1975

Spectroscopy of transition metal species in rare gas matrices: I. Vanadium metal, II. Sulfides, III. Carbonyl complexes, IV. Dinitrogen complexes, V. Homonuclear diatomic compounds

Thomas Carroll DeVore
Iowa State University

Spectroscopy of transition metal species in rare gas matrices

I. Vanadium metal

II. Sulfides

III. Carbonyl complexes

IV. Dinitrogen complexes

V. Homonuclear diatomic compounds

by

Thomas Carroll DeVore

A Dissertation Submitted to the

Graduate Faculty in Partial Fulfillment of

The Requirements for the Degree of

DOCTOR OF PHILOSOPHY

Department: Chemistry
Major: Physical Chemistry

Approved:

Signature was redacted for privacy.

In Charge of Major Work

Signature was redacted for privacy.

For the Major Department

Signature was redacted for privacy.

For the Graduate College

Iowa State University
Ames, Iowa

1975

TABLE OF CONTENTS

I. INTRODUCTION

Even the most casual glance through the literature quickly produces the realization that transition metal compounds in the form of vapor molecules exhibit a wide variety of structural and electronic configurations. Nearly 300 transition metal containing molecules of varying complexity have been identified from high temperature vaporization studies alone. In fact, a number of vapor molecules often occur in the vapor in equilibrium with a single condensed phase. For example, the vapor in equilibrium with solid WO_3 contains WO(g), WO_2(g), WO_3(g), W_2O_6(g) W_3O_8(g), W_3O_9(g) and W_4O_{12}(g).[1] The bonding in the molecular transition-metal compounds ranges from being rather ionic as found for ScF[2] to being completely covalent as found for Mn_2.[3] However, because of the large number of electrons involved, Hartree-Fock SCF-CI calculations have been performed for only the simplest of the transition metal vapor molecules including ScF,[2] Mn_2,[3] ScO,[4] TiO,[5] VO,[6] and FeO.[7] The models used to explain the bonding in the more complicated systems in a large measure result from semiempirical theoretical techniques such as liquid field theory or extended Hückel calculations. Most of the techniques used to interpret the properties of the transition metal molecules require experimental data to evaluate parameters used in the calculations. While more SCF-like calculations which require little or no experimental data, such as the approximate ab-initio calculations developed by Caulton and co-workers,[8] are rapidly becoming available, good experimental data are still needed to determine the accuracy of the calculations.

It is often experimentally difficult to obtain data for transition

metal molecules. Many transition-metal containing systems are quite refractory and do not have appreciable vapor pressures except at elevated temperatures, and many vapor molecules are quite reactive and have relatively short lifetimes making it difficult to observe their spectroscopic properties. Still other molecules which are of theoretical interest, such as the binary dinitrogen complexes, cannot be formed as vapor species using normal preparative techniques. However, the problems inherent in each of these cases can be partially solved through the use of the techniques of matrix isolation.

The matrix isolation method which was first introduced by Whittle et al.[9] in 1954, is a technique for trapping molecules as isolated entities in an inert solid (i.e. the matrix) in order to investigate some of their molecular properties. At first the method was used mainly to study radicals and other reaction intermediates. By using a large excess of the matrix gas and cooling the matrix to a temperature which was sufficiently low to prevent diffusion through the matrix, the reactive species were effectively isolated in a nonreactive environment and their lifetimes were greatly increased. Much of the work which has been done on radicals has been reviewed by Andrews.[10]

In 1961, Linevsky[11] successfully applied the matrix isolation technique to the study of high temperature vapors effusing from a Knudsen cell and observed the infrared spectra of monomeric LiF in Ar, Kr, Xe, and N_2 matrices. These experiments opened the door to the utilization of matrix isolation by high-temperature chemists, and several similar studies isolating other high temperature molecules have now been completed. Much of

the work on high temperature molecules has been reviewed by Snelson.[12]

In 1969, Rest and Turner[13] introduced the possibility of synthesizing new transition metal complexes in low temperature matrices by producing $Ni(CO)_3$ from the photolysis of $Ni(CO)_4$ in an argon matrix. Shortly thereafter, DeKock[14] demonstrated that new complexes could also be produced by codepositing metal atoms with the ligand molecules when he succeeded in producing $Ni(CO)_{1-4}$ and $Ta(CO)_{1-6}$. This field has grown rapidly and several new binary complexes have now been synthesized and identified in low temperature matrices. Part of this work was recently reviewed by Ozin and Van der Voet.[15]

The technique of matrix isolation has been successfully applied to infrared and Raman spectroscopy, ultraviolet-visible absorption and emission spectroscopy, electron spin resonance spectroscopy, and Mössbauer spectroscopy. Thus the technique has been demonstrated to be of use in obtaining much of the experimental information traditionally considered in the discussion of structure and bonding of molecules.

Although the technique of matrix isolation has several advantages for studying high-temperature molecules, reactive intermediates and unstable species, it also has the drawback that the observed spectra are altered by interactions between the trapped species and the "inert" environment. Since the molecules generally cannot rotate in the matrix, the rotational fine structure and the molecular information it contains are lost. Also the various electrostatic interactions in the matrix slightly perturb the potential well of the trapped species with a resulting shift of the observed frequencies relative to the unperturbed spectrum. In addition, if the

species is trapped in two or more unique matrix environments, or is trapped in an asymmetrical environment which can remove the degeneracy of a normal mode, then two or more frequencies may be observed for one normal mode. For example, the ground state stretching frequency of LiF, a single band at 898 cm^{-1} in the gas phase, shifts to 867 cm^{-1} in a Ne matrix, to 830 cm^{-1} in a Kr matrix, and splits into a doublet at 837/842 cm^{-1} in Ar and 814/823 in a Xe matrix.[11] In addition, there is evidence that in rare instances the structure of the reactive species may be significantly distorted by the matrix environment.[16] To determine the magnitude of the matrix shifts, the spectra of several stable molecules have been studied in various matrices. Hallam[17] recently has reviewed the results of several of these studies and found that the vibrational frequencies and the calculated bond angles for the matrix isolated molecules vary only a few percent from the gas phase values for most systems. Consequently, using uncorrected matrix data is not currently thought to introduce a large error. However, the causes of matrix effects are still not understood completely and research is continuing in this area.

Several molecular properties which reflect the bonding can be determined from the vibrational and electronic spectra. Therefore, matrix isolation absorption spectroscopy was used to collect data to be used together with semiempirical bonding models to provide information about the bonding in a variety of transition metal compounds.

The transition metal oxides rank among the better studied transition metal molecules and a considerable amount of spectroscopic data, some of which was obtained by using the technique of matrix isolation, is available

in the literature. Several review articles summarizing most of the work on the oxides have been published.[12,18,19] In contrast, the transition metal sulfides rank among the least studied transition metal systems. Prior to this study, rather incomplete spectroscopic data were available for only ScS,[20-21] YS,[21] LaS,[22] TiS,[23] and CuS.[24]

The bonding in the oxides has been investigated by a number of techniques including Hartree-Fock-SCF-CI calculations. Thus, the oxide bond is fairly well understood. Intuitively, the bonding of the sulfides is expected to be quite similar to the bonding of the oxides. To test this assumption, the first period transition metal sulfides were examined.

Obtaining information about the bonding was not the only incentive to study the transition-metal sulfides. During the past few years, several research groups have been studying the vaporization behavior of the transition metal sulfides. It is desirable to compare the values of the thermodynamic quantities obtained from these studies with the results of third law calculations using spectroscopic data. Thus, the spectra of the transition metal sulfides were also examined to obtain the spectroscopic data needed for these calculations.

Since the pioneering work of Rest and Turner[13], several transition metal carbonyl systems have been investigated in low temperature matrices. One interesting system which surprisingly had not been previously investigated, was the vanadium carbonyl system. $V(CO)_6$ is the only known stable binary carbonyl which violates the 18 electron rule[25] and is the only known stable binary carbonyl system which is paramagnetic. Thus $V(CO)_6$ is the only stable hexacarbonyl which should not have octahedral

symmetry, since octahedral $V(CO)_6$ would have a $^2T_{2g}$ ground state which is expected to distort via either the E_g or the T_{2g} vibrational mode according to the theorem of Jahn and Teller.[26]

Several of the models used to explain the bonding in the transition metal carbonyls have been reviewed by Braterman.[27] Since the calculated orbital energy levels of the isoelectronic ligands N_2 and CO are quite similar,[28] the bonding in the end-bonded complexes formed from these ligands is expected to be quite similar. Since the original report of Burdett et al.[29] that binary dinitrogen complexes could be synthesized in low temperature matrices, several investigators have succeeded in preparing a number of such complexes in matrices. In general, these complexes are isostructural with the corresponding carbonyls. However, no analog of the well studied hexacarbonyl systems, which are often used as the model systems for the carbonyls, had previously been reported. Thus the dinitrogen systems for two metals, V and Cr, which are expected to form hexacoordinated dinitrogen complexes, were examined.

In addition, the pure covalent metal-metal bond without the influence of coordinated ligands was examined by studying the spectra of the homonuclear diatomic molecules of several transition metals.

One other "bond" which always exists in matrices is the bond between the reactive molecule and the matrix. Transition metal atoms have provided much experimental information about matrix effects. The spectrum of vanadium in rare gas matrices was analyzed and an attempt was made to explain the data by assuming the vanadium "bonded" to the matrix, a model which provided considerable insight into the perturbation of the vanadium

electronic energy levels by the inert gas matrix.

There are several studies relevant to the systems considered in this thesis which have not been discussed in this brief introduction. In the introduction to each section which describes the results, specific studies appropriate to that study will be discussed to provide the necessary literature background.

II. EXPERIMENTAL TECHNIQUE

A. Apparatus

The stainless steel dewar and the matrix gas delivery system used in this study, and the furnace assembly used previously have been described in detail.[30]

In order to attain sample temperatures approaching 2200°K, it was necessary to completely redesign the furnace assembly. The resistively heated Knudsen cell described previously was replaced by a conical shaped (5 mm in diameter x 7 mm high) tungsten wire basket purchased from Ladd Research Industries, Inc. This basket was supported by two ceramic insulated copper leads which were supported by a stainless steel plate which bolted to the furnace housing. A 1" quartz viewing port was placed in the center of the stainless steel plate to permit the surface temperature of the basket to be determined using an optical pyrometer. A movable shutter was placed over the window between temperature determinations to prevent excessive build-up of sample on the viewing port. Unfortunately, the temperature often varied as much as 500°K from the top to the bottom of the basket. Thus the shutter was usually left partially open to monitor the rate of sample deposition.

The basket was heated resistively. Electrical power to the basket was provided by passing 120 V current through two manually controlled autotransformers wired in series. Depending upon the sample resistance, a power of $\sim$ 180 watts ($\sim$ 9 volts and $\sim$ 20 amps) was sufficient to heat the basket to 2000°K.

Three spectrometers were used in the experiments; a Beckman IR-7 to

scan the infrared region from 600 to 4000 cm^{-1}, a Beckman IR-11 to scan the infrared region from 200 - 800 cm^{-1}, and a Cary 14 to scan from the near infrared (10,000 cm^{-1}) through the ultraviolet (50,000 cm^{-1}). Both infrared instruments were calibrated by using atmospheric H_2O and CO_2 bands and are estimated to be accurate to $\pm$ 1 cm^{-1}. The Cary 14 was calibrated using matrix-isolated metal bands and is estimated to be accurate to $\pm$ 0.3 nm. for the sharper bands.

The continuum for the Cary 14 was provided by a high intensity tungsten lamp in the near infrared and the visible regions, and by a hydrogen discharge lamp in the ultraviolet.

B. Sample Preparation

1. Reagents

All metal samples were obtained from the Ames Laboratory, the Ar, CO, and OCS were obtained from Matheson, Inc., the N_2 was obtained from Air Products, enriched $^{15}N_2$ (95% $^{15}N_2$) was obtained from Merck and Co., and Kr was obtained from J. T. Baker Chemical Co.

The solid transition-metal sulfide samples were prepared in one of two ways. MnS, FeS, and NiS were prepared by mixing an acidified aqueous solution of the metal dihalide ("Baker Analyzed" Reagent) with a solution of of Na_2S ("Baker Analyzed" Reagent). The insoluble sulfide was then dried under vacuum and outgassed prior to use.

VS and CrS were prepared by heating stoichiometric quantities of the elements (sulfur from American Smelting and Refining Co.) in sealed Vicor tubes. The samples were preheated to 750°K for four days. The temperature

was then slowly raised to 1200°K for ten days.

2. General Procedure

All matrices were formed using the same general procedure. After the sample was placed in the tungsten basket, the cryostat and the furnace assembly were evacuated using a 2 inch oil diffusion pump. When a residual pressure of 5×10^{-4} Torr or less was obtained ($\sim$ 4 hours), the CsI cold window was pre-cooled to 77°K by pouring liquid N_2 into both dewars. Once the window reached 77°K, the liquid N_2 was blown out of the inner dewar using pressurized He, and liquid He was transferred. To prevent pumping on the diffusion pump by the liquid He cryopump, the valves between the cryostat and the diffusion pump were closed when the inner dewar contained liquid helium.

Once the inner dewar was filled with liquid He, the residual pressure in the cryostat fell to $\sim 10^{-6}$ Torr. Once the temperature of the block reached 10°K or less (usually within 5 minutes after finishing the transfer of the liquid He), the cold windows were turned to face the furnace assembly and $\sim$ 3 millimoles of matrix gas were deposited on the cold window. The furnace was then brought to temperature and the sample was deposited. After the deposition of the sample was completed, the matrix gas was allowed to flow for approximately five minutes to insure that the furnace had cooled.

Generally the furnace was adjusted to produce a sample vapor pressure between 0.001 and 0.100 Torr. The average sample deposition time was approximately 20 minutes. Matrices of good optical quality were usually

produced by depositing ∿ 0.3 millimoles of matrix gas per minute. These deposition rates produce an approximately 1000-fold excess of matrix gas, which assured good isolation.

While the overall technique of forming the matrix was the same, the details of the matrix formation did vary from system to system.

In the study on matrix effects, the matrices were produced by heating vanadium metal to ∿ 2000°K and codepositing the metal atoms with the rare gas. While deposition times of 10 minutes were sufficient to observe the stronger features, deposition times up to 30 minutes were used to enhance the weaker bands.

In the metal-sulfide study, matrices were formed in two ways. One method was to codeposit the rare gas and the vapor obtained by heating the approximately stoichiometric solid monosulfide. Because of the high degrees of dissociation exhibited by these compounds upon vaporization, furnace temperatures were adjusted to give an estimated total sample vapor pressure of ∿ 0.1 Torr.

The second method of forming the matrix was to generate the sulfide in-situ by codepositing metal atoms with rare gas doped with a sulfur source. To facilitate the reaction, the furnace assembly was modified to allow the matrix gas to pass directly over the heated metal. Although H_2S, CS_2, and OCS were all tried as sulfur sources, only OCS proved satisfactory. H_2S usually failed to react, and CS_2 often formed carbonyl sulfide species which had absorptions in the M-S stretching region (see Figure 1). While considerably more productive of MS species than H_2S and CS_2, OCS also had shortcomings. A large matrix band caused by the ν_2 band of OCS obscured a

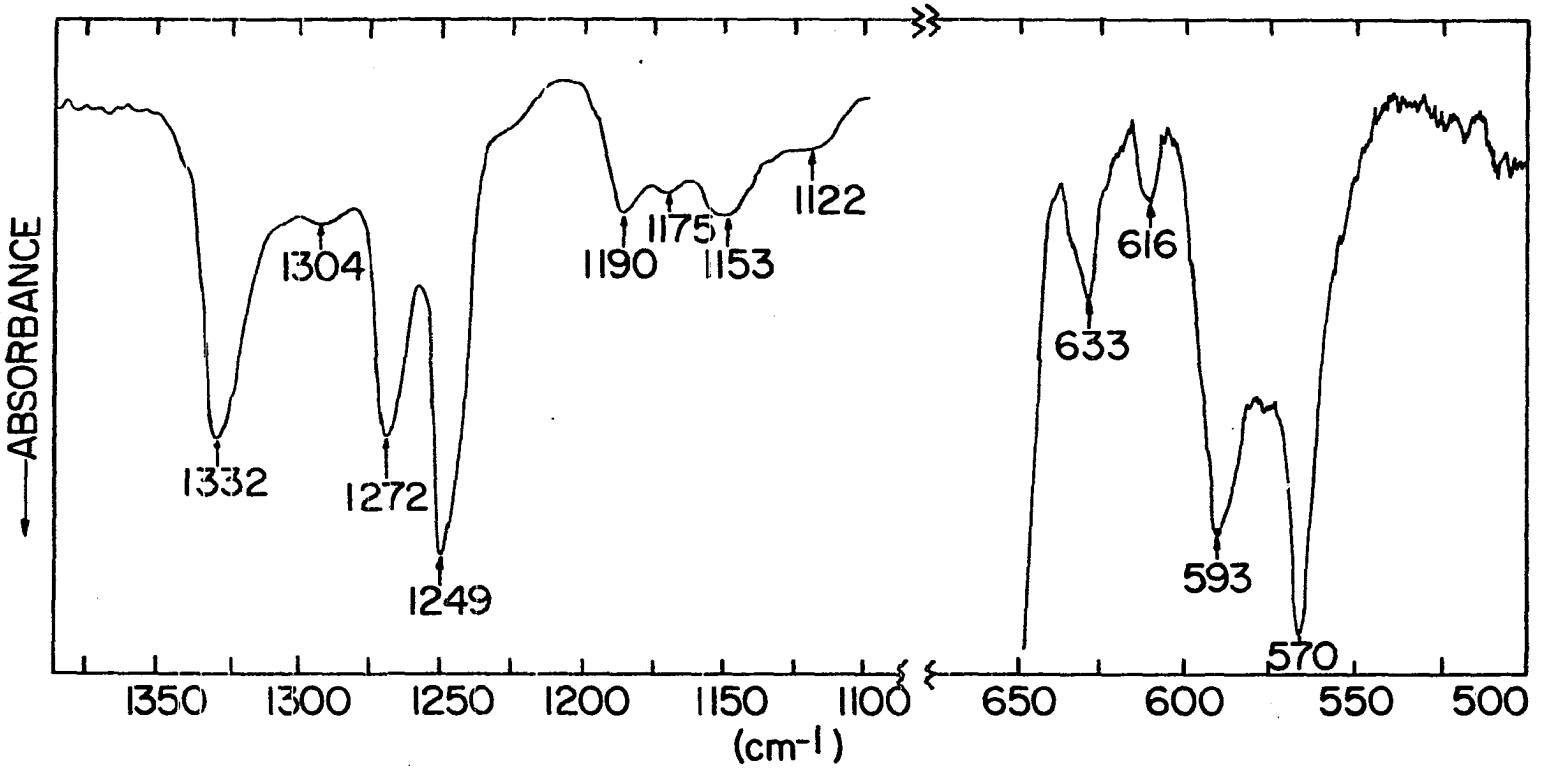

Figure 1. The infrared spectrum of V isolated in a CS_2 matrix showing the absorptions in the M-S and C-S stretching regions

region $\sim$ 40 cm^{-1} wide centered around 520 cm^{-1}. In addition, there was the possibility of the formation of metal carbonyls. Fortunately, carbonyl formation proved not to be a serious problem, although evidence of carbonyl complexes in the matrix was occasionally detected.

The matrices for the carbonyl and the dinitrogen experiments were formed in similar manner. Metal atoms with a vapor pressure of $\sim$ 0.01 Torr were codeposited with ligand/argon mixtures. The ligand concentrations were varied from 0.5 - 8 mole % CO and from 0.25 - 15 mole % N_2 for the carbonyl and the dinitrogen experiments, respectively. In addition, some spectra were observed using matrices formed totally of CO and N_2.

After the initial deposition, further reaction was accomplished by controlled annealing of the matrix. This was accomplished by radiatively heating the matrix with two 250 watt infrared heat lamps. Using this procedure it was possible to observe the growth and the disappearance of the various absorption bands providing information useful in the assignment of the spectra.

The method of matrix preparation in the homonuclear-diatomic molecule study was identical with that used for the vanadium metal study, except longer deposition periods were used.

With the exception of part of the carbonyl and the dinitrogen studies when NaCl optics were used, CsI optics were used throughout. These optics permit the observation of the spectrum from 200 cm^{-1} to $\sim$ 40,000 cm^{-1}.

III. VANADIUM METAL

A. Introduction

The work of Mann and Broida[31] has generated interest in the effect of rare gas matrices upon the spectra of isolated metal atoms. Matrix shifts relative to the gaseous atom transitions of several hundred wavenumbers have been observed, demonstrating that these effects are not negligible. However, no universal theory has been reported which can satisfactorily explain all the effects observed in the spectra of matrix isolated metal atoms. A review of several models which have been used to attempt to explain matrix effects was recently published by Barnes.[32]

Although the large number of strong transitions generally observed for atomic species makes the correlation of the matrix-shifted peaks to the corresponding gas phase frequencies difficult, reasonable correlations may generally be made by appropriately shifting the entire gas phase spectrum. However, the magnitude of this shift varies from metal to metal with no apparent regularity, and differences of several hundred wavenumbers in the shifts for a given metal in one type of matrix generally occur. For example, Schoch and Kay[33] observed for Ta in Xe, an approximate blue shift of 980 cm^{-1} for $\nu < 33{,}000$ cm^{-1} and a red shift of 3230 cm^{-1} for $\nu > 33{,}000$ cm^{-1}. In contrast the spectrum of Ta in Ar[33,34] shows a nearly constant perturbation of approximately 1000 cm^{-1} throughout.

In the hope of gaining more information about matrix shifts, the spectrum of V in Ar and Kr matrices has been examined. Based upon published oscillator strengths,[35] it was expected that the spectrum of V metal would

be relatively simple for $\nu < 30{,}000\ cm^{-1}$. Thus it was hoped that some useful insight about matrix shifts could be gained by examining this region.

B. Results and Discussion

As was anticipated the spectrum with $\nu < 30{,}000\ cm^{-1}$ is relatively simple and may readily be assigned from intensity considerations for V in both Ar and Kr matrices as shown by Figures 2 and 3. This region appears to be characterized by two distinct average matrix shifts. The low intensity bands with $\nu < 25{,}000\ cm^{-1}$ are red shifted in Ar and are randomly shifted by slight amounts in Kr, while the more intense bands with $30{,}000\ cm^{-1} > \nu > 25{,}000\ cm^{-1}$ show a substantial blue shift in both Ar and Kr. One possible explanation for this effect is that the direction and magnitude of the shift depend upon the energy of transition. Support for this explanation is found in the assignments of Schoch and Kay[33] for W/Xe and Ta/Xe and by Gruen and Carstens[36] for Ti/Ar, Xe. Oscillator strength may also have an effect upon the direction of the shift, since the oscillator strengths of the red shifted transitions are considerably less than those shifted to the blue. Support for this model is also found in the results for the Ta/Xe system.[33] In either case a blue shift for the strong transitions with $\nu > 30{,}000\ cm^{-1}$ would be expected. Figure 4 shows that a constant blue shift of $1000\ cm^{-1}$ for V in Ar in this region does a poor job of reproducing the observed spectrum. Unlike many of the transition metals which have been previously studied, the assumption of a constant matrix shift does not adequately assign the spectrum. While the failure of this model does not exclude the possibility that oscillator strength or

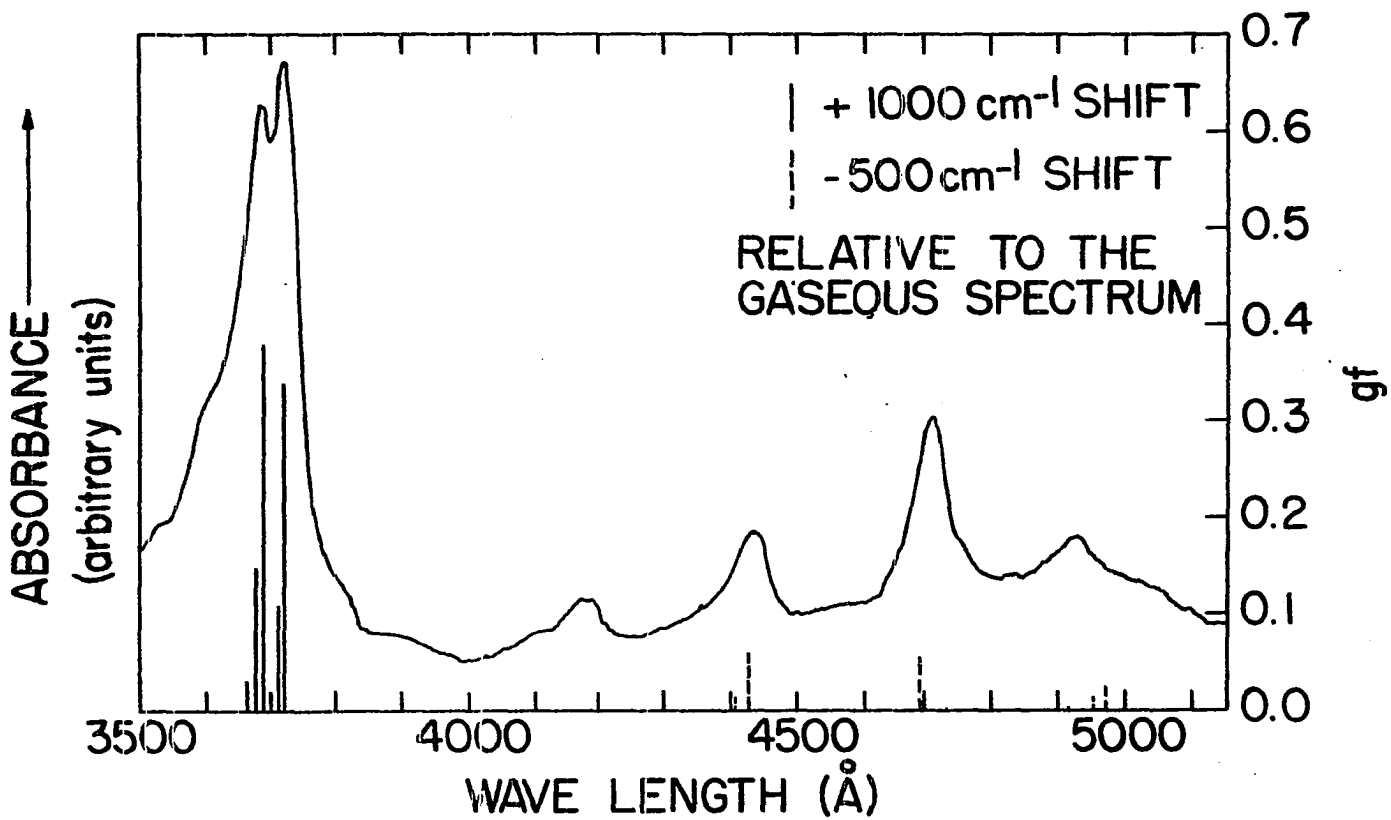

Figure 2. The spectrum of V in Ar with $\nu < 30{,}000\ cm^{-1}$. The lines represent the gas phase spectrum from the $a^4F_{3/2}$ ground state of known oscillator strength shifted as indicated to match the observed intensities with + implying a blue shift. Values of gf are from Reference 35. Assignments are given in Table 1

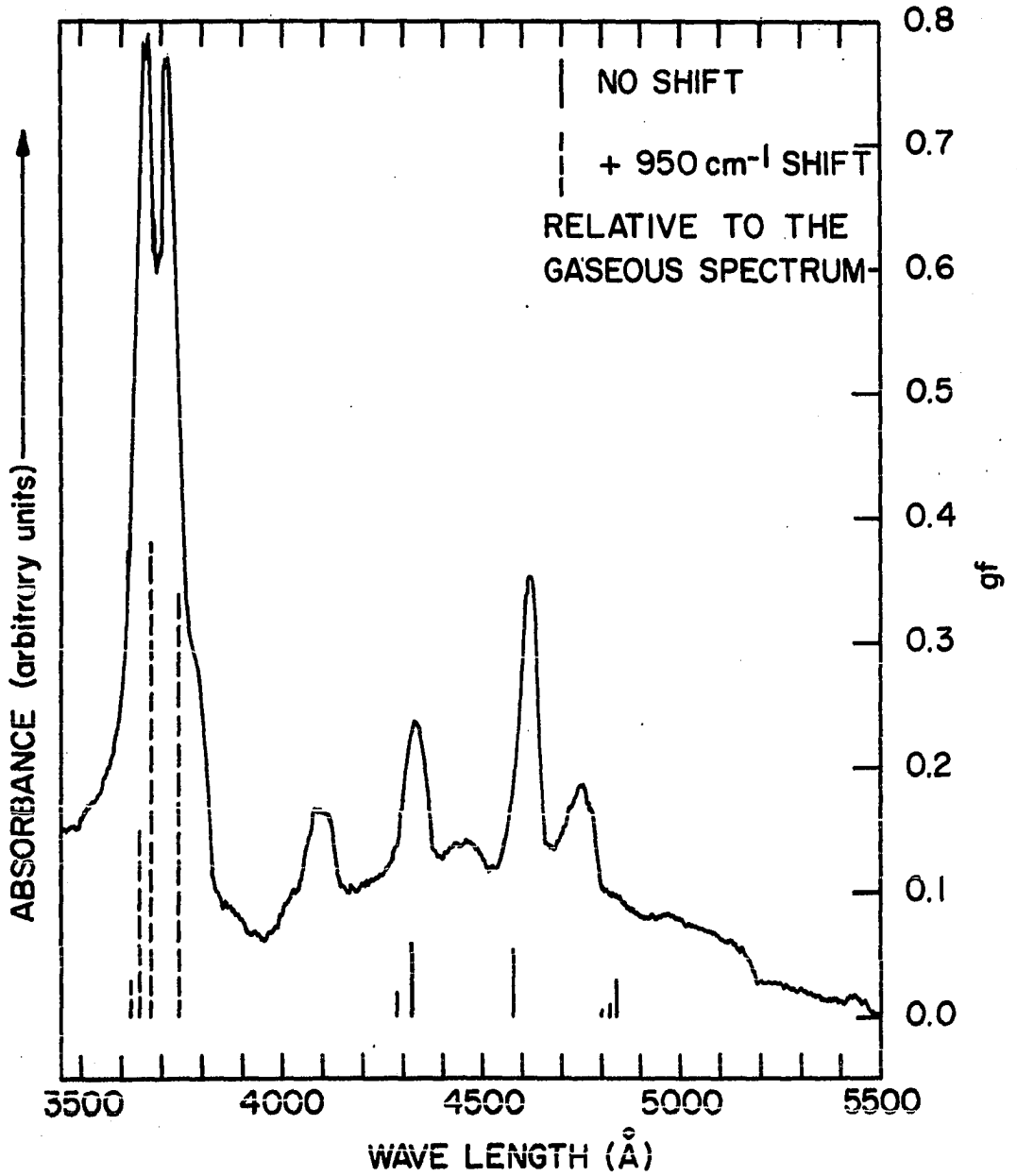

Figure 3. The spectrum of V in Kr with $\nu < 30{,}000\ cm^{-1}$. The lines represent the gas phase spectrum from the $a^4F_{3/2}$ ground state of known oscillator strength shifted as indicated to match the observed intensities with + implying a blue shift. Values of gf are from Reference 35. Assignments are given in Table 2

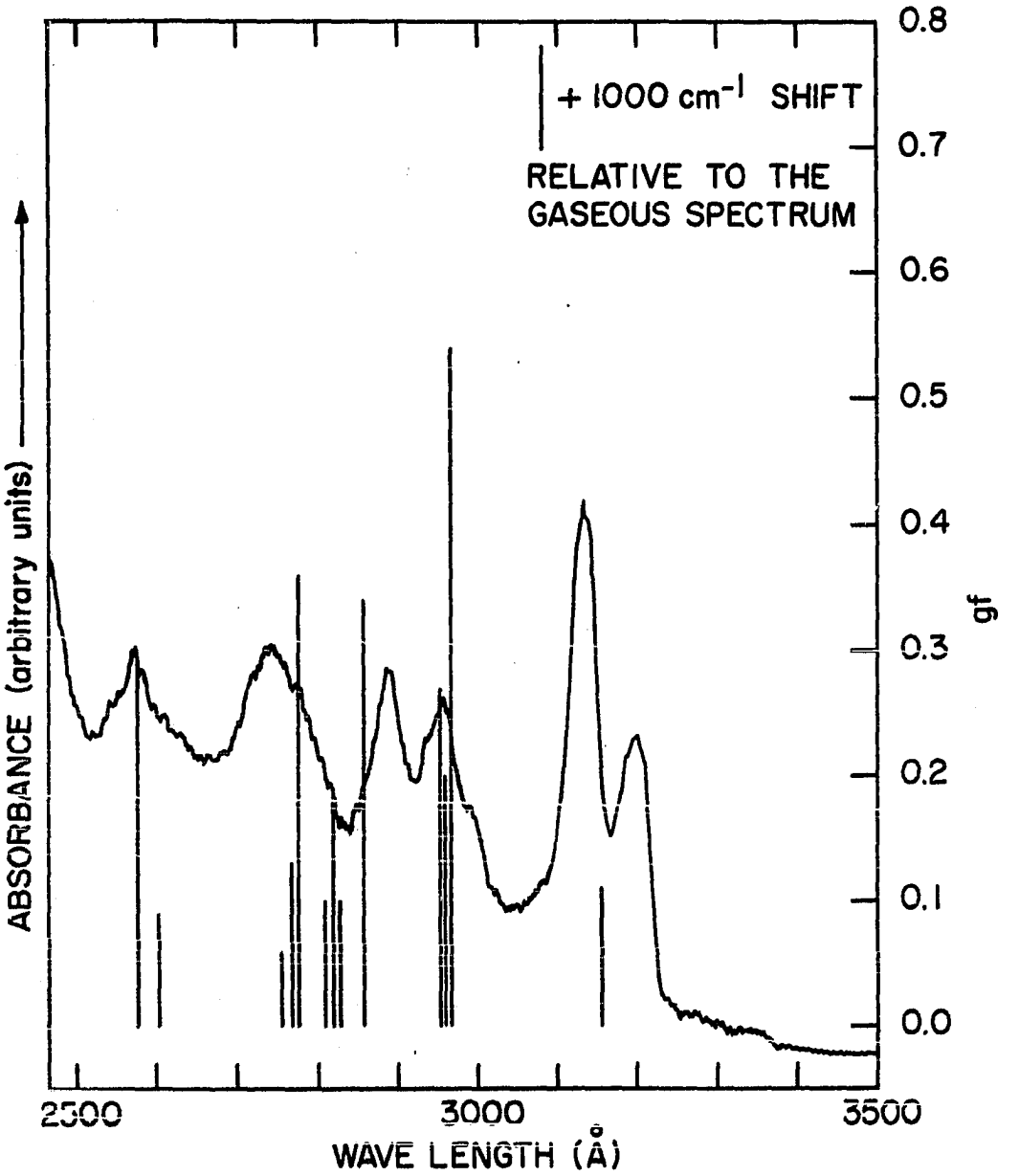

Figure 4. The spectrum of V in Ar with $\nu > 30{,}000$ cm^{-1} showing the assignments which would be made from a constant blue shift of 1000 cm^{-1}. Values of gf are from reference 35. No assignments were made from this model

energy of transition influences the matrix shift, it does indicate that neither is a significant factor in the determination of the magnitude of the shift.

Examination of the transitions in the region with $\nu < 30{,}000$ cm^{-1} for V in Ar indicates that all the red shifted transitions are to states corresponding to a $3d^3 4s[a^3F]4p$ configuration while those which are blue shifted are to states which correspond to a $3d^4[a^5D]4p$ configuration. Assuming that the degeneracy of the atomic orbitals is not broken by the matrix environment, it seems reasonable to expect that transitions to all states which arise from a $3d^3 4s[a^3F]4p$, or the closely related $3d^3 4s[a^5F]4p$ configuration, would show a red shift, while those to states originating from a $3d^4[a^5D]4p$ configuration would show a blue shift. Figure 5 shows the assignments which would result for the $\nu > 30{,}000$ cm^{-1} region from this model. Although each configuration undoubtedly has its own unique shift, in Figure 5 all transitions to states from configurations other than those specifically mentioned have been arbitrarily shifted to best match the observed intensity by assuming a constant blue shift of 1000 cm^{-1} or a constant red shift of 500 cm^{-1}.

The similarity of the gf values for the stronger gas phase transitions in this region makes several alternative assignments possible and several were considered. The assignments made using this model are believed to best fit the observed spectrum and are given in Table 1. The individual states arising from the same configuration show more fluctuation in the V/Kr system than was observed for V/Ar. However, the basic model used for V/Ar, with slight modifications which will be discussed in more detail

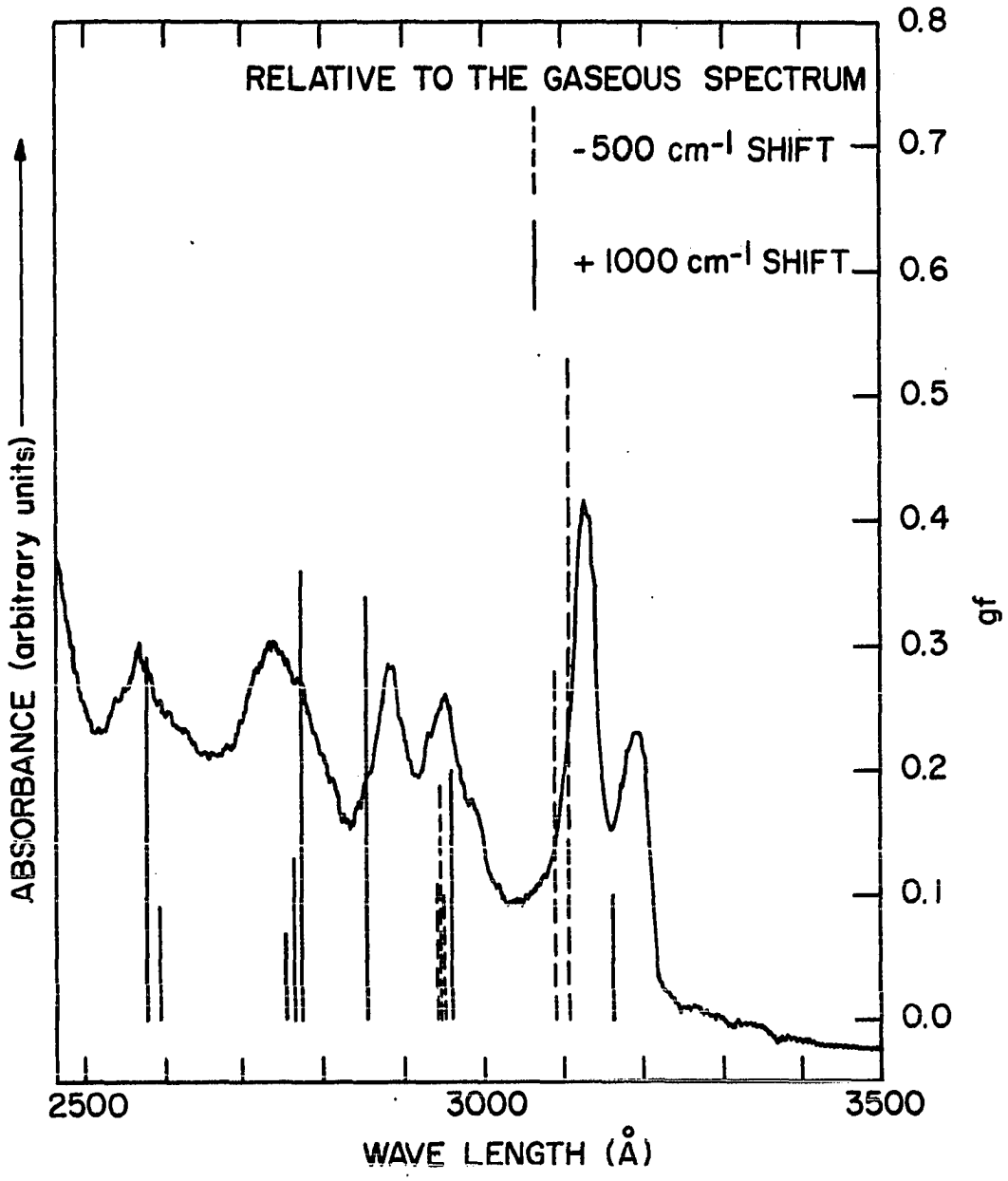

Figure 5. The spectrum of V in Ar with $\nu > 30{,}000$ cm^{-1} showing the assignments which would be made by assuming that all states which correspond to the same electron configuration show the same shift. Values of gf are from reference 35. Assignments are given in Table 1

Table 1. Assignments for V in Ar

λ(Å)	ν_{Ar} (cm^{-1})	ν_g (cm^{-1})[a]	$\nu_{Ar}-\nu_g$	Configuration[a]	Upper State[a]	gf[b]
6011	16,636					
5885	16,992					
5755	17,376					
4930	20,284	20,606	-322	$3d^3 4s(a^3F)4p$	$z^4D_{1/2}$	0.028
4704	21,259	21,841	-582	$3d^3 4s(a^3F)4p$	$z^4G_{5/2}$	0.055
4428	22,584	23,088	-504	$3d^3 4s(a^3F)4p$	$z^4F_{3/2}$	0.060
4173	23,964					
4050	24,691					
3719	26,889	25,931	958	$3d^4(a^5D)4p$	$y^4F_{3/2}$	0.34
3686	27,130	26,183	947	$3d^4(a^5D)4p$	$y^4D_{1/2}$	0.38
3198	31,270	30,636	634	$3d^3 4s(b^3G)4p(?)$	$y^4G_{5/2}$	0.11
3136	31,888	32,738	-850	$3d^3 4s(a^5F)4p$	$w^4F_{3/2}$	0.53
3121	32,041	32,847	-806	$3d^3 4s(a^5F)4p$	$w^4F_{5/2}$	0.27

[a] From reference 37.

[b] From reference 35.

Table 1. (Continued)

λ(Å)	ν_{Ar} (cm^{-1})	ν_g (cm^{-1})[a]	$\nu_{Ar}-\nu_g$	Configuration[a]	Upper State[a]	gf[b]
2998	33,356				$z^2P_{3/2}$	0.20
2960	33,784	32,768 34,477	1016 -697	$3d^3\overline{4s(a^5F)}4p$	$v^4D_{1/2}$	0.19
2892	34,578	33,967	611	$3d^34s(c^3P)4p$	$w^4D_{1/2}$	0.34
2752	36,337	35,013	1324	———	$u^4D_{1/2}$	0.36
2708	36,928					
2565	38,986	37,757	1229	$3d^4(b^3F)4p$	$t^4D_{1/2}$	0.29

later, also appears to be applicable for V/Kr and has been used to make the assignments shown in Figure 6 and summarized in Table 2.

Several of the bands observed in the spectrum apparently arise from transitions which are not allowed in the free atom. Since Moore's tables[37,38] list a number of states which could reasonably be the upper states for these transitions, they are believed to be atomic vanadium transitions rather than a transition caused by some impurity in the matrix. However, since there was no method to determine which transition had increased in intensity, assignments for these transitions could not be made. These matrix-allowed transitions illustrate that the observed intensity of a transition can also be influenced by the matrix.

It appears that for V metal the electronic configuration of the excited state is a significant factor in determining the direction and magnitude of the matrix shift. To determine if this effect is observable for other metals, the shifts observed for Ti metal in Ar and Xe by Gruen and Carstens[36] and for Nb in Ar, Kr, and Xe by Green and Gruen[39] have been examined. Although the results, which are tabulated in Tables 3 and 4, are not conclusive, it appears that the magnitudes of the shifts exhibited by these metals also depend upon the configurations of the upper states, with each inner electron state* exhibiting a corresponding shift. The outer electrons, which actually determine the final state, appear to influence the shift to a much larger extent in the matrices composed of the larger more easily polarized gases for these metals.

---

*For example, the states which arise from a $3d^3 4s\ [a^3F]4p$ configuration would have an a^3F inner state.

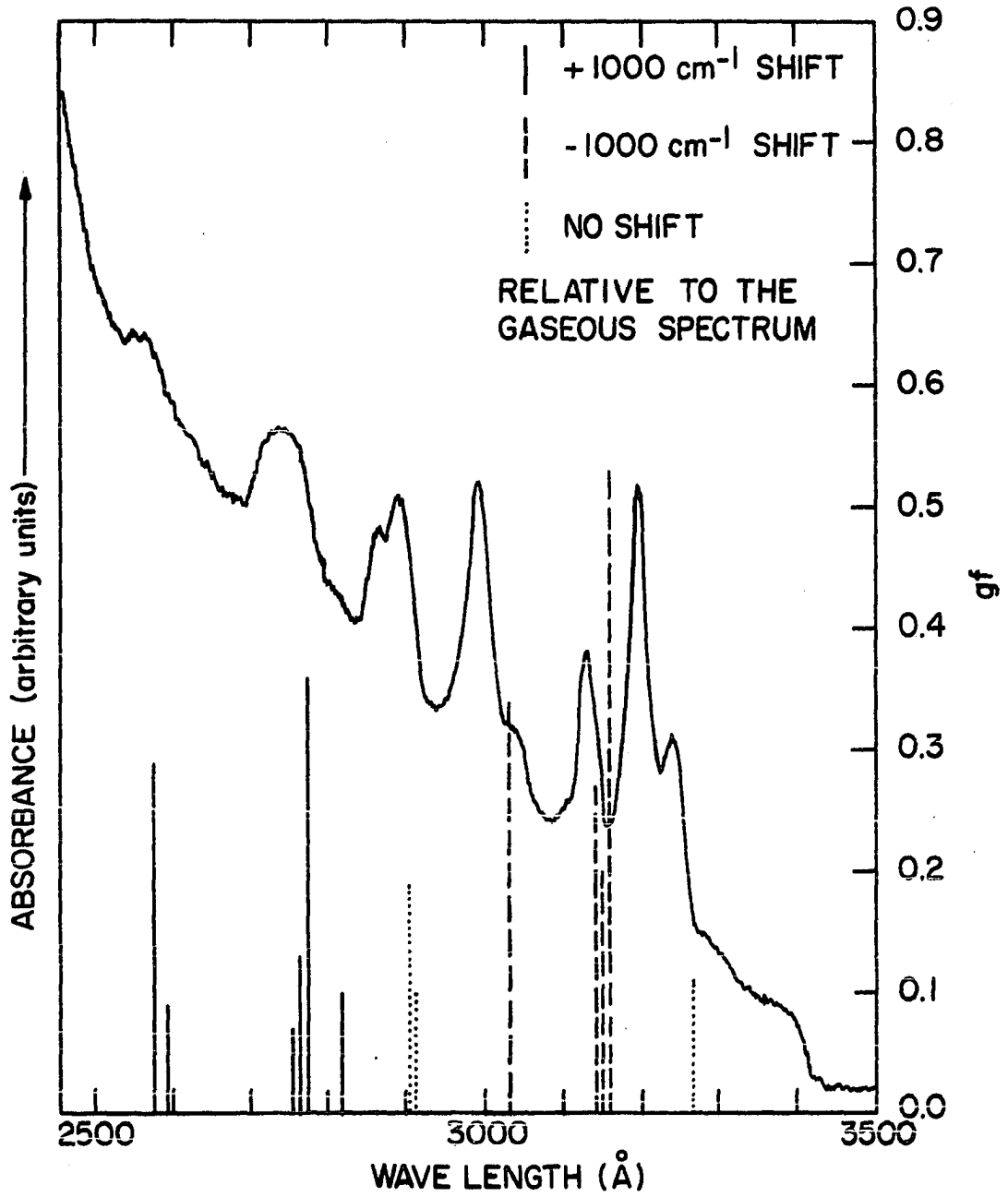

Figure 6. The spectrum of V in Kr with $\nu > 30{,}000$ cm^{-1} showing the assignments which would be made by assuming that all states which correspond to the same electron configuration show the same shift. Values of gf are from reference 35. Assignments are given in Table 2

Table 2. Assignments for V in Kr

λ(Å)	ν_{Kr} (cm^{-1})	ν_g (cm^{-1})[a]	$\nu_{Kr}-\nu_g$	Configuration[a]	Upper State[a]	gf[b]
6142	16,280					
6108	16,373					
6003	16,660					
5959	16,782					
5832	17,147					
4775	20,942	20,606	336	$3d^3 4s(a^3F)4p$	$z^4D_{1/2}$	0.028
4760	21,008	20,688	320	$3d^3 4s(a^3F)4p$	$z^4D_{3/2}$	0.011
4722	21,175	20,828	347	$3d^3 4s(a^3F)4p$	$z^4D_{5/2}$	0.002
4624	21,626	21,841	-215	$3d^3 4s(a^3F)4p$	$z^4G_{5/2}$	0.055
4478	22,334					
4341	23,035	23,088	-53	$3d^3 4s(a^3F)4p$	z^4F^0	0.060
4115	24,301					
4088	24,462					

[a] From reference 37.

[b] From reference 35.

Table 2. (Continued)

λ(Å)	ν_{Kr} (cm^{-1})	ν_g (cm^{-1})[a]	$\nu_{Kr}-\nu_g$	Configuration[a]	Upper State[a]	gf[b]
4018	24,888					
3790	26,385					
3732	26,795	25,931	846	$3d^4(a^5D)4p$	$y^4F_{3/2}$	0.34
3672	27,233	26,183	1050	$3d^4(a^5D)4p$	$y^4D_{5/2}$	0.38
3295	30,349					
3242	30,840	30,636	204	$3d^34s(b^3G)4p(?)$	$y^4G^0_{5/2}$	0.11
3195	31,299	32,738	-1439	$3d^34s(a^5F)4p$	$w^4F_{5/2}$	0.53
3132	31,923	32,768	-845	———	$z^2P_{3/2}$	0.20
3040	32,895					
2991	33,459	33,967	-508	$3d^34s(c^3P)4p$	$w^4D_{1/2}$	0.34
2902	34,459	34,416	-43	$3d^34s(a^5F)4p$	$v^4D_{5/2}$	0.10
2894	34,557	34,447	-110	$3d^34s(a^5F)4p$	$v^4D_{1/2}$	0.19
2865	34,904	34,477	427	———	y^2D	0.098
2755	36,298	35,013	1285	———	$u^4D_{1/2}$	0.36
2560	39,062	37,757	1305	$3d^4(b^3F)4p$	$t^4D_{1/2}$	0.29

Table 3. Comparison of the configuration for the upper state with the matrix shift for Ti metal

Configuration[a]	Upper State[a]	E gas (cm^{-1})[b]	ΔE/Ar[b]	ΔE/Xe[b]
$3d^2 4s(a^2F)4p$	z^3F_2	19323	580	620
$3d^2 4s(a^2F)4p$	Z^3D_1	19938	680	610
$3d^2 4s(a^2F)4p$	z^3G_3	21470	830	880
$3d^2 4s(c^4F)4p$	y^3F_2	25107	580	30
$3d^2 4s(a^4F)4p$	y^3D_1	25318	710	60
$3d^3(b^4F)4p$	x^3F_2	26803	690	___
$3d^3(b^4F)4p$	y^3G_3	27499	570	-210
$3d^2 4s(b^4P)4p$	w^3D_1	29661	___	-160
$3d^2 4s(a^4F)4p$	x^3G_3	29915	650	260
$3d^2 4s(b^2G)4p$	w^3G_3	31374	1030	30
$3d^2 4s(b^2G)4p$	v^3F_2	33981	850	-260
$3d^3(b^2D)4p$	u^3D_1	37852	1330	250

[a]Reference 37.

[b]Reference 36.

Table 4. Comparison of the configuration for the upper state with the matrix shift for Nb

Configuration[a]	Upper State[a]	E gas (cm^{-1})[b]	ΔE/Ar[b]	ΔE/Kr[b]	ΔE/Xe[b]
$4d^4(a^5D)5p$	$z^4P_{1/2}$	23007	2156	———	———
$4d^4(a^3P)5p$	$z^2D_{3/2}$	23526	2200	———	———
$4d^4(a^5D)5p$	$y^6F_{1/2}$	23985	2200	1627	736
$4d^4(a^5D)5p$	$y^6F_{3/2}$	24165	———	1548	697
$4d^4(a^5D)5p$	$x^6D_{1/2}$	26552	———	———	526
$4d^4(a^5D)5p$	$x^6D_{3/2}$	26713	2323	1504	438
$4d^4(a^5D)5p$	$y^4D_{3/2}$	26937	2363	———	397
$4d^4(a^3P)5p$	$z^4S_{1/2}$	28208	———	———	137
$4d^35s(a^5P)5p$	$y^6P_{3/2}$	28278	2558	1878	899

[a]Reference 38.

[b]Reference 39.

In an attempt to gain some insight into the mechanism by which the electronic states influence the matrix shift, an average transition from the $3d^3 4s^2[a^4F_{3/2}]$ ground state of V to some $3d^3 4s[a^{3(5)}F]4p$ state was examined in a model Ar matrix using extended Hückel theory. Since extended Hückel calculations will be discussed in detail in Appendix A, only a brief description of the calculation will be given here. For simplicity, the matrix was assumed to be an octahedral complex about the vanadium atom with only the 6 nearest neighbor V-Ar interactions of importance. The atomic screening constants for the single Slater type orbitals[40] used in the calculation were calculated from the formulas of Clementi and Raimondi.[41] The diagonal matrix elements for each configuration were assumed to be the VOIP's of Basch, Viste and Gray.[42] Off-diagonal elements were calculated using the Wolfsberg-Helmholz[43] approximation with k = 2.0. The "bond lengths" were arbitrarily chosen to be 3.83 Å, the nearest neighbor distance in solid Ar. Since spin is not included in this calculation, the effect of altering the spin-orbital states during the transition is lost. For this reason, the only transitions which were considered are the $3d^3 4s[^{3(5)}F]4p \leftarrow 3d^3 4s^2[^4F_{3/2}]$ transitions in which the total spin and the occupied d orbitals remain unaltered.

From Figure 7 one sees the main effect of the matrix is to increase the energy of the outer metal electrons, presumably due to electron-electron repulsion with the Ar electrons. This causes the total energy of the state to be increased in the matrix. However, the effect on each state is quantitatively slightly different, and this quantitative difference correlates with the observed matrix shifts.

Table 5. Input parameters for EHMOT calculation for the $3d^3 4s[a^{3(5)}F]4p^1 \leftarrow 3d^3 4s^2[a^4F_{3/2}]$ transition for V in an argon matrix

	$k = 2.0$	$r_e = 3.83$ Å
	$3d^3 4s^2[a^4F_{3/2}]$ Configuration	
Orbital	Diagonal Matrix Element (eV)	Orbital Exponent
3p	43.33	3.595
3d	8.85	2.994
4s	7.49	1.245
4p	3.10	1.245
	$3d^3 4s[a^{3(5)}F]4p^1$ Configuration	
3p	43.33	3.595
3d	8.85	2.994
4s	8.75	1.245
4p	4.51	1.245

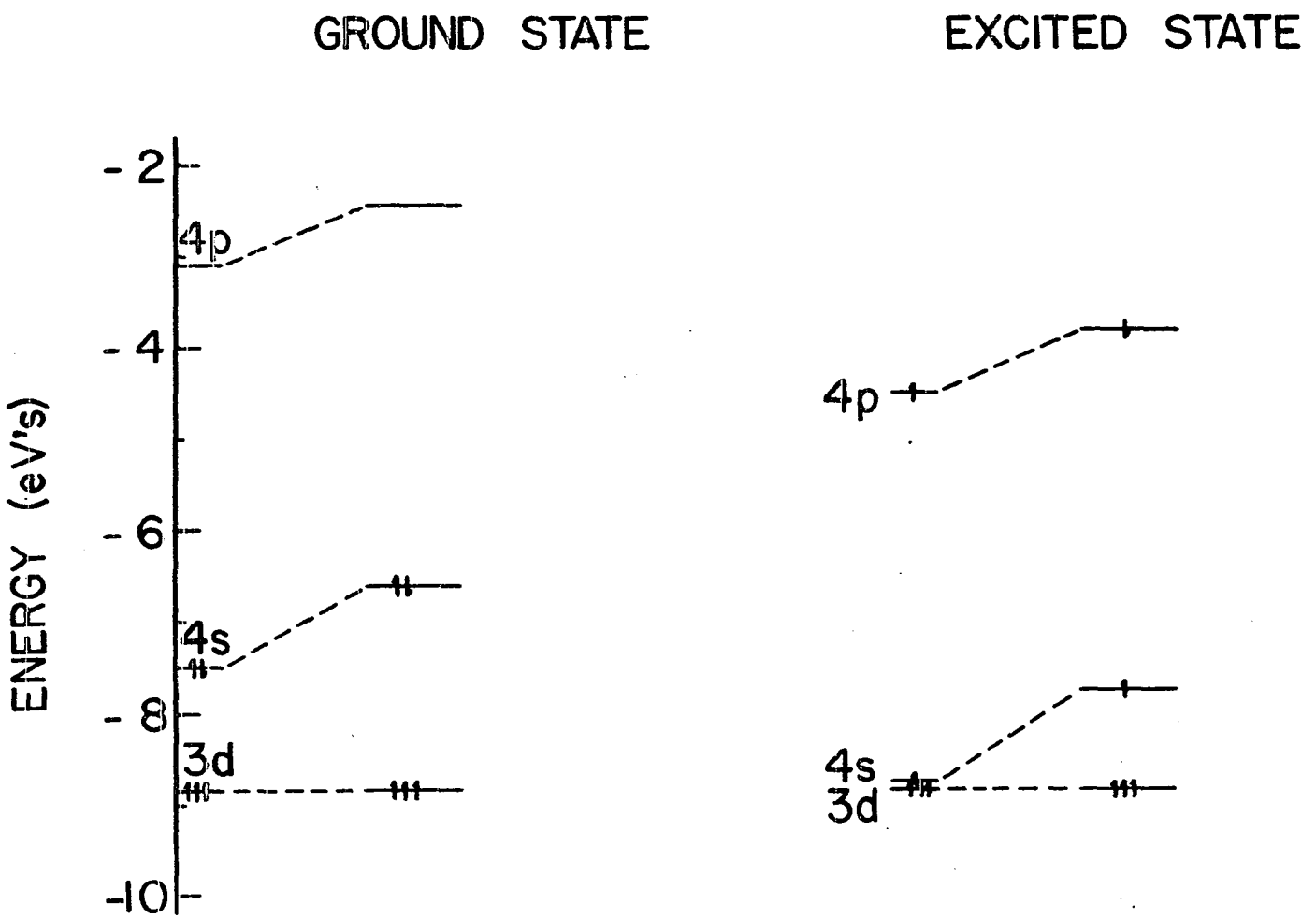

Figure 7. The effect of the model matrix upon the valance orbitals in each configuration for a $3d^3 4s^1 [a^{3(5)}F] 4p \leftarrow 3d^3 4s^2 [a^4F_{3/2}]$ transition in V. The matrix causes the energy of each configuration to be raised. The ground state configuration is raised 1.798 e.V. while the excited configuration is raised 1.687 e.V. Thus a red shift of 0.111 e.V. (895 cm^{-1}) is expected for this transition in the matrix

This model offers an explanation for another observed matrix effect. According to the model, the appropriate wavefunctions are no longer the pure metal atomic orbitals. The interaction with the matrix has caused some mixing of the metal atomic orbitals with both the ligand orbitals and other symmetry related metal orbitals. While this mixing is small, it is likely that this alteration of the atomic orbital wavefunctions gives rise to the altered intensity relationships observed in most matrices.

However V/Kr does not appear to strictly follow this model. From Table 2, it is apparent that transitions to states arising from the $3d^3 4s[a^{3(5)}F]4p$ configuration show at least two distinct matrix shifts. This effect also appears in some of the other transition metals. For example, the matrix shifts for Fe in Ar, listed in Table 8 also show two distinct matrix shifts for each electron configuration. However, the model proposed here was based upon the assumption that the orbital degeneracy of the free atom was not changed. If this degeneracy is broken then each configuration would be expected to exhibit more than one matrix shift.

C. Conclusions

The interaction with the matrix appears to cause a perturbation in the energy of each atomic state, and differences in the amount of the perturbation accounts for the observed matrix shifts. In a totally symmetric environment all transitions to states which arise from the same electronic configuration are expected to have the same matrix shift in the absence of second-order effects. As the site symmetry is decreased, the number of

Table 6. Eigenvalues and eigenvectors for the $3d^3 4s^2 [a^4F_{3/2}]$ state of V in a model Argon matrix

	T_{1u_2}	A_{1g}	E_g	T_{2g}	T_{1u_2}
E_i(eV)	-2.463	-6.591	-8.850	-8.850	-43.33
3p(V)	0.0001	0.0	0.0	0.0	1.0000
3d(V)	0.0	0.0	1.0000	1.0000	0.0
4s(V)	0.0	1.0076	0.0	0.0	0.0
4p(V)	1.0121	0.0	0.0	0.0	0.0000
3s(Ar_1)	0.0	-0.0581	-0.0002	0.0	0.0
3p(Ar_1)	-0.0198	0.0906	0.0016	-0.0002	0.0
3s(Ar_2)	0.0	-0.0581	-0.0002	0.0	0.0
3p(Ar_2)	-0.0198	-0.0906	-0.0016	0.0002	0.0
3s(Ar_3)	0.0	-0.0581	0.0002	0.0	0.0
3p(Ar_3)	-0.0198	0.0906	-0.0016	-0.0002	0.0
3s(Ar_4)	0.0	-0.0581	0.0002	0.0	0.0
3p(Ar_4)	-0.0198	-0.0906	0.0016	0.0002	0.0
3s(Ar_5)	-0.0818	-0.0581	0.0	0.0	0.0001
3p(Ar_5)	0.1013	0.0906	0.0	0.0	-0.0002
3s(Ar_6)	0.0818	-0.0581	0.0	0.0	-0.0001
3p(Ar_6)	0.1013	-0.0906	0.0	0.0	-0.0002

Table 7. Eigenvalues and eigenvectors for the $3d^3 4s^1 [a^{3(5)}F] 4p$ state of V in an Argon matrix

	T_{2u_2}	A_{1g}	E_g	T_{2g}	T_{1u_1}
E_i(eV)	-3.818	-7.755	-8.850	-8.850	-43.33
3p(V)	0.0001	0.0	0.0	0.0	1.0000
3d(V)	0.0	0.0	0.0	0.0	0.0
4s(V)	0.0	1.0034	1.0000	1.0000	0.0
4p(V)	1.0114	0.0	0.0	0.0	0.0
$3s(Ar_1)$	0.0	-0.0612	-0.0002	0.0	0.0001
$3p(Ar_1)$	-0.0221	0.1038	0.0019	-0.0003	-0.0002
$3s(Ar_2)$	0.0	-0.0612	-0.0002	0.0	-0.0001
$3p(Ar_2)$	-0.0221	-0.1038	-0.0019	0.0003	-0.0002
$3s(Ar_3)$	0.0	-0.0612	0.0002	0.0	0.0
$3p(Ar_3)$	-0.0221	0.1038	-0.0019	-0.0003	0.0
$3s(Ar_4)$	0.0	-0.0612	0.0002	0.0	0.0
$3p(Ar_4)$	-0.0221	-0.1038	0.0019	0.0003	0.0
$3s(Ar_5)$	-0.0863	-0.0612	0.0	0.0	0.0
$3p(Ar_5)$	0.1130	0.1038	0.0	0.0	0.0
$3s(Ar_6)$	0.0863	-0.0612	0.0	0.0	0.0
$3p(Ar_6)$	0.1130	-0.1038	0.0	0.0	0.0

Table 8. Comparison of the configuration of the upper state with the matrix for Fe

Configuration[a]	Upper State[a]	E gas (cm^{-1})[b]	ΔE/Ar[b]	ΔE/Kr[b]	ΔE/Xe[b]
$3d^6 4s(a^6D)4p$	z^5D_4	25,900	548	1000	350
$3d^6 4s(a^6D)4p$	z^5D_3	26,140	1440	1050	390
$3d^6 4s(a^6D)4p$	z^5F_5	26,375	1535	1125	465
$3d^6 4s(a^6D)4p$	z^5P_3	29,056	1634	1110	347
$3d^7(a^4F)4p$	y^5D_4	33,096	314	194	-676
$3d^7(a^4F)4p$	y^5D_3	33,507	443	163	-727
$3d^7(a^4F)4p$	y^5F_5	33,695	645	605	-305
$3d^7(a^4F)4p$	y^5F_4	34,040	920	550	-290
$3d^6 4s(a^4D)4p$	y^5P_3	36,767	633	483	-417
$3d^6 4s(a^4D)4p$	x^5D_4	39,626	1414	524	-576
$3d^6 4s(a^4D)4p$	x^5F_5	40,257	1783	633	-747

[a]Reference 39.

[b]Reference 31.

distinct matrix shifts is increased. Also different configurations which arise from similar orbital combinations, for example the $3d^3 4s[a^3F]4p$ and the $3d^3 4s[a^5P]4p$ configurations of V, may markedly differ in the direction and magnitude of their shift. One may qualitatively model the system by assuming the argon and the metal interact to form a "complex." The changes in the energy levels of the metal atom as a result of the formation of this complex are responsible for the observed matrix shifts, while the alterations in the atomic wavefunctions through the formation of this complex account for the differences in the observed intensities.

Since the matrix wavefunctions are no longer the free atom wavefunctions, the two electron energy terms can no longer be considered to be identical with the two electron terms exhibited by the free atom. Since these terms affect the energy differences between states, the difference in these integrals could account for at least part of the fluctuation around the average value of the matrix shift.

IV. TRANSITION METAL SULFIDES

A. Introduction

Knowledge of several molecular parameters is needed to provide a fundamental understanding of the chemical behavior of molecules in the vapor phase. Most of these constants are not known for the transition metal sulfides. Consequently, several empirical correlations have been developed[44-47] relating the sulfide molecular constants to those of the corresponding oxides. However, these correlations were developed from observed trends in the oxides and sulfides with nontransition metal cations, and lack of experimental data has prevented an adequate testing of these correlations for the sulfides of the transition metals. The purpose of this study was to determine experimentally as many molecular constants as possible for the first period transition metal sulfides, and to use the data to test the empirical correlations.

The spectra observed for the transition metal sulfides tended to be of rather poor quality. In many experiments no bands were observed which could be assigned as transition metal sulfide bands in either the infrared or the visible spectrum. Although this could partially be attributed to the tendency of the transition metal sulfides to vaporize as atoms and the inefficient molecular vaporizer used in this study, there is also reason to believe that matrix interactions played a significant part in generating the low intensities observed for these bands. Cater[48] failed to observe the infrared spectra of several rare earth sulfides in rare gas matrices, even though the mass spectrometrically verified that molecular species were

present in the vapor effusing from a Knudsen cell.

However, while the infrared bands were weak, they were observable and spectra were obtained for each of the first period transition metal sulfides except Co. Co reacted with the tungsten basket and formed a low melting solution which resulted in a break in the electrical circuit. This melting coupled with the low intensities generally observed for the transition metal sulfides, resulted in the deposition of an inadequate amount of CoS to permit the observation of the infrared spectrum.

Surprisingly, the near infrared-visible absorption spectrum was even harder to observe than was the infrared spectrum. Electronic spectra were not observed for several of the transition-metal sulfide systems examined. This result is consistent with a similar study for ScS reported previously by McIntyre et al.[21] They observed the IR and ESR spectra of ScS, but also failed to observe the electronic spectrum. In general, the transitions which were observed contained weak, rather broad, highly overlapping bands. This observation supports McIntyre et al.'s conclusion that matrix broadening and/or weak oscillator strengths are responsible for obscuring the electronic spectra of the transition metal sulfides in rare gas matrices.

The large concentrations of free metal atoms which accompanied all spectra made attempts to observe the ultraviolet spectrum impractical.

B. Results and Discussion

1. TiS

Since the ground state vibrational frequency of TiS is known from the work of Clements and Barrow,[23] the Ti system was used to test the efficiency of the sulfur sources. The infrared spectra obtained from the species produced by the reaction of Ti with OCS in an OCS matrix (trace a), and with 5% OCS in an argon matrix (trace b) are shown in Figure 8. The observed frequencies of 552 cm^{-1} in an OCS matrix and of 556 cm^{-1} in an argon matrix agree with the gas-phase frequency of 558.3 cm^{-1}, and verify that TiS was produced in both cases. The TiS frequency is red shifted by only $\sim$ 2 cm^{-1} in the argon matrix. A red shift of comparable magnitude was found for ScS in Ar by McIntyre, Lin and Weltner,[21] namely $\sim$ 4 cm^{-1} relative to the gas phase value reported by Marcano and Barrow.[20] These results taken together indicate that the error generated by using the argon matrix frequency in place of the true gas phase frequency is only $\sim$ 1%.

Although electronic transitions are known to exist for TiS in the near infrared-visible region studied, no electronic transitions were observed.

2. VS

Figure 9 shows the infrared spectra obtained by reacting vanadium with OCS (trace a) and from codepositing the vapor from stoichiometric VS with argon (trace b). Although each spectrum was found to contain two bands, the band around 580 cm^{-1} which is common to both systems has been assigned as the VS stretching frequency. The band at 598 cm^{-1} was found in the spectrum of V/CO/Ar, and is assigned as $V(CO)_6$. Since Owzarski and

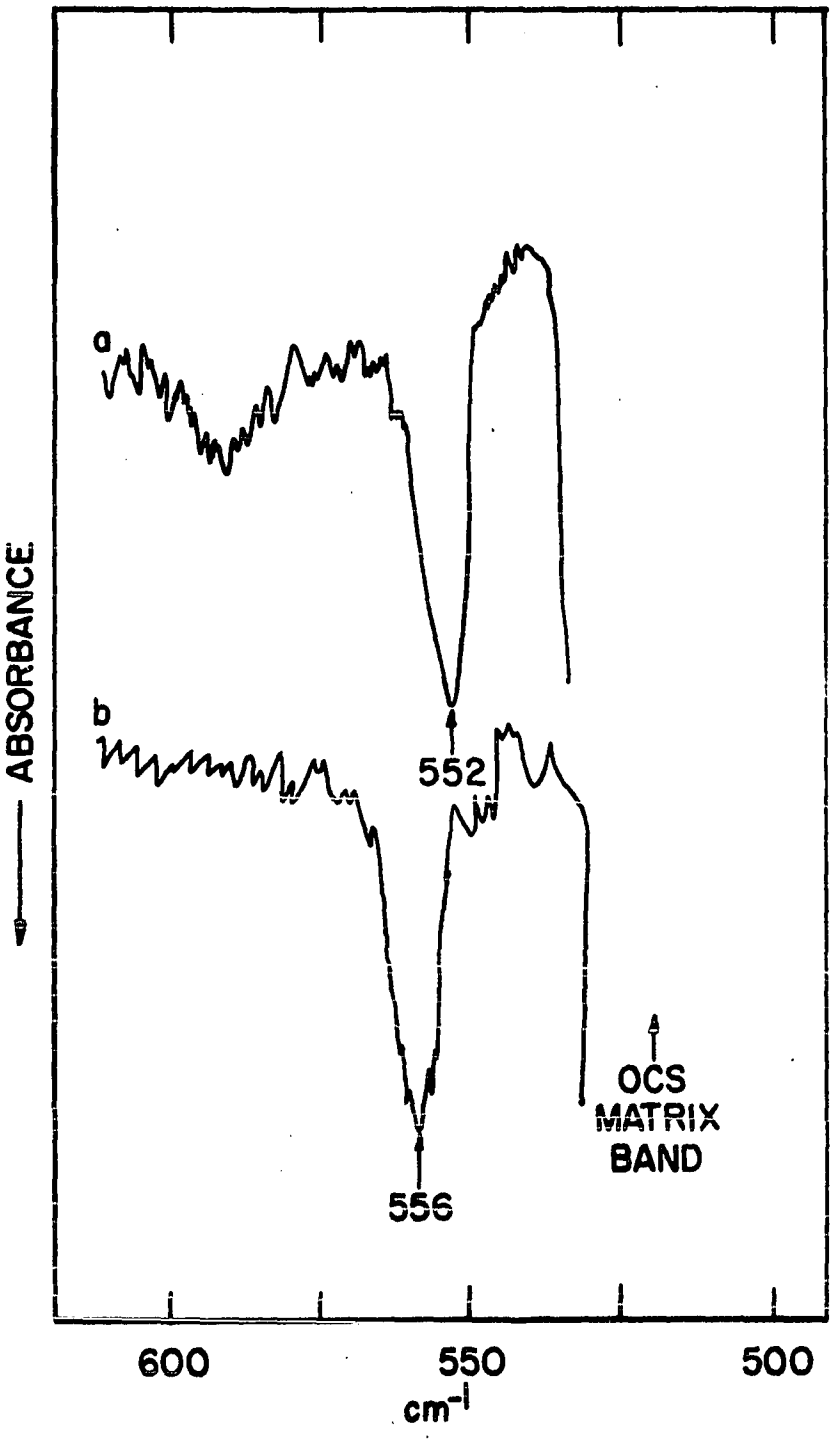

Figure 8. The infrared spectrum of TiS isolated in an OCS (trace a) and in a 5% OCS/Ar (trace b) matrix

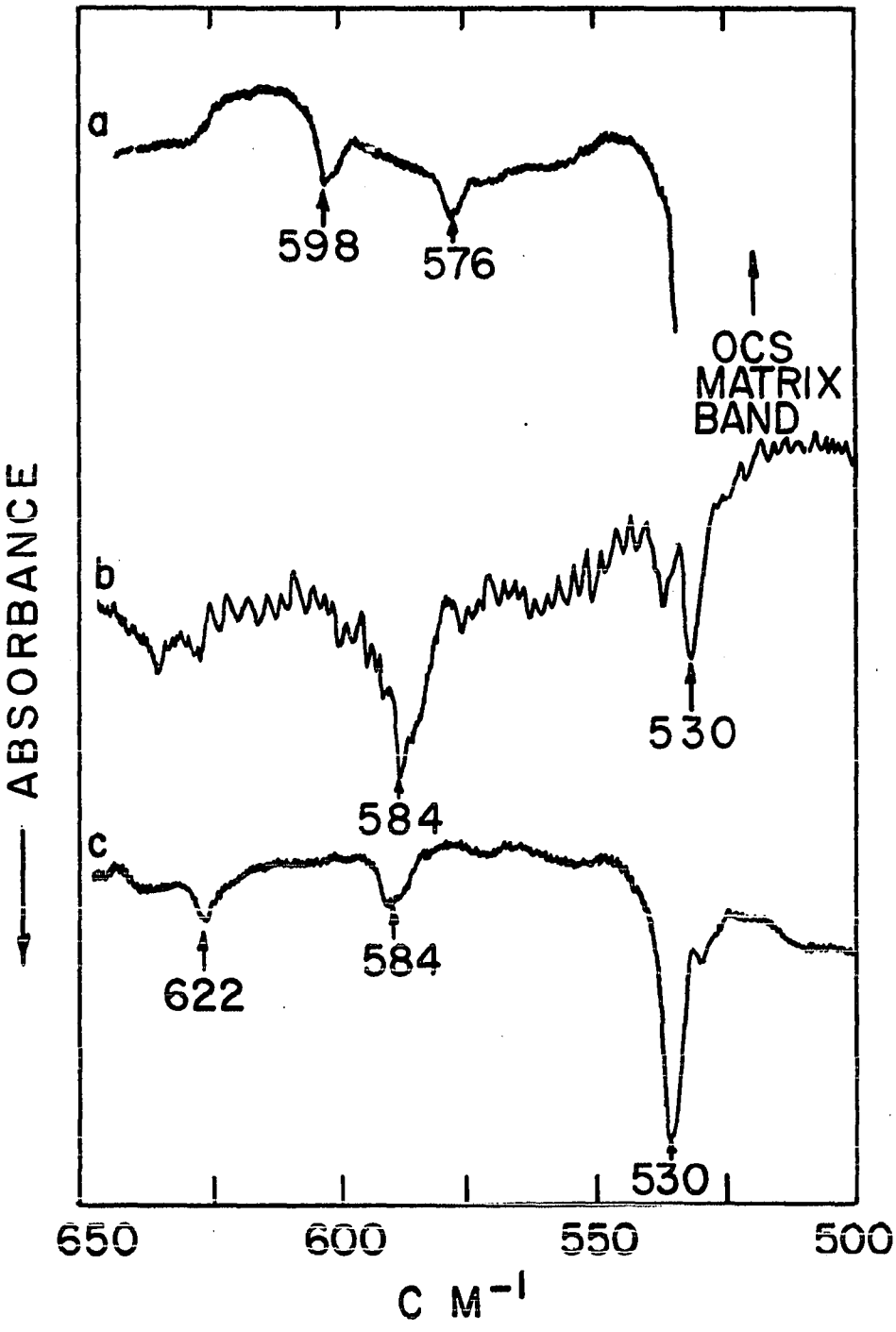

Figure 9. The infrared spectrum of VS and VS_2 isolated in an OCS (trace a) and in argon matrices (traces b and c)

Franzen[49] have found a small amount of $VS_2(g)$ in the vapor in equilibrium with solid VS, the band observed at 530 cm^{-1} in Ar is believed to arise from VS_2. Further support for this assignment was obtained by codepositing the vapor from a phase richer in sulfur than the monosulfide, V_3S_5, with Ar (trace c). In this spectrum, the intensity of the 530 cm^{-1} band was greatly increased and a new band was observed at 622 cm^{-1}. Since the amount of VS_2 in the matrix is expected to increase with increasing sulfur content of the vaporizing solid, this result supports the assignment of the 530 cm^{-1} band as the ν_3 frequency of VS_2. The 622 cm^{-1} band is assigned as the ν_1 frequency of VS_2.

The observation of the ν_1 band is in agreement with Owzarski's[50] prediction of C_{2v} symmetry for VS_2. It is interesting to note that, as is true for TiO_2,[51] TaO_2,[52] CeO_2,[53] ThO_2,[54] WO_2,[55] and ZrO_2,[56] VS_2 is apparently a molecule for which $\nu_1 > \nu_3$ for the ground state frequencies, rather than the more usual case $\nu_3 > \nu_1$.

A progression of overlapping bands observed in the near infrared spectrum of VS/Ar is shown in Figure 10. The average vibrational spacing of 458 cm^{-1}, which was determined by graphically resolving the spectrum into component gaussians, is reasonable for a metal sulfide, therefore this progression is tentatively assigned as the $A \leftarrow X$ transition of VS. The assignments made by assuming the longest wavelength band to be the 0-0 band are given in Table 9. The band marked with the asterisk was observed in several vanadium containing matrices in which the VS progression was not observed. Although this band has not been definitely assigned, it probably arises from vanadium metal atoms in the matrix.

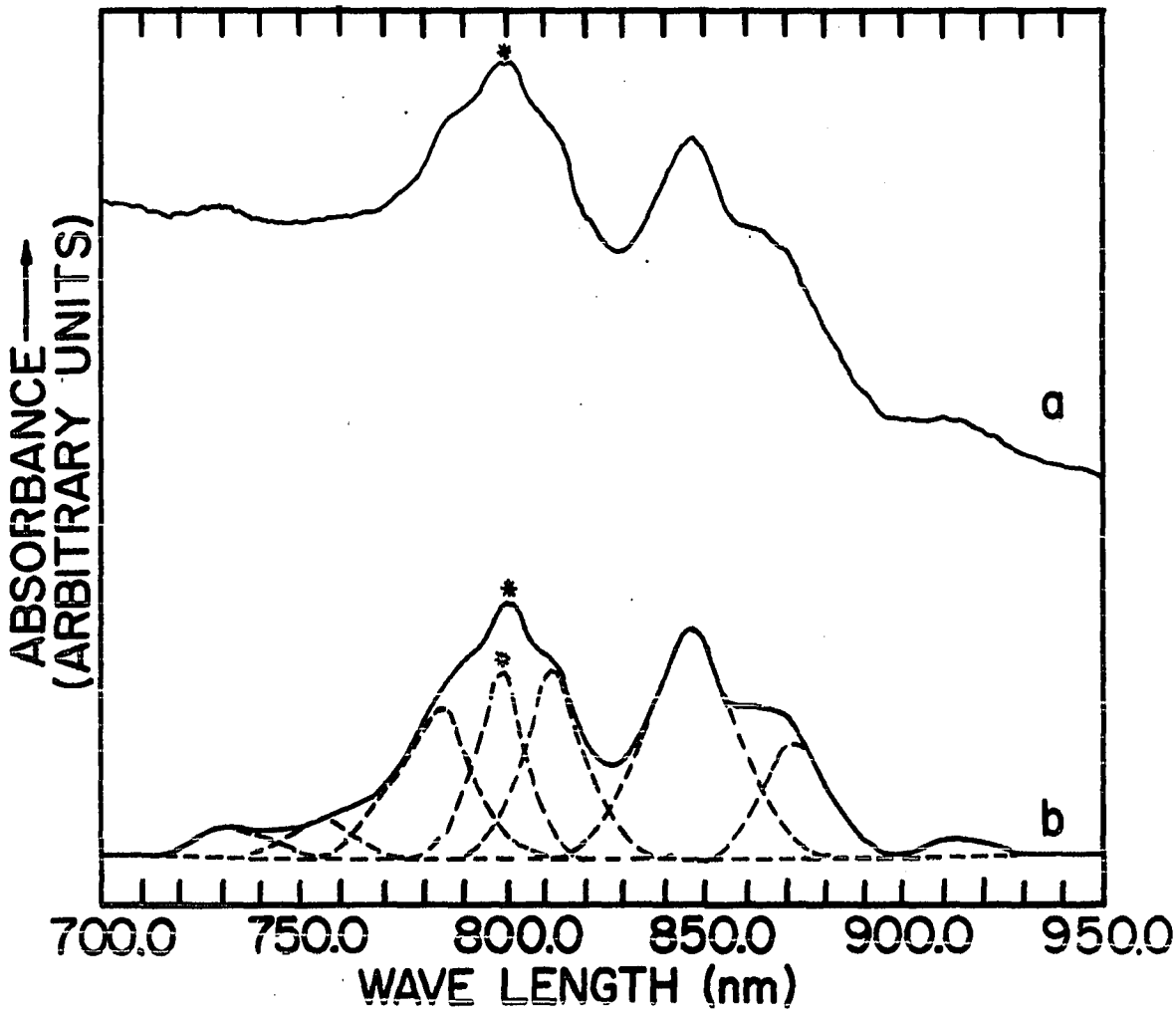

Figure 10. The near infrared absorption spectrum of VS in an argon matrix. Trace b is a gaussian resolution of the observed spectrum shown in trace a. The asterisk denotes an impurity band

Table 9. Assignments for the A ← X transition of VS in an Ar matrix assuming the longest wavelength band is the 0-0 band

ν'	λ(nm)	$\bar{\nu}$(cm^{-1})	$\Delta G'_{1/2}$ (cm^{-1})
0	913.8	10943	473
1	876.0	11416	435
2	843.8	11851	464
3	812.0	12351	450
4	783.4	12765	476
5	755.2	13241	450
6	730.4	13691	———
		Ave.	458

There appears to be a second progression of bands in the visible region starting around 600 nm. Unfortunately, interference of known matrix isolated vanadium bands with this progression prevented the accurate determination of the 0-0 band or the vibrational spacing. Since the vibrational spacing appears to be $\sim$ 450 cm^{-1}, this progression has tentatively been assigned as the B $\leftarrow$ X transition of VS.

3. CrS

The infrared spectrum of CrS isolated in OCS and Ar matrices is shown in Figure 11. Although two possible frequencies for CrS were observed in argon matrices, only one band at 560 cm^{-1} was observed for CrS in OCS matrices. Consequently the band at 558 cm^{-1} in Ar has been assigned as the stretching frequency of CrS. Further support for this assignment is obtained from the behavior of the 576 cm^{-1} band. The intensity of this band was found to decrease with annealing of the matrix and with increasing vaporization temperature of the sample. This type of behavior was not expected nor was it observed for any of the other sulfides studied. Consequently, this 576 cm^{-1} band is probably not due to a Cr sulfide species and has not been assigned.

Two definite vibrational progressions found in the near infrared-visible spectrum of CrS in Ar and Kr matrices are shown in Figures 12 and 13. Both progressions have tentatively been assigned as electronic transitions of CrS. The assignments are given in Tables 10 and 11.

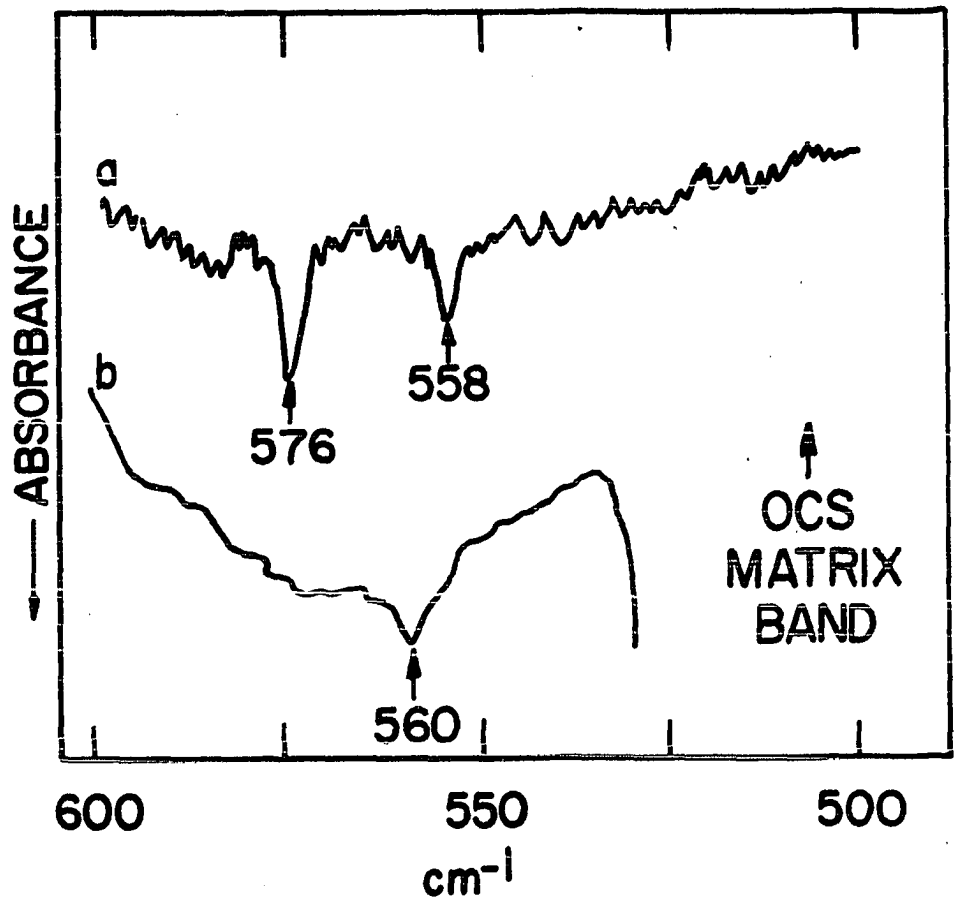

Figure 11. The infrared spectrum of CrS isolated in an Ar (trace a) and in an OCS (trace b) matrix

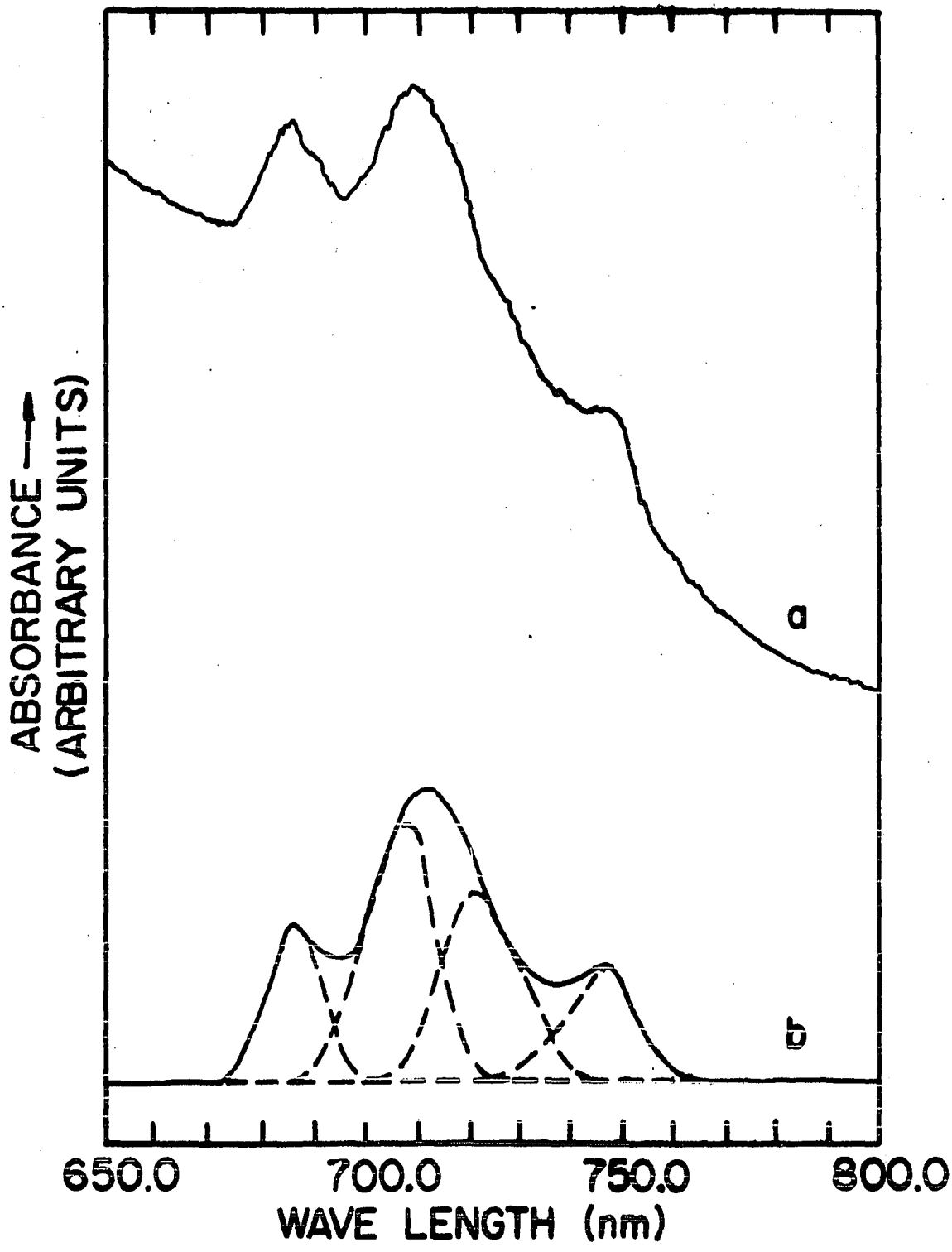

Figure 12. The near infrared absorption spectrum of CrS isolated in an Ar matrix. Trace b is a gaussian resolution of the observed spectrum shown in trace a

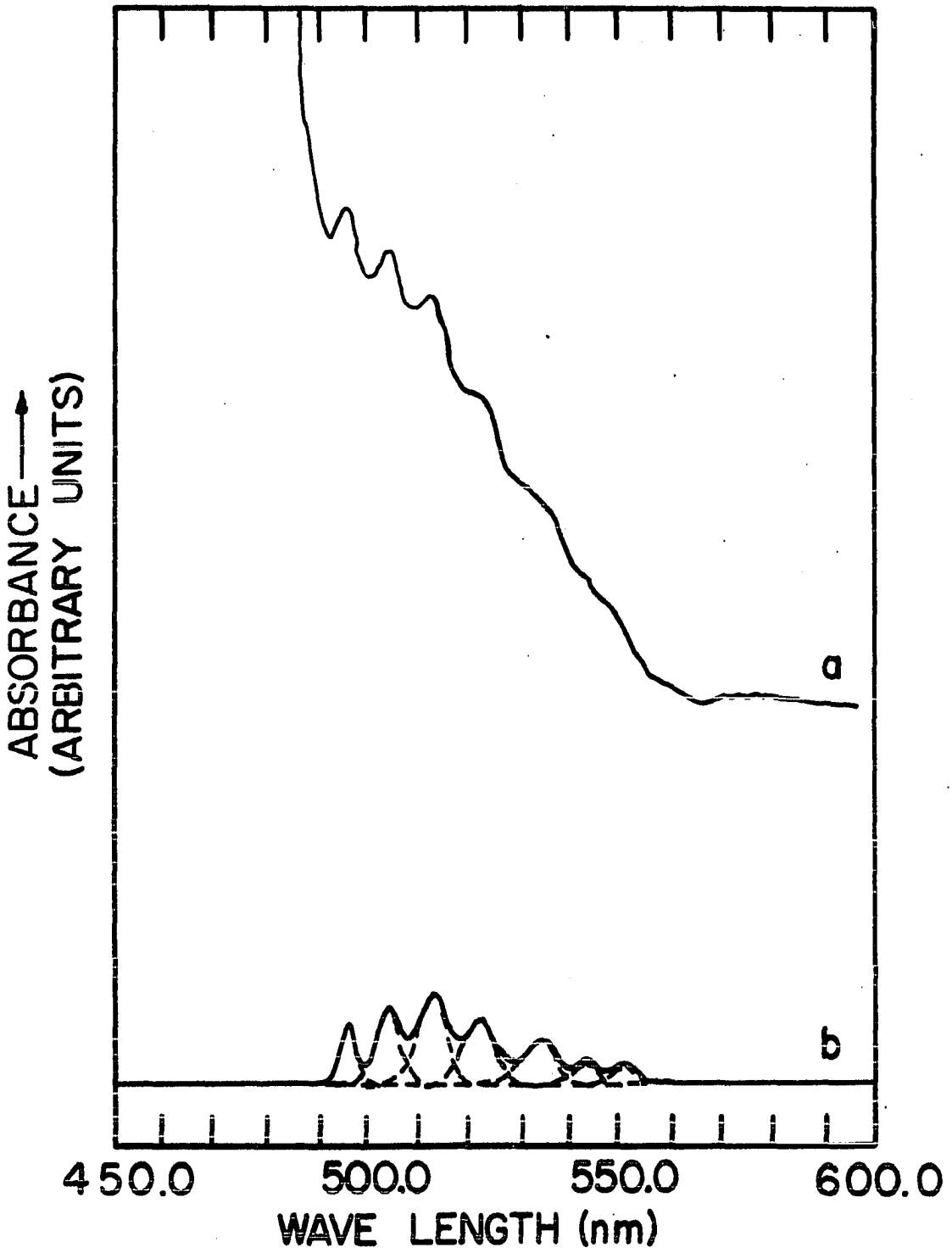

Figure 13. The visible absorption spectrum of CrS isolated in a Kr matrix. Trace b is a gaussian resolution of the observed spectrum shown in trace a

Table 10. Assignments for the A ← X transition of CrS in an Argon matrix assuming the longest wavelength band is the 0 - 0 band

ν'	λ(nm)	$\bar{\nu}(cm^{-1})$	$\Delta G'_{1/2}(cm^{-1})$
0	747.6	13376	402
1	725.8	13778	396
2	705.6	14172	405
3	686.0	14577	
			Ave. 400

Table 11. Assignments for the B ← X transition of CrS in a Krypton matrix assuming the longest wavelength band is the 0 - 0 band

ν'	λ(nm)	$\bar{\nu}$(cm^{-1})	$\Delta G'_{1/2}$ (cm^{-1})
0	553.4	18070	346
1	543.0	18416	346
2	533.0	18762	344
3	523.4	19106	342
4	514.2	19448	346
5	505.2	19794	343
6	496.6	20137	
			Ave. 343

4. MnS

The infrared spectrum of MnS isolated in an argon matrix is shown in Figure 14. The band at 508 cm^{-1} was observed only for MnS/Ar and has been assigned as the MnS stretching frequency. Unfortunately, the large matrix band prevented the verification of this frequency using OCS. No electronic transitions were observed for MnS.

5. FeS

The infrared spectra of FeS isolated in OCS, Ar, and Kr matrices are shown in Figure 15. The large band ∿520 cm^{-1} is always accompanied by two other bands at ∿1150 cm^{-1} and ∿1350 cm^{-1}. Comparison of this spectrum with the spectrum observed by Allavena et al.[57] for SO_2 in Kr matrices readily identifies the 520 cm^{-1} band as the ν_2 bending frequency of SO_2. Thus the band at ∿540 cm^{-1} is assigned as the FeS stretching frequency.

One highly overlapping vibrational progression was observed in the visible spectrum of FeS/Ar and it has tentatively been assigned as the $A \leftarrow X$ transition of FeS.

6. NiS

The infrared spectrum of NiS isolated in an Ar matrix is shown in Figure 17. As with FeS, the band at 522 cm^{-1} was assigned as the ν_2 band of SO_2, leaving only the band at 536 cm^{-1} as a possible NiS band. Since this band was observed only for the Ni-S system, it has been assigned as the stretching frequency of NiS. Like MnS, the OCS matrix band prevented the verification of this frequency by using OCS. No electronic transitions were observed for NiS.

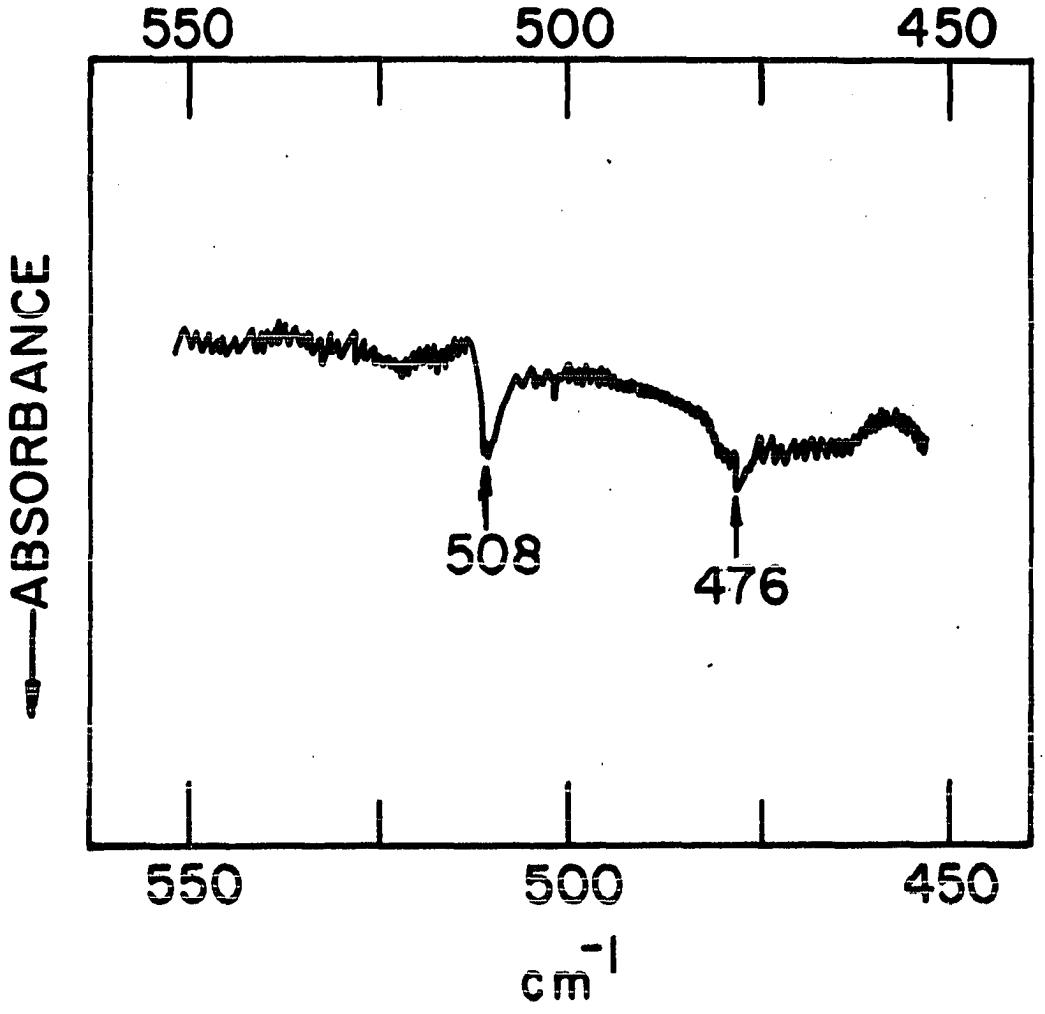

Figure 14. The infrared spectrum of MnS isolated in an Ar matrix

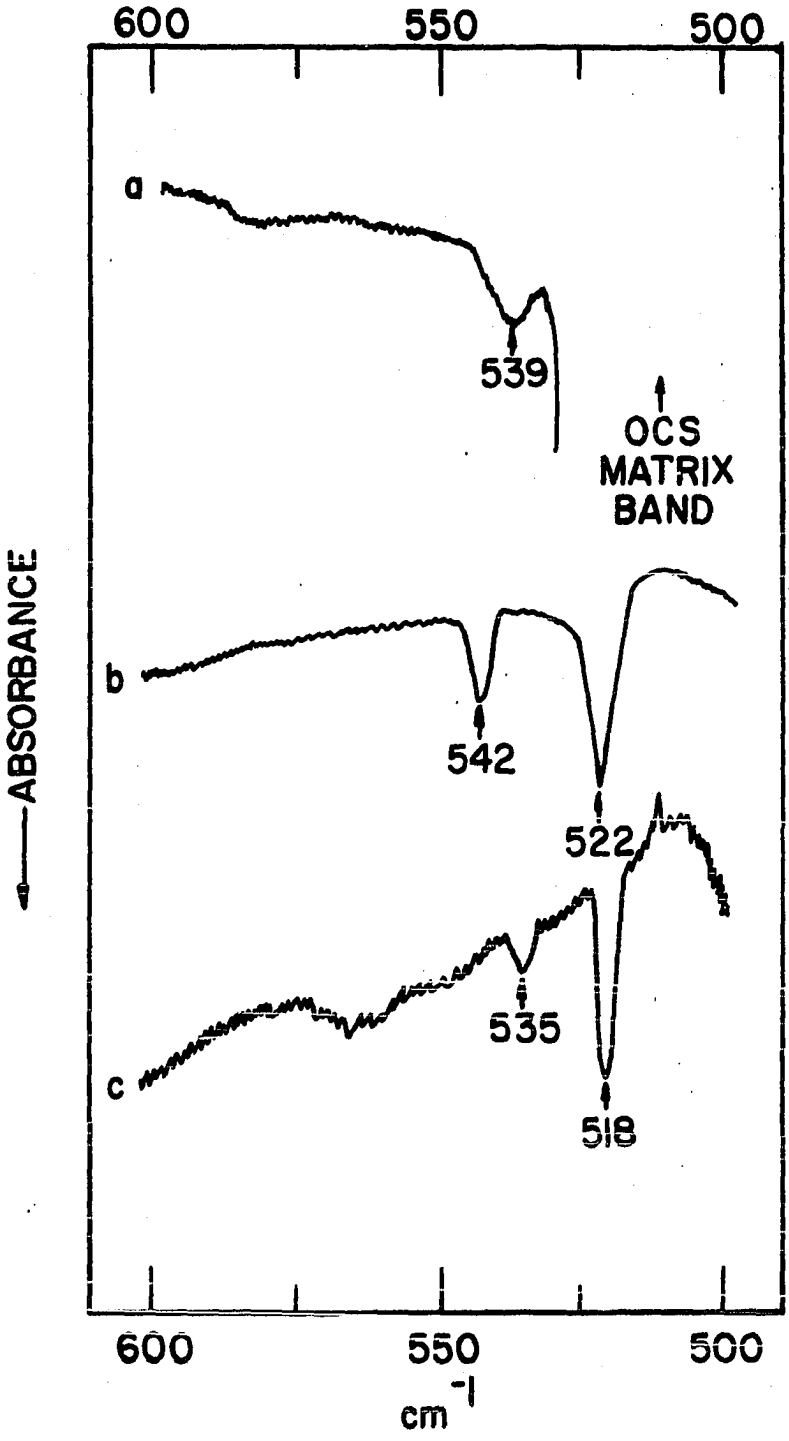

Figure 15. The infrared spectrum of FeS isolated in an OCS (trace a), in an Ar (trace b), and in a Kr (trace c) matrix

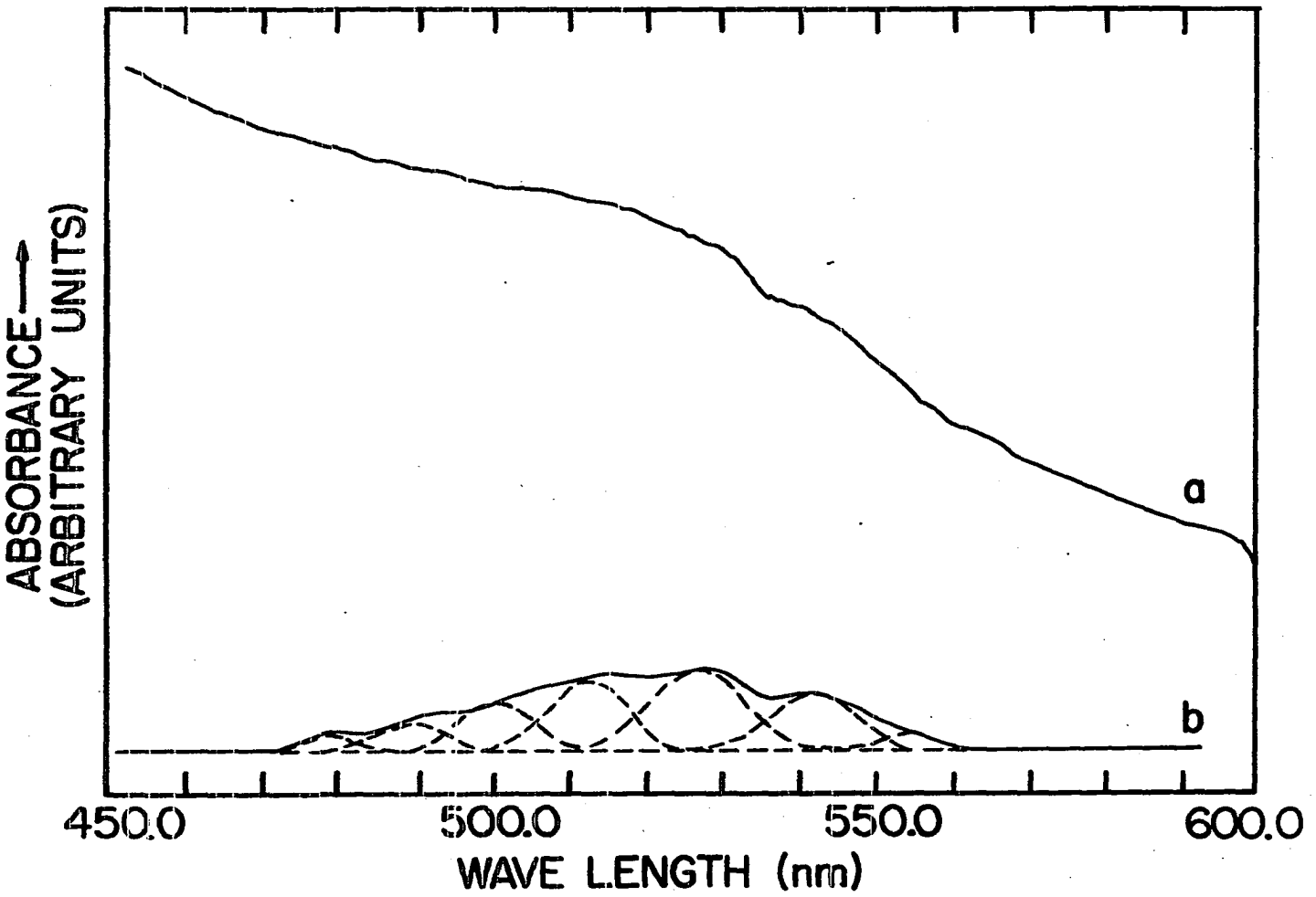

Figure 16. The visible absorption spectrum of FeS isolated in an Ar matrix. Trace b is a gaussian resolution of the observed spectrum shown in trace a

Table 12. Assignments for the A ← X transition of FeS in Ar matrices assuming the longest wavelength band is the 0-0 band

ν'	λ(nm)	$\bar{\nu}$(cm^{-1})	$\Delta G'_{1/2}$ (cm^{-1})
0	555.8	17992	485
1	541.2	18477	506
2	526.8	18983	505
3	513.4	19478	498
4	500.6	19976	501
5	488.4	20475	498
6	476.8	20973	
			Ave. 497

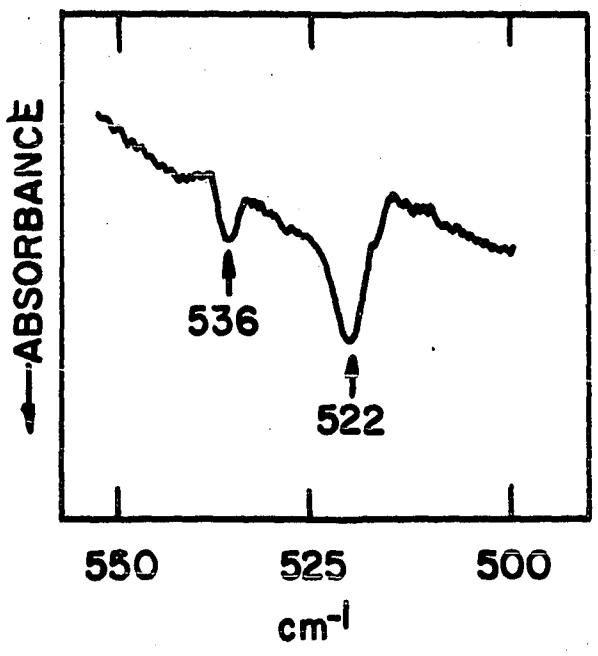

Figure 17. The infrared absorption spectrum of NiS isolated in an Ar matrix

7. S_x

Infrared bands were observed at 680 cm^{-1}, 668 cm^{-1}, 646 cm^{-1}, 588 cm^{-1}, 480 cm^{-1} and 440 cm^{-1} in the spectra obtained by vaporizing several different transition metal sulfides. From the work of Meyer and coworkers,[58,59] the bands at 668 cm^{-1} and 480 cm^{-1} can be assigned as S_4 and the band at 588 cm^{-1} can be assigned as S_3. However, the origin of the remaining bands is not known.

The electronic spectra at S_3 and S_4 were also observed and are shown in Figure 18. The band centered $\sim$ 400 nm is S_3 and the band centered at 530 nm is S_4. The band centered about 620 nm was not definitely assigned previously. However, it most likely is also due to S_4, although Meyer[58] has suggested that it may also arise from S_6.

8. Force constants

Table 13 summarizes the observed matrix frequencies for each monosulfide. In addition, Table 13 contains an estimate of the gas phase harmonic frequencies and the gas phase harmonic force constants. The harmonic frequencies were estimated by assuming the argon matrix frequencies were red shifted by $\sim$ 3 cm^{-1} and using the modified Birge-Sponer[60] relationship.

$$4\omega_e\chi_e \approx 4\omega_o\chi_o = \omega_o^2/D_o \qquad (1)$$

to estimate $\omega_e\chi_e$.

Obviously too little experimental information is available to rigorously calculate the force constants for VS_2. However, if the apex angle is estimated, approximate force constants can be calculated by using

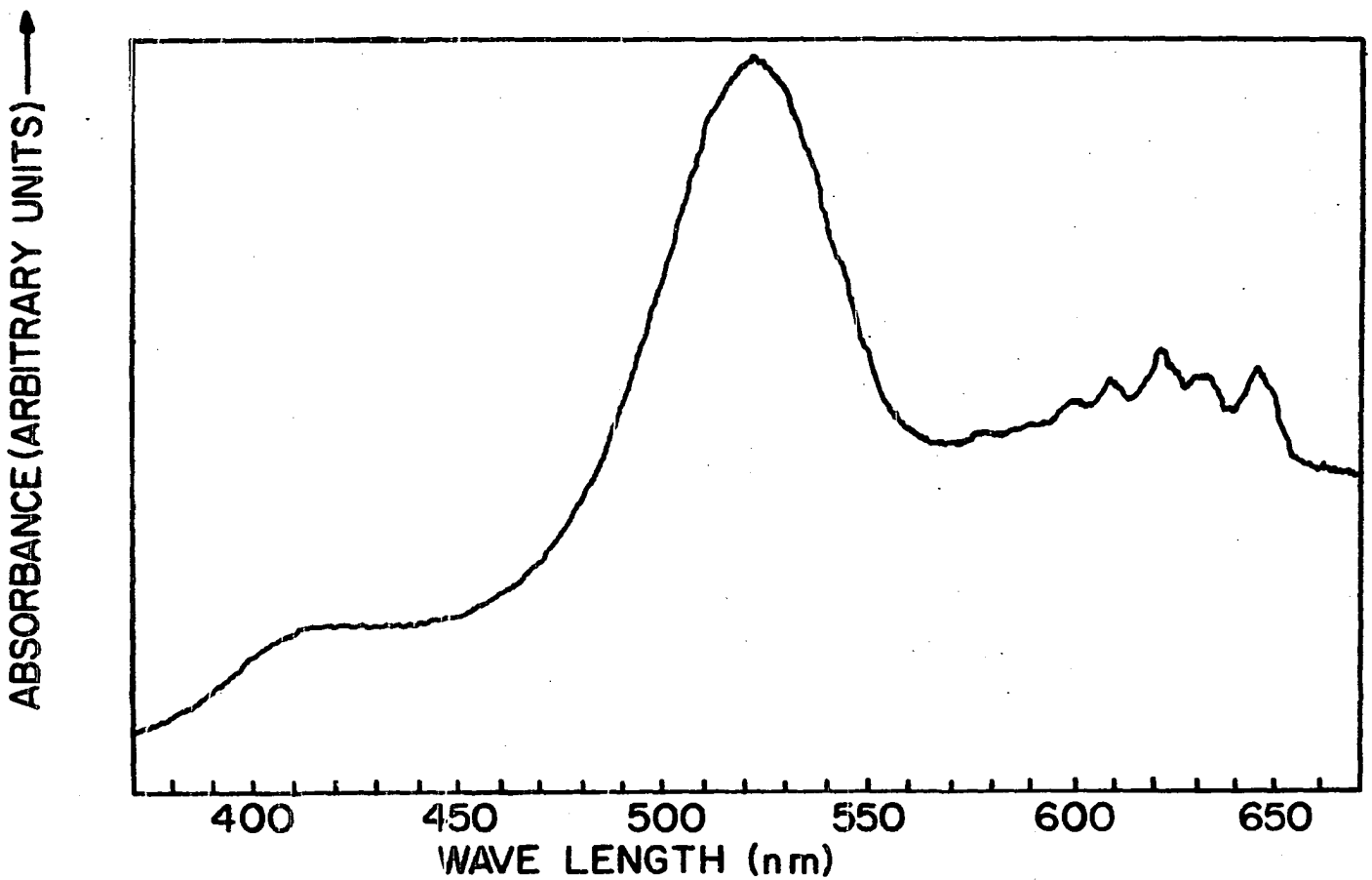

Figure 18. The electronic spectrum of S_3 and S_4 in an argon matrix (from NiS/Ar)

Table 13. Frequencies and force constants for the first period transition force constants

Molecule	OCS Matrix	Ar Matrix	Gas	
	$\omega_o(cm^{-1})$	$\omega_o(cm^{-1})$	$\omega_e(cm^{-1})$	K(millidynes/Å)
ScS	____	554[a]	526.07[b]	3.48
TiS	552	556	562.18[b]	3.57
VS	576	584	591[c]	4.04
CrS	560	558	566[c]	3.74
MnS	____	508	516[c]	3.17
FeS	539	542	550[c]	3.63
NiS	____	536	544[c]	3.59
CuS	____	____	414.2[a]	2.40

[a]Reference 21.

[b]Reference 44.

[c]Estimated value (see text).

the uncoupled oscillator approximation[61] for the three term valence potential

$$2V = k_1(\Delta r_1^2 + \Delta r_2^2) + 2k_{12}\Delta r_1 \Delta r_2 + k_2 \Delta\theta^2 \tag{2}$$

where Δr_1, Δr_2 and $\Delta\theta$ are displacements from the equilibrium displacement of the two bonds and the apex angle respectively, and k_1, k_2, and k_{12} are valence force constants. In this approximation, the equations relating the harmonic frequencies to the force constants for a nonlinear XY_2 molecule[62]

$$\lambda_1 + \lambda_2 = 4\pi^2 c^2(\omega_1^2 + \omega_2^2) = \left[\frac{1}{m_y} + \frac{2}{m_x}\cos^2\alpha\right] K_{11} + 2\left[\frac{1}{m_y} + \frac{2}{m_x}\sin^2\alpha\right] K_{22}, \tag{3}$$

$$\lambda_1\lambda_2 = 16\pi^4 c^4 \omega_1^2 \omega_2^2 = 2\left[\frac{1}{m_y} + \frac{2}{m_x m_y}\right] K_{11}K_{22}, \tag{4}$$

$$\lambda_3 = 4\pi^2 c^2 \omega_3^2 = \left[\frac{1}{m_y} + \frac{2}{m_x}\sin^2\alpha\right] K_{33}, \tag{5}$$

where m_x = mass of atom X, m_y = mass of atom Y, the symmetry force constants $K_{11} = k_1 + k_{12}$, $K_{22} = k_2/r^2$, $K_{33} = k_1 - k_{12}$, 2α is the apex angle, and r is the equilibrium bond distance are simplified to

$$\lambda_1 = \left[\frac{1}{m_y} + \frac{2}{m_x}\cos^2\alpha\right] K_{11}, \tag{6}$$

$$\lambda_2 = \left[\frac{1}{m_y} + \frac{2}{m_x}\sin^2\alpha\right] K_{22}, \tag{7}$$

$$\lambda_3 = 2[\frac{1}{m_y} + \frac{2}{m_x} \sin^2 \alpha] K_{33}. \quad (8)$$

Owzarski[50] has calculated the apex angle of VS_2 using extended Hückel theory. His calculated apex angle of 108.8° is quite close to the apex angle of 110° observed for TiO_2[51] and is therefore taken as a reasonable estimate to be used in the calculation of K_{11} and K_{33} using the uncoupled oscillator approximation. The values obtained for K_{11} and K_{33} were 5.12 millidynes/Å and 2.89 millidynes/Å, respectively. In his calculation, Owzarski also calculated the bending frequency of VS_2. This value for ν_2 was used to calculate the force constants given in Table 14. The close agreement of the calculated value of K_{11} using Owzarski's value of ν_2 and the value of K_{11} obtained here using the uncoupled oscillator approximation indicate that this value of ν_2 is close to the true value, since the uncoupled oscillator approximation is expected to work rather well for molecules like VS_2.[61]

9. Oxide-sulfide correlation

Barrow and Cousins[44] were the first to observe that special relationships seem to exist between the dissociation energies (D) and the force constants (K) of the oxides and sulfides with nontransition metal cations. However, they found a number of exceptions to their general rules which tended to make them rather unreliable for estimating unknown molecular parameters. A more reliable correlation was developed by Hauge and Margrave.[45] They found the ratio $D_{mo}K_{ms}/D_{ms}K_{mo}$ to be approximately constant for the elements of one group in the periodic table. Nearly simultaneously,

Table 14. Force constants of VS_2 using a 3 term potential

$\omega_1 = 622\ cm^{-1}$	$\omega_2 = 117^a\ cm^{-1}$	$\omega_3 = 530\ cm^{-1}$
$2\alpha = 108.8^a$		
K_{11} (millidynes/Å)	K_{22} (millidynes/Å)	K_{33} (millidynes/Å)
5.09	0.08	2.89

[a]Calculated value (reference 50).

Yanishevskii[46] developed a similar more general relationship to be used to estimate the molecular properties of any diatomic molecule from any other diatomic molecule. It is

$$\frac{K' D}{K D'} = \frac{\chi' r}{\chi r'} \tag{9}$$

where χ is the electronegativity of the cation and r is the bond length. Ideally the ratio of the electronegativities would equal one for oxides and sulfides having the same cation. However, Hauge and Margrave computed some values for the ratio

$$\frac{D_{mo} K_{ms} r_{ms}}{D_{ms} K_{mo} r_{mo}}$$

and found this ratio could differ from the ideal value of unity by as much as 18% if one of the molecules was significantly more ionic than the other (e.g., O_2 and SO). Hence, the Yanishevskii equation would probably be improved by replacing the electronegativity of the cation with a quantity which reflects the tendency toward ionic bonding in the diatomic molecule. Recently Chang[47] has presented a new set of empirical equations which can be universally used to estimate either a dissociation energy or a force constant from known properties of the diatomic molecules. From these equations one predicts

$$\frac{D_{mo} K_{ms}}{D_{ms} K_{mo}} \approx \left(\frac{D_{O_2}}{D_{S_2}}\right)^{1/2} \left(\frac{K_{S_2}}{K_{O_2}}\right)^{1/2} \approx 0.70 \tag{10}$$

for all cations.

The data needed to determine this ratio are collected in Tables 15 and 16. Table 17 contains the calculated ratios for the transition metal cations. The computed values of the ratio are all within ten percent of the average value of 0.769, suggesting that, within experimental error, this ratio is approximately constant for all transition metals. However, the average value is nearly 10% greater than the universal value predicted by Chang.

10. Trends in the oxide and sulfide

As shown in Figure 19, plots of the dissociation energies and the force constants of the oxides and the sulfides as functions of atomic number are qualitatively similar. This qualitative trend can be explained by the remarkably useful schematic molecular orbital (MO) diagram which was derived from the observed ground states[19] of the oxides of Ca-Cr, shown in Figure 20. Consider the trends in the ground state force constants and bond energies.

Since only sufficient electrons are available to fill the predominately nonmetal molecular orbitals, both chalcogenides of calcium are expected, as has been observed,[19,44] to have $^1\Sigma^+$ ground states. Both experiment[44] and nonempirical calculations[4] indicate a $^2\Sigma^+$ ground state for ScO and experiment[21] indicates a $^2\Sigma^+$ ground state for ScS. Hence, the first electron to fill a predominantly metal orbital in a metal monochalcogenide gaseous molecule has sigma symmetry. The observed increase in molecular properties suggests that this orbital is slightly bonding. The ground states of TiO and VO are known to be $^3\Delta$ and $^4\Sigma^-$ corresponding to a $\sigma\delta$ and

Table 15. Dissociation energies, vibrational frequencies and force constants for the transition metal oxides[a]

Molecule	ω_e (cm^{-1})	D_o^o (Kcal/mole)	K_e (millidynes/Å)
CaO	732.1	93 ± 5	3.61
SrO	653.5	102 ± 5	3.41
BaO	669.8	130 ± 5	3.79
ScO	971.6	161.0	6.56
YO	852.5	168.5	5.81
LaO	811.6	192.5	5.57
TiO	1008.3	167.4 ± 2.3	7.18
VO	1011.6	147.5 ± 4.5	7.34
CrO	898.8	101.1 ± 7	5.82
MnO	839.5	85.4 ± 4	5.14
FeO	880.8	90.3 ± 5	5.68
NiO	(826)	86.5 ± 5	5.04
CuO	628	62.7 ± 3	2.96

[a]Data from references given in reference 19.

Table 16. Dissociation energies, vibrational frequencies, and force constants for the transition metal sulfides

Molecule	ω_e (cm^{-1})	D_o^o (Kcal/mole)	K_e (millidynes/Å)
CaS	462.23[a]	79.9 ± 4.5[a]	2.24
SrS	388.38[a]	80.2 ± 4.5[a]	2.09
BaS	370.42[a]	100.6 ± 4.5[a]	2.10
ScS	562.07[a]	113.4 ± 2.5[a]	3.48
YS	490[b]	125.7 ± 2.5[a]	3.33
LaS	456.93[a]	137.5 ± 2.5[a]	3.20
TiS	562.18[a]	100.8 ± 1.8[c]	3.57
VS	591[d]	116.4 ± 4[e]	4.04
CrS	566[d]	77.6 ± 3.5[a]	3.74
MnS	516[d]	65.7 ± 2.5[a]	3.17
FeS	550[d]	76.3 ± 3.0[a]	3.63
NiS	544[d]	80.5 ± 3.5[a]	3.59
CuS	414.2[a]	66.9 ± 3.5[a]	2.40

[a]Reference 44.

[b]Reference 21.

[c]Reference 63.

[d]This work.

[e]Reference 49.

Table 17. Computed value of the ratio of the dissociation energies, force constants, and $D_{mo}K_{ms}K_{mo}$

Cation	D_{mo}/D_{ms}	K_{mo}/K_{ms}	$D_{mo}K_{ms}/D_{ms}K_{mo}$
Ca	1.16	1.61	0.720
Sr	1.27	1.63	0.799
Ba	1.30	1.80	0.722
Sc	1.42	1.88	0.753
Y	1.34	1.74	0.770
La	1.40	1.74	0.804
Ti	1.66	2.01	0.825
VS	1.27	1.86	0.700
CrS	1.30	1.56	0.837
MnS	1.30	1.62	0.801
FeS	1.18	1.56	0.757
NiS	1.07	1.40	0.766
CuS	0.937	1.23	0.759
		Ave.	0.769 ± 0.041

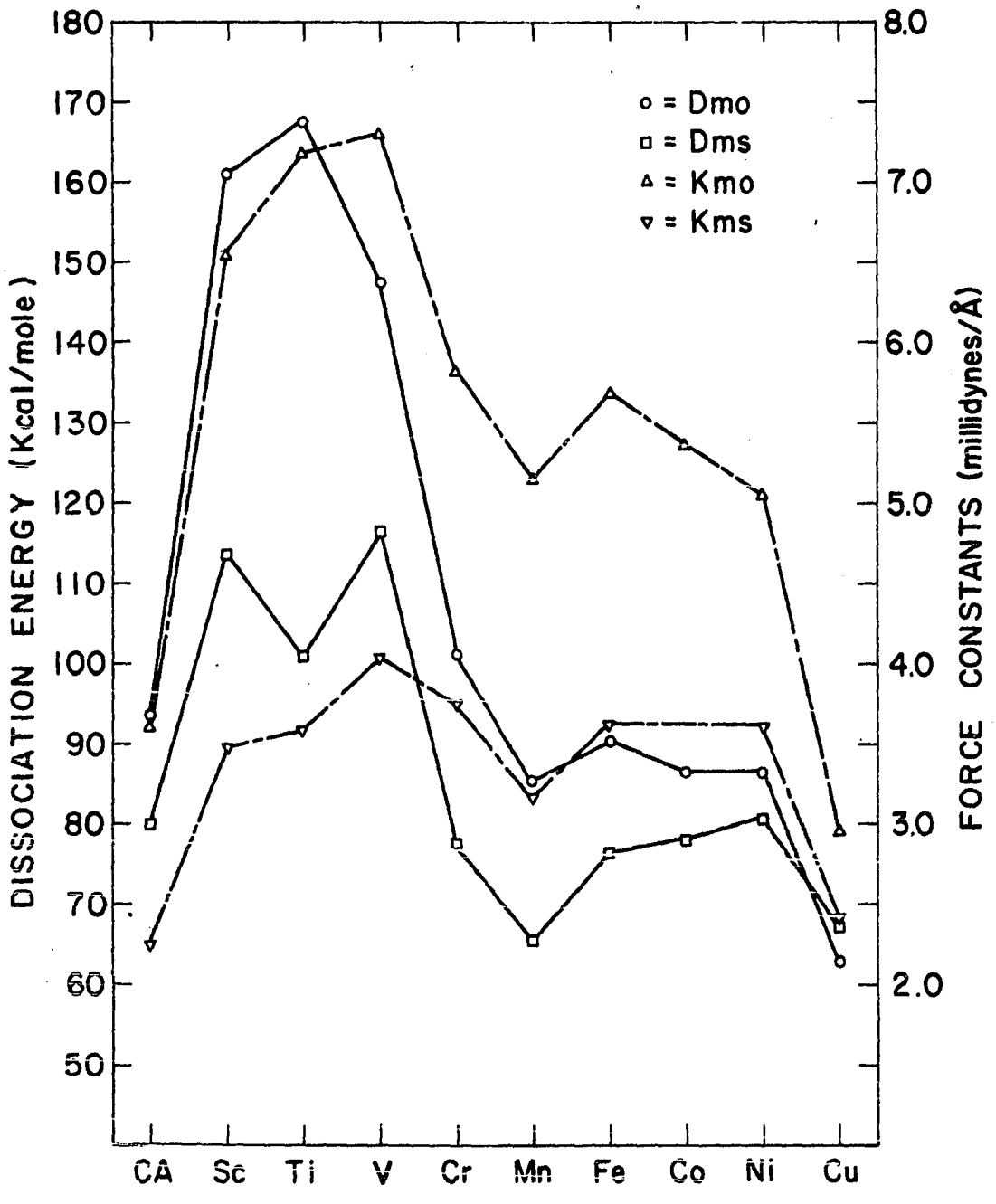

Figure 19. Plots of the dissociation energies and force constants versus atomic number for the first period transition metal chalcogenides

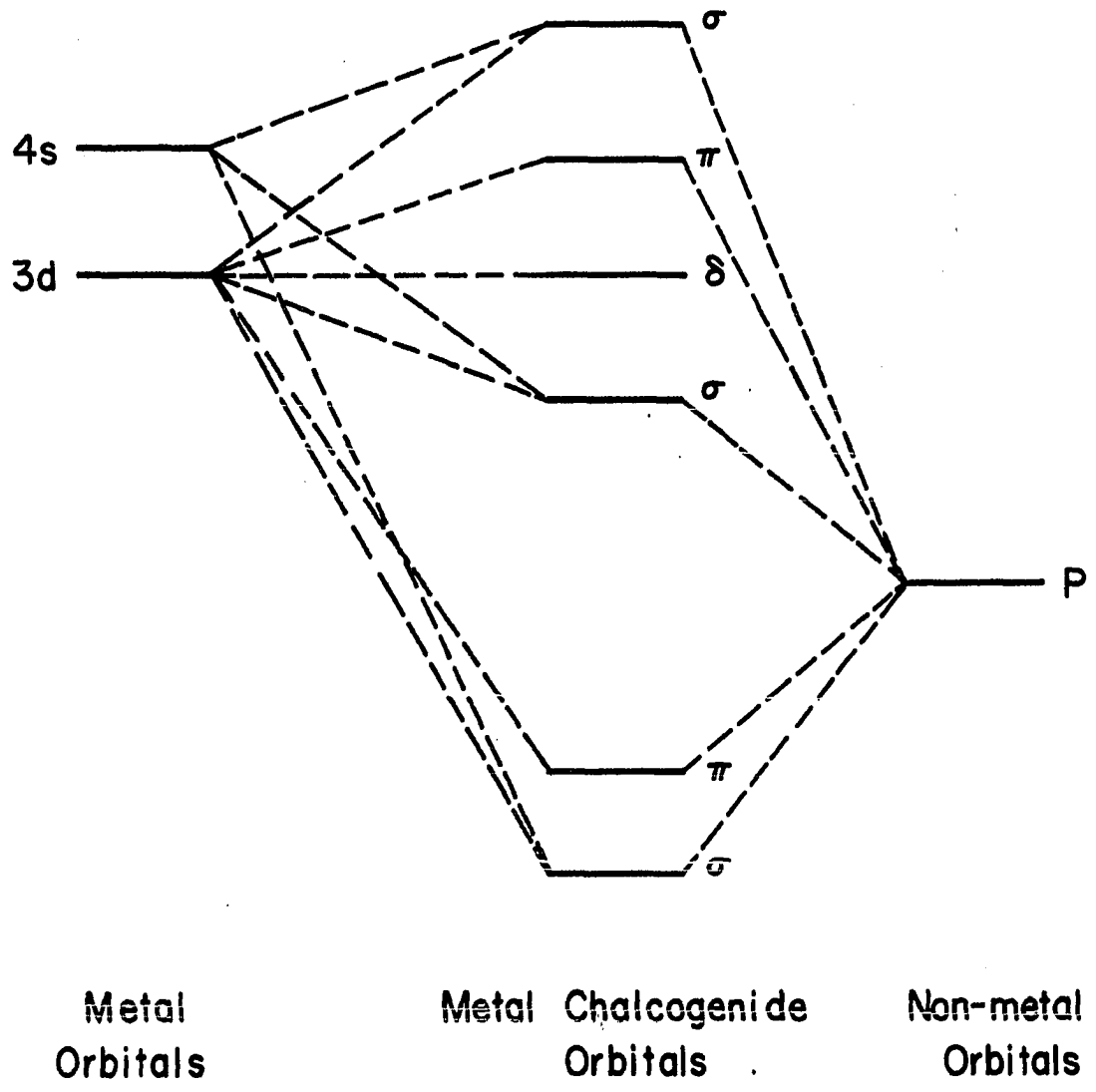

Figure 20. A schematic MO diagram for the first period transition metal chalcogenides

a $\sigma\delta^2$ configuration[5,6,44] respectively. Since the δ orbital is expected to be nonbonding, the molecular properties of these oxides whould be quite similar to those observed for ScO. This is observed, although small variations due to quantitative differences in the orbitals do occur. TiS is known to have a $(\sigma\delta)\ ^3\Delta$ ground state.[23] From the similarity in the oxide and sulfide trends, VS is inferred to have a $(\sigma\delta^2)\ ^4\Sigma^-$ ground state.

Ninomiya[64] has concluded from rotational analysis that CrO has a $(\sigma\delta^2\pi)^5\pi$ configuration. Since the molecular constants decrease at Cr, this π orbital must be antibonding. Again the observed trend for the sulfides suggests CrS also has a $^5\pi$ ground state. The ground state of MnO is unknown. However, since the molecular properties continue to decrease, it appears likely that the chalcogenides of manganese have $\sigma\delta^2\pi^2$ configurations. Although this configuration produces several states, the state of highest multiplicity, the $^6\Sigma^+$ state, is most likely the ground state. Barrow and Senior[65] have concluded the ground state of FeO is most likely $^7\Sigma$ or $^5\Sigma$. The increase in the molecular properties at Fe suggests the next electron is added to the sigma bonding orbital producing a $\sigma^2\delta^2\pi^2$ configuration. Three sigma states, $^5\Sigma^+$, $^3\Sigma^-$ and a $^1\Sigma^+$ state correspond to this configuration, with the $^5\Sigma^+$ apparently the ground state. A recent spectroscopic study by West and Broida[66] has established that the ground state of FeO is in fact $^5\Sigma^+$. According to this scheme, each of the next two electrons would be added to the nonbonding δ orbitals most likely producing a $(\sigma^2\delta^3\pi^2)^4\Delta$ and a $(\sigma^2\delta^4\pi^2)^3\Sigma^-$ state for the chalcogenides of Co and Ni, respectively. Although the actual ground states are unknown, the small fluctuation observed in the trends supports this model. For the

chalcogenides of copper a $(\sigma^2\delta^4\pi^3)^2\pi$ state is predicted. Since the electron would be added to an antibonding orbital a decrease in the molecular properties would be expected, and is observed. The observed ground state of $^2\pi$ for both CuO[19] and CuS,[24] further supports this prediction.

The suggested MO diagram also explains the observed electronic transitions for the oxides in the near infrared-visible region. Since the 0-0 bands of the sulfide were generally found at similar wavelengths to known oxide transitions, the MO diagram has been used to assign the states involved for the observed sulfide transitions. The assignments of the states made using this model are compared to the known states for the isoelectronic oxide transitions in Table 18.

C. Conclusions

Reasonable estimates of the molecular properties of the transition metal sulfides can be obtained from empirical correlations such as the Hauge-Margrave equations, providing sufficient data are known. The observed trends in the dissociation energies and the force constants of the transition metal oxides and sulfides suggests the bonding in these systems is quantitatively similar. A qualitative MO diagram has been presented which explains the observed trends in these systems. From this MO diagram, the ground states of the transition metal sulfides have been predicted and the states involved in the observed electronic transitions of the sulfides have been assigned.

Table 18. Comparison of the 0-0 bands and the states involved in the observed electronic transitions of the transition metal oxides and sulfides

Vanadium

Oxide[a]		Sulfide	
Band System	λ (nm)	Band System	λ (nm)
$A(^4\Sigma^-) - X(^4\Sigma^-)$	573.9	$B(^4\Sigma^-) - X(^4\Sigma^-)$	∿ 600
$C(^4\pi) - X(^4\pi)$	797.3	$A(^4\pi) - X(^4\Sigma^-)$	913.8

Chromium

Oxide[b]		Sulfide	
Band System	λ (nm)	Band System	λ (nm)
$B(^5\pi) - X(^5\pi)$	605.1	$B(^5\pi) - X(^5\pi)$	553.4
		$A(^5\Sigma^+) - X(^5\pi)$	747.6

Iron

Oxide[c]		Sulfide	
Band System	λ (nm)	Band System	λ (nm)
$A(^5\Sigma^+) - X(^5\Sigma^+)$	558.3	$A(^5\Sigma^+) - X(^5\Sigma^+)$	555.8

[a]Reference 67.
[b]Reference 64.
[c]Reference 66.

V. THE VANADIUM CARBONYL SYSTEM

A. Introduction

The spectra of metal carbonyls have been widely studied because of the qualitative insight they provice into metal-carbon bonding. Several new binary carbonyls with from one to six CO molecules per metal atom have been synthesized using the technique of matrix isolation including $Ni(CO)_{1-4}$ and $Ta(CO)_{1-6}$,[14] $Pd(CO)_{1-4}$,[68] $Pt(CO)_{1-4}$,[69] $Cu(CO)_x$,[70] $U(CO)_{1-6}$[71] $Nd(CO)_{1-6}$ and $Yb(CO)_x$,[72] and $Pr(CO)_{1-6}$, $Eu(CO)_{1-6}$, $Gd(CO)_{1-6}$ and $Ho(CO)_{1-6}$.[73]

$V(CO)_6$ has been investigated by a large number of techniques, including infrared and ultraviolet spectroscopy,[74] photoelectron spectroscopy,[75] electron spin resonance spectroscopy,[76] and magnetic measurements.[77,78] At room temperature $V(CO)_6$ has one unpaired electron and virtual octahedral geometry producing a $^2T_{2g}$ ground state. However, the Jahn-Teller theorem[26] predicts that this structure should undergo some distortion along either the E_g or the T_{2g} vibrational normal mode to remove the orbital degeneracy. In fact, there is strong experimental evidence of a dynamic Jahn-Teller distortion at room temperature.[74] At $\sim$ 66°K both ESR[13] and magnetic measurements[77,78] indicate this dynamic distortion is replaced by a static distortion to D_{4h} symmetry, producing a $^2B_{2g}$ ground state. In addition, magnetic measurements[77] have indicated $V_2(CO)_{12}$ may form in solid $V(CO)_6$ at low temperatures. However, neither $V_2(CO)_{12}$ nor D_{4h} $V(CO)_6$ has been previously observed spectroscopically. Among other features, the technique of matrix isolation provides a convenient method for studying the spectrum of isolated

molecules at low temperatures. Consequently, this technique was chosen to investigate the low temperature structure of $V(CO)_6$.

B. Results and Discussion

The infrared spectra obtained from one annealing experiment of vanadium atoms in a 1 mole % CO/Ar matrix are shown in Figure 21. In addition to the bands shown in the figure, all spectra contained intense sharp bands at 2138 cm^{-1} and 2092 cm^{-1}, due to ^{12}CO and ^{13}CO respectively, which are not shown. While this experiment was above average in the amount of information contained, it was typical of the spectra obtained using low CO concentrations. In general, the bands were rather weak and quickly disappeared upon warming the matrix, producing a few relatively stable species which tended to resist further annealing.

Prior to annealing, the band at 1874 cm^{-1} clearly dominated the spectrum as shown in spectrum 21a. Upon annealing (spectrum 21b), new bands appeared in the spectrum at 1896 cm^{-1}, 1910 cm^{-1}, and 1948 cm^{-1}. Further annealing (spectrum 21c) caused the bands at 1874 cm^{-1} and 1896 cm^{-1} to decrease in intensity and generated new bands at 1948 cm^{-1}, 1955 cm^{-1}, 1963 cm^{-1}, 1975 cm^{-1}, 1981 cm^{-1} and 2030 cm^{-1}. The bands at 1896 cm^{-1}, 1922 cm^{-1} and 1948 cm^{-1} diminished to unobservable intensity with further annealing (spectra 21d and 21e). In addition, the bands at 1975 cm^{-1} and 1981 cm^{-1} increased in intensity and new bands were observed at 2014 cm^{-1} and 2021 cm^{-1}. Increasing the CO concentration to 5% produced the infrared spectra shown in Figure 22. All the bands observed in the 1% CO/Ar experiments plus new bands at 1866 cm^{-1} and 2045 cm^{-1} were initially present in

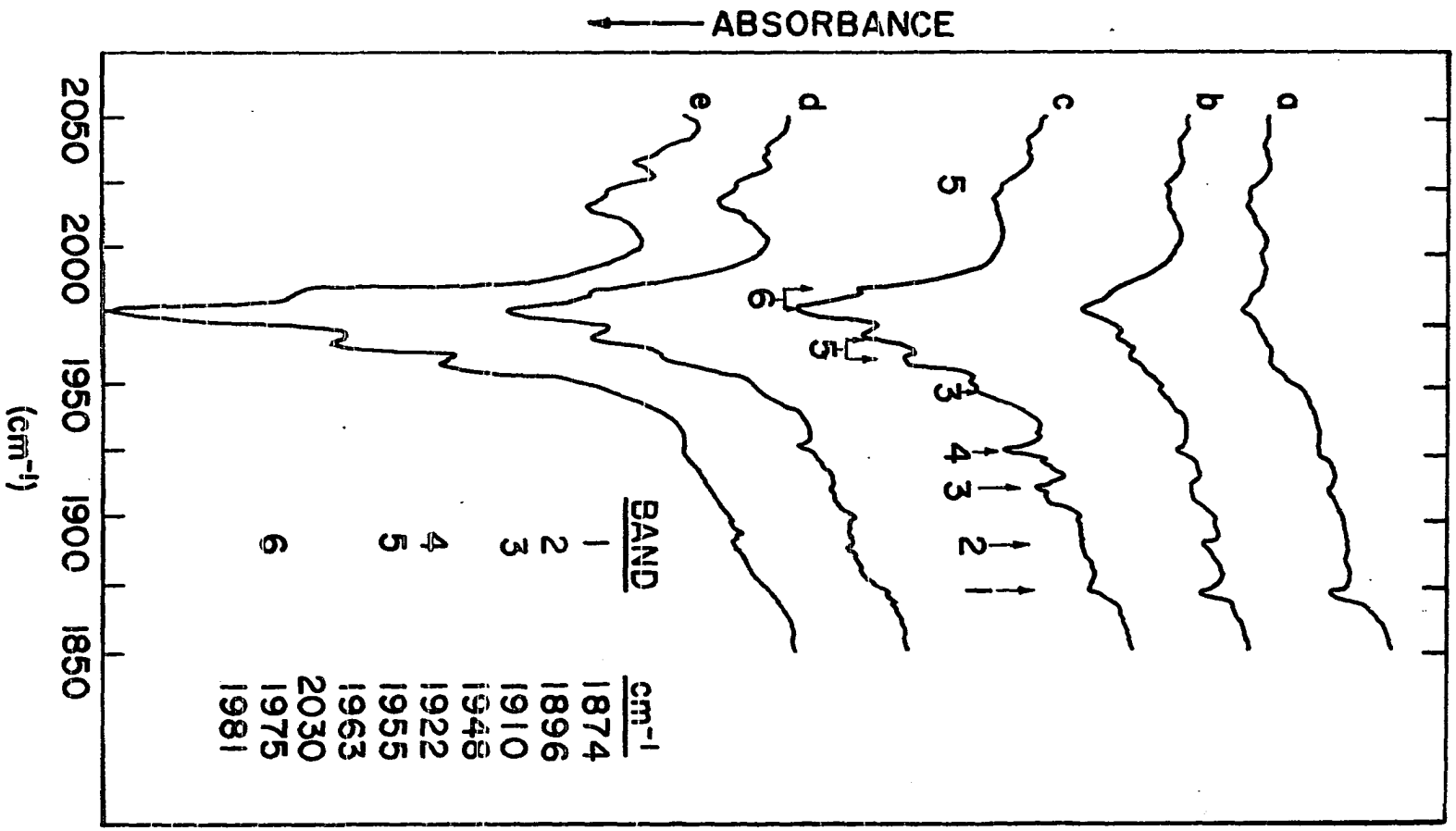

Figure 21. The infrared spectra of the vanadium carbonyl complexes in 1% CO/Ar. Trace a is prior to annealing. Traces b-e are after warming the matrix to 30°K for several minutes

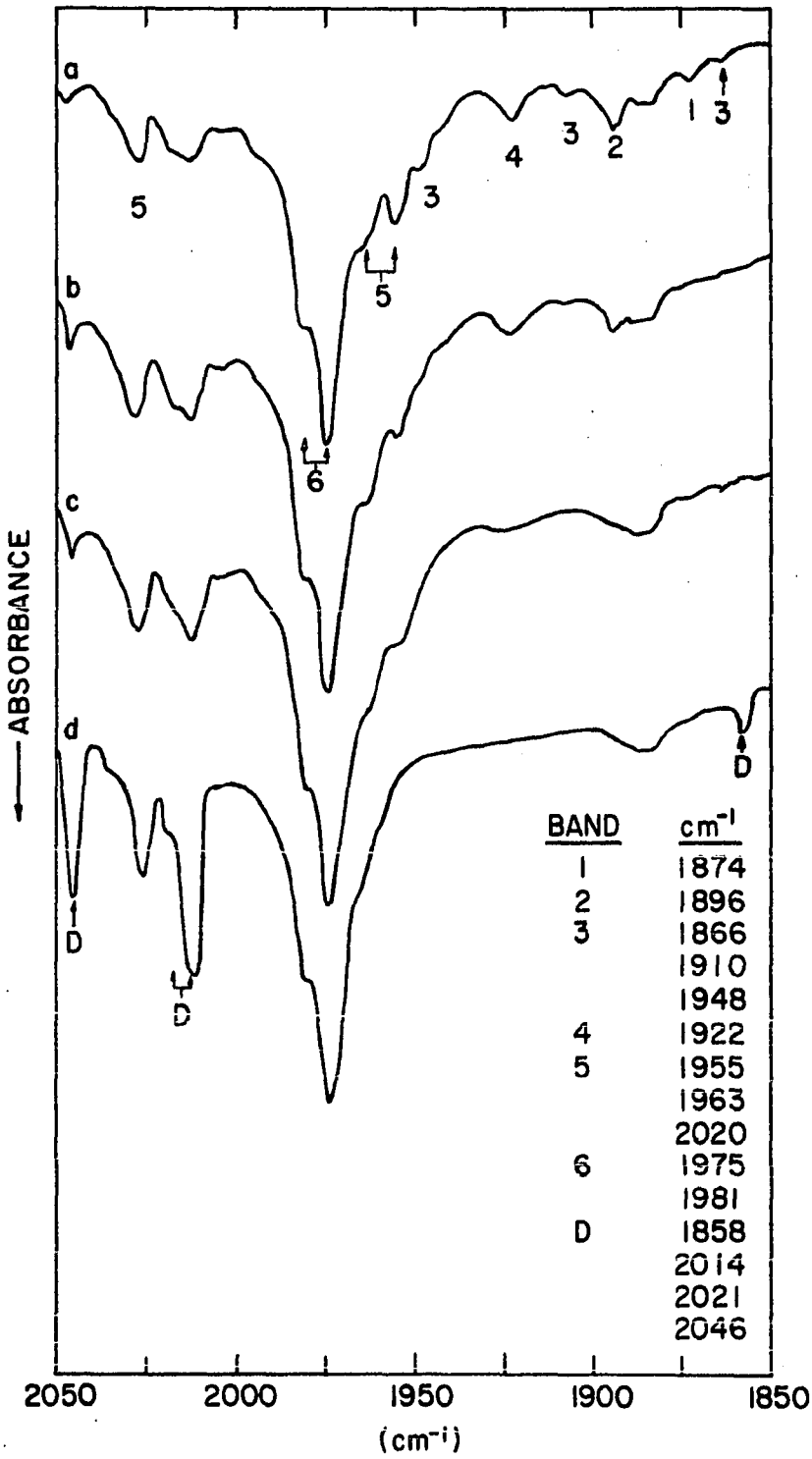

Figure 22. The infrared spectra of the vanadium carbonyl complexes in 5% CO/Ar. Trace a is prior to annealing. Traces b-d are after warming the matrix to 30°K for several minutes

the spectrum (spectrum 22a). The bands at 1866 cm^{-1}, 1874 cm^{-1}, 1910 cm^{-1} and 1948 cm^{-1} quickly lost intensity upon annealing (spectrum 22b). With further annealing the band at 1922 cm^{-1} lost intensity (spectrum 22c). Finally the bands at 1955 cm^{-1}, 1963 cm^{-1}, and 2030 cm^{-1} began to lose intensity, the bands at 1975 cm^{-1} and 1981 cm^{-1} remained fairly constant and the bands at 1858 cm^{-1}, 2014 cm^{-1}, 2021 cm^{-1}, and 2046 cm^{-1} showed a marked increase in intensity (spectrum 22d).

When CO was used as the matrix, the infrared spectra shown in Figure 23 were obtained. Prior to annealing, two very strong bands at 1972 cm^{-1} and 1980 cm^{-1} and a weak band at 2014 cm^{-1} were observed. Upon annealing and/or photolysis of the matrix caused by prolonged exposure to the hydrogen lamp used to obtain the ultraviolet spectrum, several new bands which are shown in spectrum 23b were observed.

Seven binary vanadium carbonyl complexes were synthesized during these experiments. Several other less successful experiments with CO concentrations of 8%, 6%, 3%, 2.5%, and 0.5% were done to aid in the assignment of frequencies to each species. If more than one band appeared to originate from one species, the ratio of the intensities of these bands were determined in a number of different experiments to further verify that they were related. The area under each band was used as a measure of the intensity. The areas were determined by tracing the spectrum on graph paper and counting the number of squares under each band. Unfortunately, low intensities and a number of highly overlapping features made it difficult to accurately determine the intensity of several of the vanadium carbonyl bands, which hindered the assignments of the spectra.

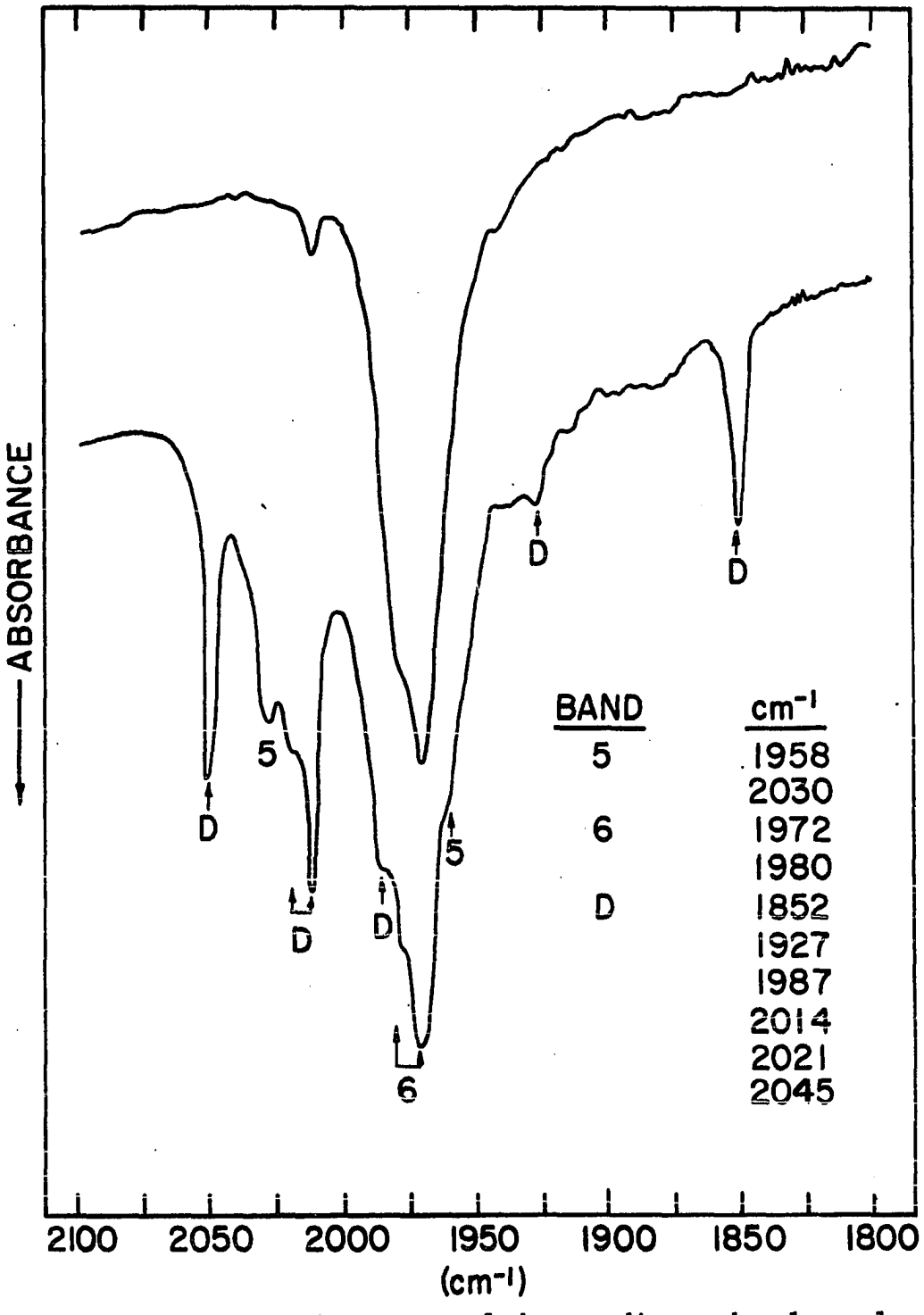

Figure 23. The infrared spectra of the vanadium carbonyl complexes observed in a CO matrix. Trace a is prior to annealing. Trace b is after annealing

While the bands may be assigned to a species on the basis of their observed intensity relationships as the matrix is annealed or as the concentration of the ligand in the matrix is changed, the species must either be identified from mixed isotope studies or from assumptions made about the expected behavior of the species trapped in the matrix. Since many of the bands were quite weak, there was little chance of the mixed isotope experiments succeeding. Consequently the assignments were based upon the following assumptions:

a. The metal atom can only react with ligands in adjacent sites. Consequently the species should be formed in a ratio which reflects the statistical probability for the number of nearest neighbor ligands, making some allowance for ligand mobility as the matrix is being formed.

b. Steric effects are minimal so that ligands may add in a step-wise fashion upon annealing.

c. The oscillator strengths of the ligand stretching modes are approximately equal for all complexes.

The assignments based on these assumptions and the infrared bands which have been assigned to each are given in Table 19. While these assignments are thought to be the best interpretation of the observed spectra, the IR frequencies assigned to $V(CO)_5$ do not agree with the IR frequencies previously reported for this complex[79] (one strong matrix split band at 1947 cm^{-1} and a medium intensity band at 1920 cm^{-1}). Bands within experimental error of both frequencies were observed. However, the relative intensities of these bands seemed to vary randomly which suggests their spectrum may have been misassigned. It is possible that differences in experimental procedure may have produced slightly different matrix environments which altered the observed spectrum. However, since neither the

Table 19. Tentative assignments and the observed vibrational frequencies for $V(CO)_{1-6}$ and V_2CO_{12}

Species	$\nu(cm^{-1})^a$	$\nu(cm^{-1})^b$
V(CO)	1874	———
$V(CO)_2$	1896	———
$V(CO)_3$	1866	———
	1910	———
	1948	———
$V(CO)_4$	1922	———
$V(CO)_5$	1955	1958
	1963	
	2030	2030
$V(CO)_6$	1975	1972
	1981	1980
$V_2(CO)_{12}$	1855	1852
	———	1927
	———	1987
	2015	2014
	2020	2021
	2045	2046

[a] In argon matrix.

[b] In CO matrix.

experimental details nor the observed spectrum have been published, the reason for the disparity could not be determined.

Since two infrared bands were observed for $V(CO)_6$ in both CO and Ar matrices, it is unlikely that the splitting is the result of matrix effects. Since two infrared bands are expected for a D_{4h} structure, this observation can be taken as proof that the low temperature structure of $V(CO)_6$ is D_{4h}.

The structure of the partially coordinated complexes can be determined by comparing the number of observed infrared bands to the number of infrared bands calculated for possible structures with the same stoichiometry. Since some bands may not have been observed because of low intensity and/or close proximity to other stronger bands, and since the matrix may distort the structure of the trapped species, the structures determined must be regarded as tentative. The structures predicted by Burdett[80] for low, intermediate and high spin d^5 ions with from one to six coordinated ligands and the number of infrared bands expected for each structure are given in Table 20. By comparing the number of infrared bands expected for each structure in Table 20 with the number of infrared bands observed for each complex tabulated in Table 19, the structure of each complex was determined. The observed structures are tabulated in Table 21.

The Jahn-Teller theorem predicts that the D_{3h} symmetry observed for $V(CO)_5$ should not be stable. The splitting of the E' made in the argon matrix may indicate the presence of a Jahn-Teller distortion. However, since this splitting was not observed in CO matrices, it is not known whether this splitting represents a true molecular distortion or a

Table 20. The structures and the number of infrared bands calculated for each structure for low, intermediate, and high spin d^5 ions with from 1 to 6 ligands per ion[a]

Species	Low Spin		Intermediate Spin		High Spin	
	Symmetry Point Group	Number of IR Active Bands	Symmetry Point Group	Number of IR Active Bands	Symmetry Point Group	Number of IR Active Bands
M(AB)	$C_{\infty v}$	1	$C_{\infty v}$	1	$C_{\infty v}$	1
$M(AB)_2$	C_{2v}	2	C_{2v}	2	$D_{\infty h}$	1
$M(AB)_3$	C_{3v}	2	C_{2v}	3	D_{3h}	1
$M(AB)_4$	C_{2v}	4	D_{4h}	1	T_d	1
$M(AB)_5$	D_{3h}[b]	2	D_{3h}[b]	2	D_{3h}	2
$M(AB)_6$	O_h[c]	1	O_h[c]	1	O_h	1

[a]Reference 80.

[b]Possible Jahn-Teller distortion to C_{2v} producing 4 IR bands.

[c]Possible Jahn-Teller distortion to D_{4h} producing 2 IR bands.

Table 21. Observed structures and point group symmetries for $V(CO)_{1-6}$

Species	Structure	Point group symmetries
V(CO)	linear	$C_{\infty v}$
$V(CO)_2$	linear	$D_{\infty h}$
$V(CO)_3$	Y-shaped	C_{2h}
$V(CO)_4$	square planar or tetrahedral	D_{4h} T_d
$V(CO)_5$	trigonal bipyramid	D_{3h}[a]
$V(CO)_6$	tetragonal bipyramid	D_{4h}

[a]May be slightly distorted to C_{2v}.

distortion resulting from matrix effects.

The structure of $V_2(CO)_{12}$ can also be partially deduced from the infrared spectrum. Since bridging CO groups usually show infrared frequencies in the range 1700 - 1850 cm^{-1},[81] the band at 1852 cm^{-1} in CO matrices indicates the presence of one or two bridging CO groups in the dimer. Since only six IR bands were observed, the molecule probably has an inversion center. Since a metal-metal band is needed to satisfy the 18 electron rule, $V_2(CO)_{12}$ is probably structurally similar to the double bridged structure shown in Figure 24.

Approximate force constants can be calculated by using the Cotton-Kraihanzel[82] approximation. The force constants for $V(CO)_{1-6}$ are given in Table 22.

The electronic spectrum of $V(CO)_6$ in a CO matrix is shown in Figure 25. Unfortunately, the massive overlap of the bands prevented a clear-cut resolution of the spectrum into its component bands. An attempt was made to resolve the spectrum by using the following method. The observed spectrum was carefully traced onto a piece of graph paper. The observed absorbance was corrected for baseline shift caused by matrix scatter by linearly extrapolating the observed baseline and subtracting the baseline absorbance from the total absorbance. The spectrum was then graphically resolved into approximately Gaussian shaped bands. Although several spectral resolutions are obviously possible, the resolution shown in Figure 25b, which represents a composite of the best features of several possible resolutions, is thought to best reproduce the observed spectrum.

An analysis of this spectrum was attempted by using a combination of

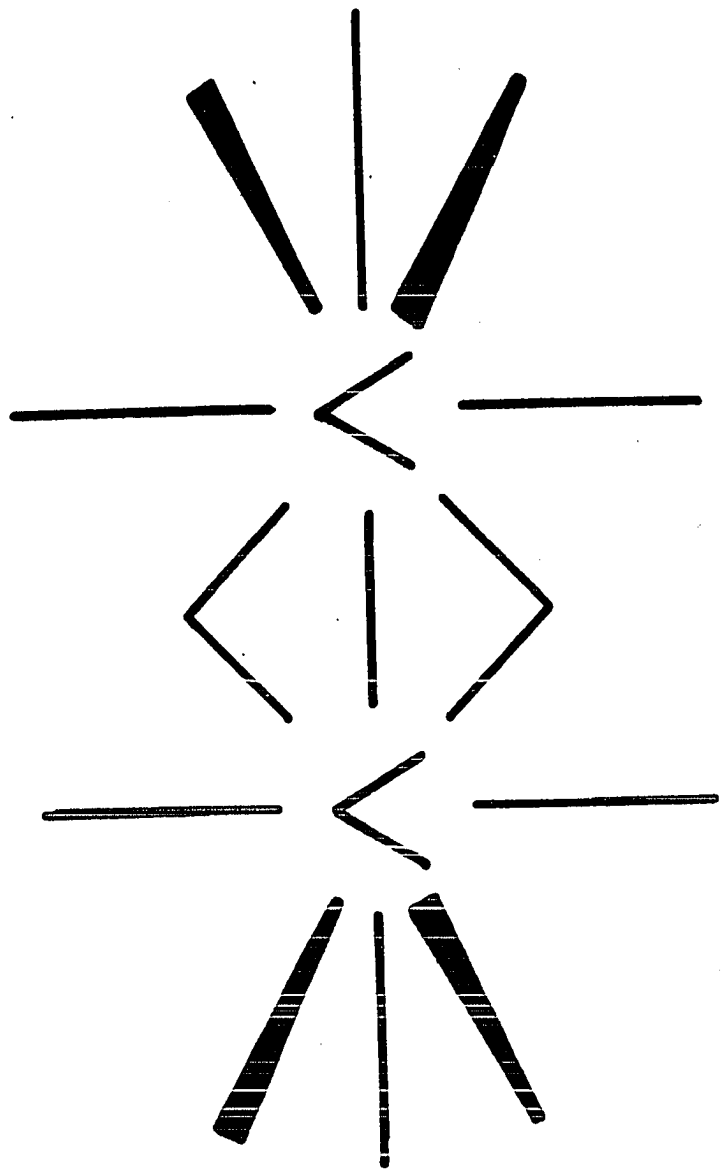

Figure 24. Tentative structure for $V_2(CO)_{12}$

Table 22. Cotton-Kraihanzel force constants for $V(CO)_{1-6}$

Species	$\nu(cm^{-1})$	Normal mode	Force constant (m dyn/Å)
V(CO)	1874	Σ^+	14.18[a]
$V(CO)_2$	1896	Σ_u^+	14.52[a]
$V(CO)_3$	1866	A_1	14.02[b]
	1910	B_2	14.73[a]
	1948	A_1	15.28[c]
$V(CO)_4$	1922	E_u or T_{2u}	14.92[a]
$V(CO)_5$	1958	E'	15.48[a]
	2030	A_2	16.64[b]
$V(CO)_6$	1975	E_u	15.75[a]
	1981	A_{2u}	15.85[b]

[a] $K - K_r$.

[b] $K' - K_s$.

[c] $K + K_r$.

Figure 25. The electronic spectrum of $V(CO)_6$ in a CO matrix. Trace a is the observed spectrum. Trace b is an approximate Gaussian resolution of the spectrum. Trace c is the calculated d-d spectrum for $V(CO)_6$

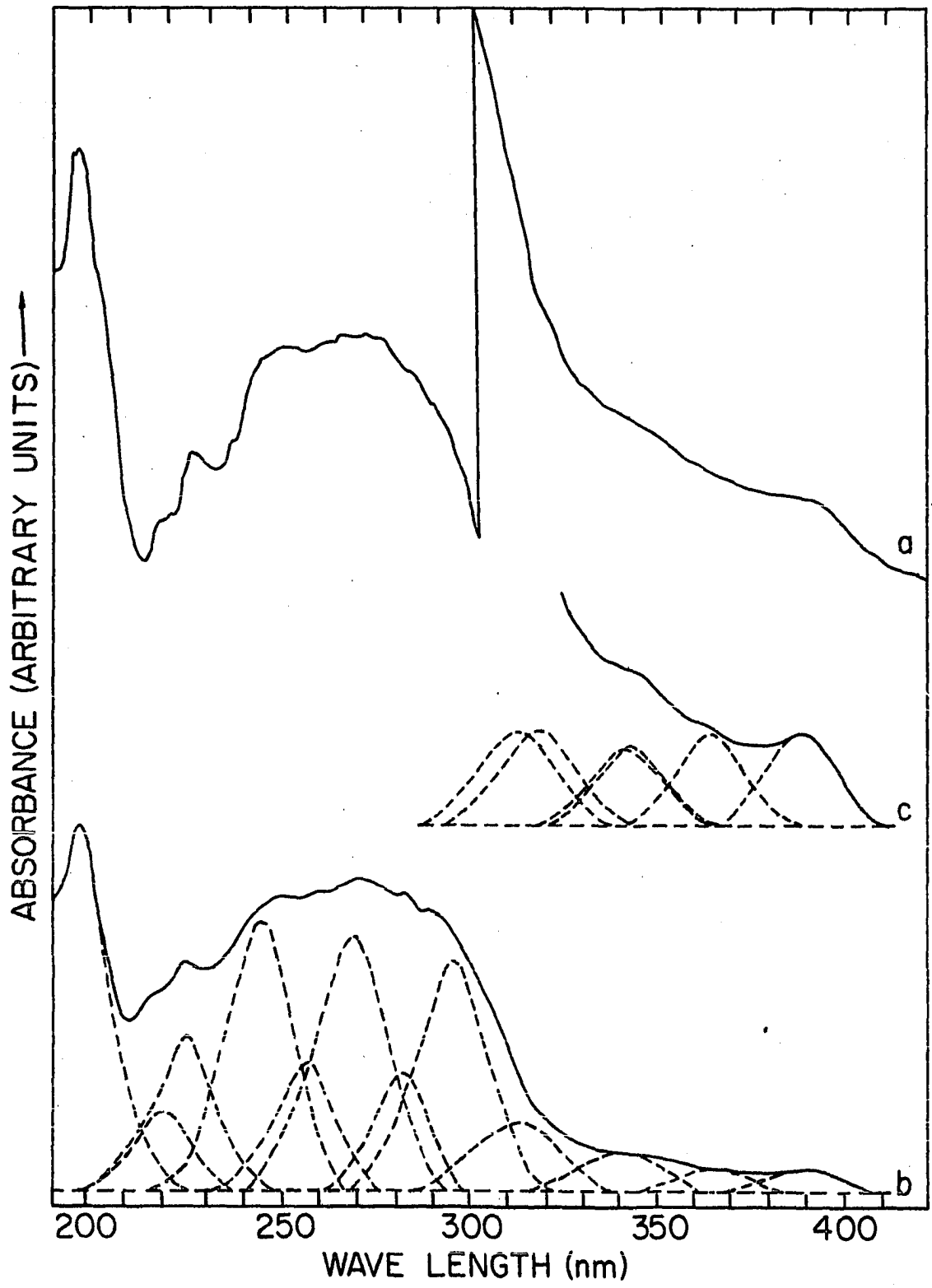
ABSORBANCE (ARBITRARY UNITS)
a
c
b
200
250
300
350
400
WAVE LENGTH (nm)

ligand field and molecular orbital theory. The lowest doublet energy states for d^5 ions in a strong tetragonally distorted octrahedral ligand field in terms of crystal field and Racah parameters[83] are given in Table 23. Ds and Dt are parameters which represent the distortion from O_h symmetry. A value greater than zero for Dt, a parameter directly related to the tetragonal distortion, corresponds to a lengthening of the bond along the four-fold axis. If the Tanabe-Sugano approximation[84] ($C \simeq 4B$) is adopted, crystal field and Racah parameters can be calculated from the four lowest energy bands of $V(CO)_6$.

From a first order analysis of the ESR spectrum, Pratt and Meyers[76] have calculated that $10\ Dq \leq 36{,}200\ cm^{-1}$ and $3\ Ds - 5\ Dt \leq 1880\ cm^{-1}$. Several sets of assignments can reasonably be made for the observed d-d transitions. Crystal field parameters were calculated for each set of assignments. These parameters were then tested by calculating the expected d-d spectrum and comparing it to the observed d-d spectrum. The parameters listed in Table 24 reproduced the observed spectrum quite well as shown in spectrum 24c and satisfied both upper limits for the crystal field parameters. Consequently, these parameters were used to assign the observed d-d spectrum.

Since the photoelectron spectrum of $V(CO)_6$ indicates the ligand bonding molecular orbitals are at least 5 e.v. lower in energy than are the metal-like d orbitals,[72] the charge transfer bands are most likely transitions from the b_{2g} and e_g π^* orbitals to the a_{2u} and e_u σ^* orbitals. The states expected for these one electron transitions are listed in Table 25. Since only the two ^2E_u states and the $^2B_{1u}$ state are electronic dipole allowed,

Table 23. Lowest spin doublet energy states for d^5 ions in a strong crystal field with D_{4h} symmetry

Electron Configuration	Designation	Total Orbital Energy[a]	Racah Energy (+ 10 A)
$e_g^4\ b_{2g}$	$^2B_{2g}$	$5\ \varepsilon_o - 20\ Dq - 2Ds + 15\ Dt$	$- 20B + 10C$
$e_g^3\ b_{2g}^2$	$^2E_g(1)$	$5\ \varepsilon_o - 20\ Dq + Ds + 10\ Dt$	$- 20B + 10C$
$e_g^4\ a_{1g}$	$^2A_{1g}$	$5\ \varepsilon_o - 10\ Dq - 6\ Ds + 10\ Dt$	$+ 10C$
$e_g^3\ b_{2g}\ a_{1g}$	$^2E_g(2)$	$5\ \varepsilon_o - 10\ Dq - 3\ Ds + 5\ Dt$	$- 13B + 9C$
	$^2E_g(3)$	$5\ \varepsilon_o - 10\ Dq - 3\ Ds + 5\ Dt$	$- 9B + 9C$

[a]The one electron orbital energies are

$E(b_{1g}) = \varepsilon_o + 6\ Dq + 2Ds - Dt$

$E(a_{1g}) = \varepsilon_o + 6Dq - 2Ds - 6Dt$

$E(b_{2g}) = \varepsilon_o - 4Dq + 2Ds - Dt$

$E(e) = \varepsilon_o - 4Dq - Ds + 4Dt.$

Table 23. (Continued)

Electron Configuration	Designation	Total Orbital Energy[a]	Racah Energy (+ 10 A)
$e_g^4\ b_{1g}$	$^2B_{1g}$	$5\ \varepsilon_o - 10\ Dq - 2\ Ds + 15\ Dt$	$- 20B + 10C$
$e_g^3\ b_{2g}\ b_{1g}$	$^2E_g(4)$	$5\ \varepsilon_o - 10\ Dq + Ds + 10\ Dt$	$- 20B + 9C$
	$^2E_g(5)$	$5\ \varepsilon_o - 10\ Dq + Ds + 10\ Dt$	$- 14B + 9C$

Table 24. Crystal field and Racah parameters for $V(CO)_6$ in cm^{-1}

10 Dq	Ds	Dt	B	C[a]
29,300	1215	365	450	1800

[a]Estimated value.

Table 25. States expected for the charge transfer bands from the e_g and b_{2g} π^* orbitals to the a_{2u} and e_u σ^* orbitals

Electron configuration	Designation
eg^4 a_{2u}	$^2A_{2u}$
e_g^3 b_{2g} a_{2u}	$^2E_u(1)$
e_g^4 e_u	$^2E_u(2)$
e_g^3 b_{2g} e_u	$^2A_{1u}$
	$^2A_{2u}$
	$^2B_{1u}$
	$^2B_{2u}$

these transitions are expected to give rise to the three strongest bands observed in the spectrum. Using this and the calculated d orbital energies, tentative assignments for the charge transfer spectrum have been made. The assignments for all of the observed electronic transitions of $V(CO)_6$ are given in Table 26.

C. Conclusions

As expected from previous studies, $V(CO)_6$ was found to have D_{4h} symmetry in matrices at low temperatures. The electronic spectrum of $V(CO)_6$ in a CO matrix was examined and tentative assignments have been made for the bands contained in the spectrum. Approximate crystal field and Racah parameters have been determined.

The binary vanadium carbonyls $V(CO)_{1-5}$ and $V_2(CO)_{12}$ have been prepared in Ar matrices and identified using IR spectroscopy. Tentative structures have been determined for each complex.

As expected, the bonding models developed for the other hexacarbonyl systems work quite well for the vanadium carbonyl system indicating that the bonding in these systems is quite similar.

Table 26. Tentative assignments for the electronic spectrum of $V(CO)_6$

Transition	λ (nm)	$\bar{\nu}$ (cm^{-1})
$^2E_g(2) \leftarrow {}^2B_{2g}$	388.2	25 758
$^2E_g(3) \leftarrow {}^2B_{2g}$	363.0	27 546
$^2B_{1g} \leftarrow {}^2B_{2g}$	341.6	29 274
$^2E_g(4) \leftarrow {}^2B_{2g}$	341.0[a]	29 317[a]
$^2A_{1g} \leftarrow {}^2B_{2g}$	317.2	31 526
$^2E_g(5) \leftarrow {}^2B_{2g}$	312.5	32 000
$^2E_u(1) \leftarrow {}^2B_{2g}$	295.4	33 852
$^2A_{2u} \leftarrow {}^2B_{2g}$	283.0	35 336
$^2E_u(2) \leftarrow {}^2B_{2g}$	269.2	37 147
$^2B_{2u} \leftarrow {}^2B_{2g}$	260.0	38 462
$^2B_{1u} \leftarrow {}^2B_{2g}$	242.5	41 237
$^2A_{2u} \leftarrow {}^2B_{2g}$	226.0	44 248
$^2A_{1u} \leftarrow {}^2B_{2g}$	220.0	45 455

[a]Calculated value.

VI. THE DINITROGEN COMPLEXES OF CHROMIUM AND VANADIUM

A. Chromium

1. Introduction

Since the calculated orbital energies of CO and N_2 are surprisingly similar,[28] it is of theoretical interest to compare binary complexes with these isoelectronic molecules as ligands. Several new binary dinitrogen complexes with from one to four N_2 molecules per metal atom have been synthesized in low temperature matrices including those of Ni,[29,85] Pt,[29,86,87] Cr,[29] Cu,[29] Pd,[85] and Rh.[88] Both experimental evidence[15] and empirical calculations[89] indicate that these complexes are generally structurally similar to the corresponding carbonyl complexes. However, no binary dinitrogen analog to the well-studied six-coordinated octahedral complexes found for the carbonyls of the VA and VIA metals,[90] the rare earth metals,[72,73] and uranium[71] has previously been reported. A non-empirical calculation for $Cr(N_2)_6$[8] suggested that this molecule should be stable, at least at low temperatures. However, a previous investigation of the chromium dinitrogen system[29] failed to produce evidence of any complex with more than one coordinated dinitrogen molecule per metal atom. While this result appeared to be inconsistent with the results of similar experiments using different cations, there was no a-priori reason to question its validity. Thus an attempt was made to examine the electronic spectrum of this three atom "complex." However, the observed electronic spectrum was incompatible with the assumption of but one coordinated dinitrogen per metal atom. Consequently, the chromium dinitrogen system has

been re-examined and binary dinitrogen complexes, $Cr(N_2)_n$, n = 1-6, have tentatively been identified from the infrared spectrum. In addition the electronic spectrum of $Cr(N_2)_6$ has been analyzed.

2. Results and discussion

Figure 26 contains the infrared spectra observed for $Cr(N_2)_n$; where n = 4-6, in N_2 matrices. If mild deposition conditions were used, the infrared spectrum contained one band at 2136 cm^{-1} (spectrum 26a). Photolysis of the matrix occurred from exposure to the hydrogen lamp used to obtain the ultraviolet spectrum. After photolysis, a new band was observed in the infrared spectrum at 2112 cm^{-1} (spectrum 26b). The 2112 cm^{-1} band could also be obtained prior to photolysis by using more rigorous deposition conditions. Spectrum 26c is an example of a spectrum obtained using these conditions. In addition, this spectrum contained three additional bands at 2028 cm^{-1}, 2072 cm^{-1}, and 2195 cm^{-1}.

The ultraviolet spectrum of a highly photolyzed Cr containing N_2 matrix, containing only the 2112 cm^{-1} infrared band, is shown in Figure 27. Spectrum 27a is the uncorrected spectrum actually observed and spectrum 27b is the same spectrum corrected for baseline drift and resolved into component gaussians using the procedure described previously for the vanadium carbonyls. The two bands marked with asterisks are "window bands" which were observed in blank N_2 matrices. The spectrum resolves into four bands; two weak bands centered at 367.2 nm and 340.8 nm, a medium intensity band centered at 311.5 nm and a weak to medium intensity band centered at 297.2 nm. In addition, there is a very strong band centered at $\sim$ 230 nm,

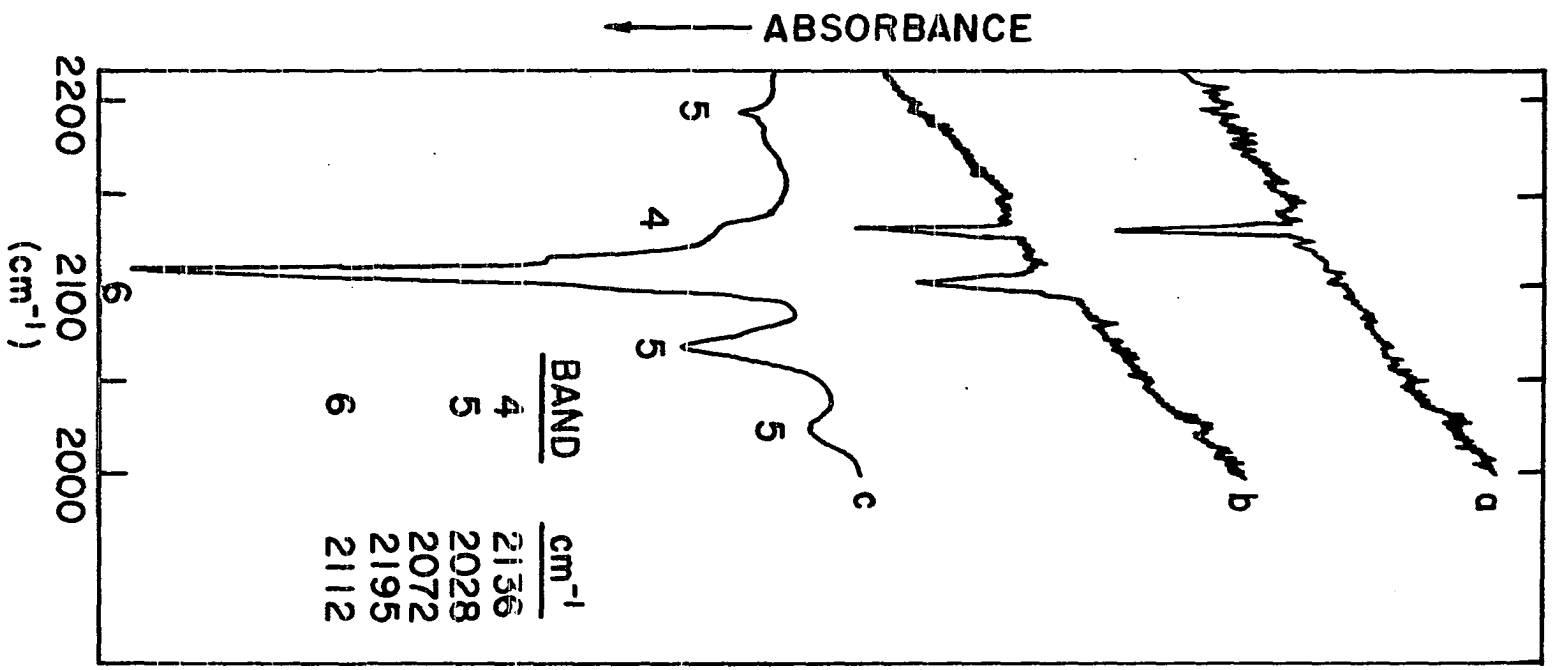

Figure 26. The infrared spectra of $Cr(N_2)_n$, n = 4 - 6 in N_2 matrices during photolysis

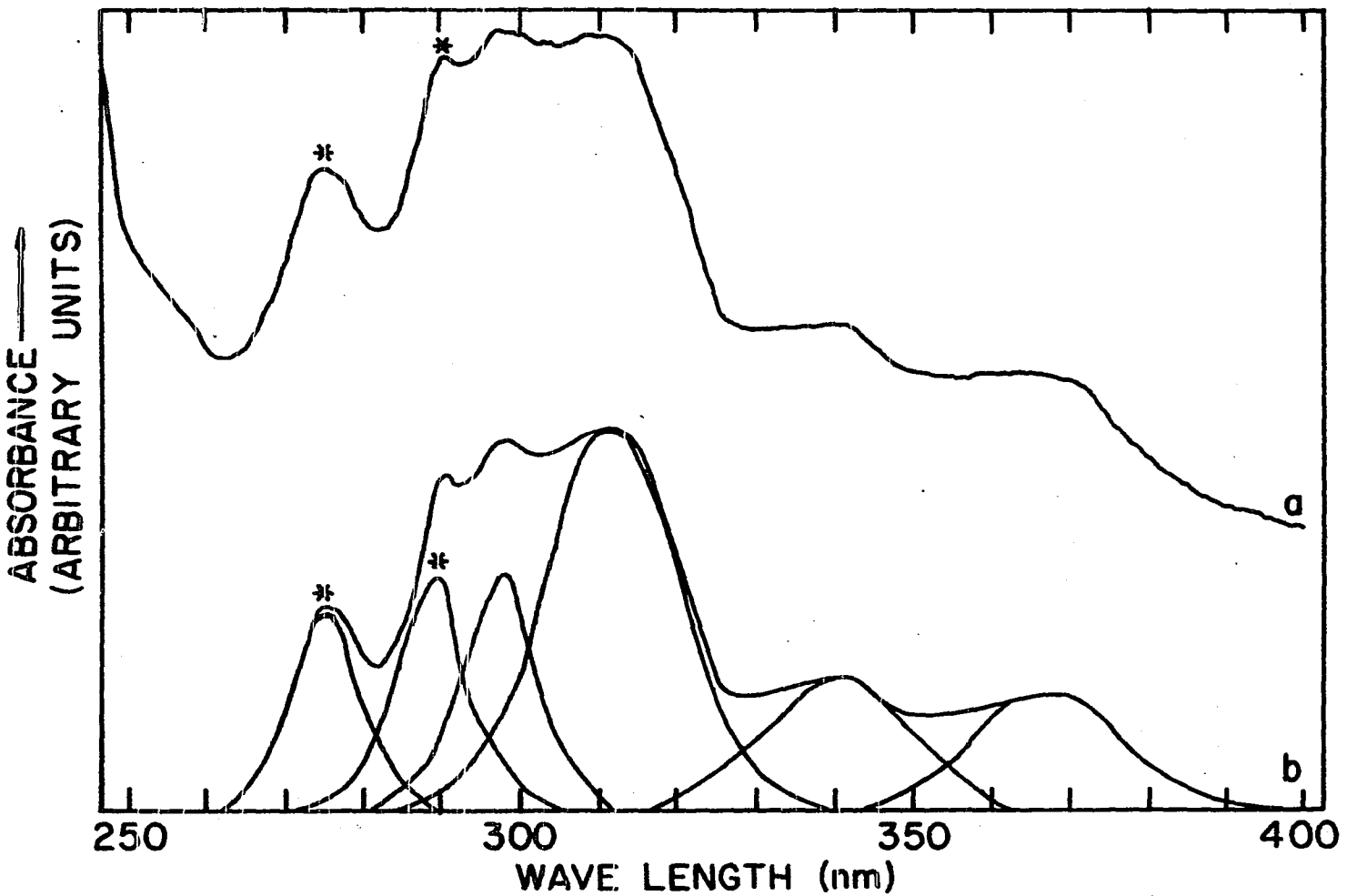

Figure 27. The UV spectrum of $Cr(N_2)_6$ in a N_2 matrix. Trace a is the observed spectrum. Trace b shows the spectrum resolved into Gaussians

which is not shown in this figure.

Qualitatively, this spectrum is identical to the electronic spectrum reported by Beach and Gray[91] for $Cr(CO)_6$. Consequently, the species giving rise to the infrared band at 2112 cm^{-1} in N_2 matrices is assigned as $Cr(N_2)_6$. As shown in Table 27, the observed electronic transitions can readily be assigned by analogy with the observed electronic spectrum for $Cr(CO)_6$. The energy of the lowest singlet energy states for d^6 ions in an octahedral field are given in Table 28. By assuming that $C \approx 4B$, approximate crystal field and Racah parameters were calculated for $Cr(N_2)_6$ and they are compared to the crystal field and Racah parameters calculated for $Cr(CO)_6$ and $Cr(CN)_6^{3-}$ in Table 29. The magnitude of the d-d splitting parameter (Δ) clearly shows that N_2 is a strong field ligand of similar magnitude as the isoelectronic ligands CO and CN^-.

Figure 28 is a composite of several experiments showing the observed changes in the dinitrogen stretching region of the infrared spectrum upon increasing the amount of N_2 in the matrix and/or annealing. Spectrum 28a is the spectrum of Cr in 1% N_2/Ar prior to annealing. After annealing a band is observed at 2215 cm^{-1}. If the N_2 concentration in the matrix is increased to 3.5% N_2, spectrum 28c is obtained prior to annealing. In addition to the 2215 cm^{-1} band, a second band at 2253 cm^{-1} is observed. Increasing the N_2 concentration to 10% N_2 (spectrum 28d) produces two new bands at 2130 cm^{-1} and 2178 cm^{-1}. As shown in spectrum 28e, both bands increase in intensity upon annealing. Further annealing, or increasing the concentration of N_2 in the matrix to 15% prior to annealing, produces three new bands at 2035 cm^{-1}, 2068 cm^{-1}, and 2273 cm^{-1} (spectrum 28f).

Table 27. Comparison of the observed electronic transitions for $Cr(N_2)_6$ and $Cr(CO)_6$[a]

Assignment	$Cr(N_2)_6$			$Cr(CO)_6$[a]		
	λ(nm)	$\bar{\nu}(cm^{-1})$	$\Delta G'_{1/2}$	λ(nm)	$\bar{\nu}(cm^{-1})$	$\Delta G'_{1/2}$
$^1T_{1g} \leftarrow {}^1A_{1g}$	367.2	27218	2254	344.8	29000	2550
	339.3	29472		317.0	31550	
$^1T_{1u} \leftarrow {}^1A_{1g}$	311.5	32103	___	279.3	35800	___
$^1T_{2g} \leftarrow {}^1A_{1g}$	297.2	33647	___	256.8	38970	___
$^1T_{1u} \leftarrow {}^1A_{1g}$	∿230	43478	___	226.2	44200	___

[a]From reference 91.

Table 28. The lowest energy singlet states for d^6 ions in an octahedral field in terms of crystal field and Racah parameters

Electron configuration	Designation	Total orbital energy	Racah energy (+ 15A)
t_g^6	$^1A_{1g}$	$6\,\varepsilon_o - 24\,D_q$	$- 16B + 8C$
$t_g^5\,e_g^1$	$^1T_{1g}$	$6\,\varepsilon_o - 14\,D_q$	$- 16B + 7C$
$t_g^5\,e_g^1$	$^1T_{2g}$	$6\,\varepsilon_o - 14\,D_q$	$+ 7C$

Table 29. Crystal field and Racah parameters for $Cr(CO)_6$, $Cr(N_2)_6$ and $Cr(CN)_6^-$

Parameter	$Cr(CO)_6$ [a]	$Cr(N_2)_6$	$Cr(CN)_6^{3-}$ [b]
$\Delta(cm^{-1})$	32,200	28,800	26,600
$B(cm^{-1})$	520	400	____
$C(cm^{-1})$	1700[c]	1600[c]	____
$\beta = B_{exp}/B_{Free}$ [d]	0.66	0.51	____

[a] From reference 91.

[b] From reference 92.

[c] Estimated value.

[d] $B_{Free} = 790\ cm^{-1}$.

Figure 28. The infrared spectra of the chromium dinitrogen complexes with increasing N_2 concentrations and/or annealing

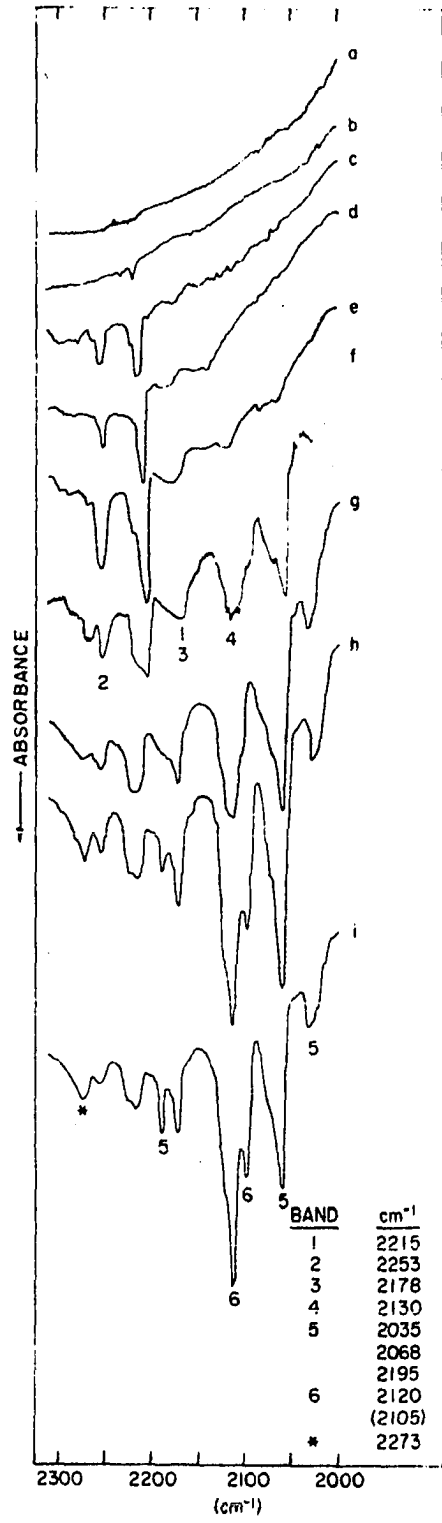
a
b
c
d
e
f
g
h
i
ABSORBANCE
1
2
3
4
5
6
5
6
5
5
*
BAND
cm⁻¹
1 2215
2 2253
3 2178
4 2130
5 2035
2068
2195
6 2120
(2105)
* 2273
2300
2200
2100
2000
(cm⁻¹)

Annealing the 15% matrix causes a marked increase in the 2034 cm^{-1} and the 2068 cm^{-1} bands and three new bands at 2105 cm^{-1}, 2120 cm^{-1} and 2195 cm^{-1} appear. With further annealing these five bands increasingly dominate the spectrum (spectrum 28h). With still more annealing the bands at 2035 cm^{-1}, 2068 cm^{-1} and 2195 cm^{-1} decrease in intensity with the bands at 2120 cm^{-1} and 2105 cm^{-1} finally dominating the spectrum. The assignments based upon this annealing and concentration dependence made using the assumptions listed previously are given in Table 30. Mixed isotope experiments were attempted to confirm these assignments. However, low intensities and highly overlapping bands prevented an accurage determination of either the relative intensities or the frequencies of the mixed isotope species. Consequently little useful information was obtained from these experiments.

The structures predicted by Burdett[80] for low, intermediate and high spin d^6 ions with from 1 to 6 coordinated ligands and the number of IR active bands expected for each structure are given in Table 31. Although some bands may not have been observed because of low intensity and/or the close proximity of other stronger bands, tentative structures were determined for each observed dinitrogen complex. If, as is usually found, all complexes are end-bonded, then $Cr(N_2)$ and $Cr(N_2)_2$ are linear molecules with $C_{\infty v}$ and $D_{\infty h}$ point group symmetries, respectively. Only one IR band could definitely be assigned to $Cr(N_2)_3$ indicating trigonal planar (D_{3h}) symmetry. However, two weaker bands, which appeared as shoulders at $\sim$ 2190 cm^{-1} and 2225 cm^{-1}, seem to be related to the $Cr(N_2)_3$ band. If these bands are truly related, then the symmetry of this molecule may actually be

Table 30. Assignments for $Cr(N_2)_n$ n = 1 - 6

Species	ν_{N_2} (cm^{-1})[a]	ν_{N_2} (cm^{-1})[b]	ν_{N_2} (cm^{-1})[c]
$Cr(N_2)$	2215	____	2142
$Cr(N_2)_2$	2253	____	2178
$Cr(N_2)_3$	2178	____	2108
$Cr(N_2)_4$	2130	2136	2060
$Cr(N_2)_5$	2035 2068 2195	2028 2072 2195	1966 2000 ____
$Cr(N_2)_6$	2120 (2105)[d]	2112	2042

[a]Argon matrix.

[b]Nitrogen matrix.

[c]$^{15}N_2$ in argon matrix.

[d]Matrix splitting.

Table 31. Predicted structures and the number of infrared active N-N stretching modes for complexes with low, intermediate, and high spin d^6 ions

Species	Low Spin		Intermediate Spin		High Spin	
	Symmetry Point Group	Number of IR Active Bands	Symmetry Point Group	Number of IR Active Bands	Symmetry Point Group	Number of IR Active Bands
M(L)	$C_{\infty v}$	1	$C_{\infty v}$	1	$C_{\infty v}$	1
$M(L)_2$	C_{2v}	2	$D_{\infty h}$	1	$D_{\infty h}$	1
$M(L)_3$	C_{3v}	2	C_{2v}	3	D_{3h}	1
$M(L)_4$	C_{2v}	4	D_{4h}	1	D_{4h}	1
$M(L)_5$	C_{4v}	3	D_{3h}	2	D_{3h}	2
$M(L)_6$	O_h	1	O_h	1	O_h	1

[a]From reference 80.

Y or even T shaped, having C_{2v} symmetry. Only one IR band was observed for $Cr(N_2)_4$ in both Ar and N_2 matrices, which suggests either tetrahedral (T_d) or square planar (D_{4h}) symmetry. Unfortunately, it is not possible to distinguish between these structural alternatives. The observation of 3 IR bands for $Cr(N_2)_5$ indicates this molecule has a tetragonal pyramid (C_{4v}) structure. $Cr(N_2)_6$ has octahedral symmetry. The splitting of the IR band for $Cr(N_2)_6$ in argon matrices is due to matrix effects. However, the failure of the chromium dinitrogen complexes to follow the trend of increased frequency with increased coordination, which was found to the hexacarbonyls,[73] could indicate the presence of side-bonded N_2 in the lower coordinated species. The IR spectra strongly suggest $Cr(N_2)_n$, n = 4-6, contain only end-bonded N_2. However, only one infrared band would be expected for side-bonded $Cr(N_2)$, $Cr(N_2)_2$, and $Cr(N_2)_3$ with C_{2v}, D_{2h}, and D_3 symmetries, respectively. Thus the structures of the lower coordinated species cannot definitely be established until the type of bonding has been determined.

Cotton-Kraihanzel (C-K) Force constants can also be calculated for dinitrogen complexes. For reasons which will be more fully developed in the next section, $Cr(N_2)$ and $Cr(N_2)_2$ are thought to be side-bonded and $Cr(N_2)_3$ is thought to be at least partially side-bonded. C-K force constants have been tabulated for the chromium dinitrogen complexes assuming the side-bonded structures in Table 32.

Table 32. Cotton-Kraihanzel force constants for $Cr(N_2)_{1-6}$

Species	$\nu(cm^{-1})$	Normal mode	Force constant (m dyn/Å)
$Cr(N_2)$	2215	A_1	20.22
$Cr(N_2)_2$	2253	B_{1u}	20.92
$Cr(N_2)_3$	2178	E	19.55
$Cr(N_2)_4$	2130	E_u or T_2	18.70[a]
$Cr(N_2)_5$	2035	A_1	17.70[b]
	2068	E	17.63[a]
	2195	A_1	19.86[c]
$Cr(N_2)_6$	2112	T_{1u}	18.39[a]

[a] $K - K_r$.

[b] $K + K_r - 2K_c$.

[c] K'.

B. Vanadium

1. Introduction

The failure of the chromium dinitrogen complexes to follow the trend of increased frequency with increased coordination found for most carbonyl systems which have a maximum coordination of six suggests there are either structural and/or quantum mechanical differences in the bonding of the chromium dinitrogen complexes. The vanadium dinitrogen system was examined to determine if this "unusual" behavior is characteristic of all dinitrogen complexes which have a maximum coordination of six.

2. Results and discussion

Unlike the previous studies, warming the matrix had little effect on the spectrum. Consequently changes in the spectrum could only be produced by changing the concentration of N_2 in the matrix.

Figure 29 is a composite of infrared spectra which shows the observed changes in intensity as the N_2 concentration in the matrix is increased from 1/4 to 8 mole %. Only bands at 1996 cm^{-1} and 2156 cm^{-1} were observed in 0.25% N_2 (spectrum 29a). Increasing the N_2 concentration to 0.5% (spectrum 29b), produced new bands at 1970 cm^{-1}, 2013 cm^{-1}, 2025 cm^{-1}, 2038 cm^{-1}, 2075 cm^{-1}, 2092 cm^{-1}, 2102 cm^{-1}, 2141 cm^{-1} and 2169 cm^{-1}. In addition, the band at 1996 cm^{-1} decreased in intensity. Increasing the N_2 concentration to 1% (spectrum 29c) produced no new bands. However, several changes in intensity did occur. Further increasing the N_2 concentration to 2% (spectrum 29d), 3% (spectrum 29e), and to 8% (spectrum 29f) produced further intensity changes. By making the usual approximations about the

Figure 29. The infrared spectrum of vanadium codeposited in argon matrices containing increasing quantities of nitrogen

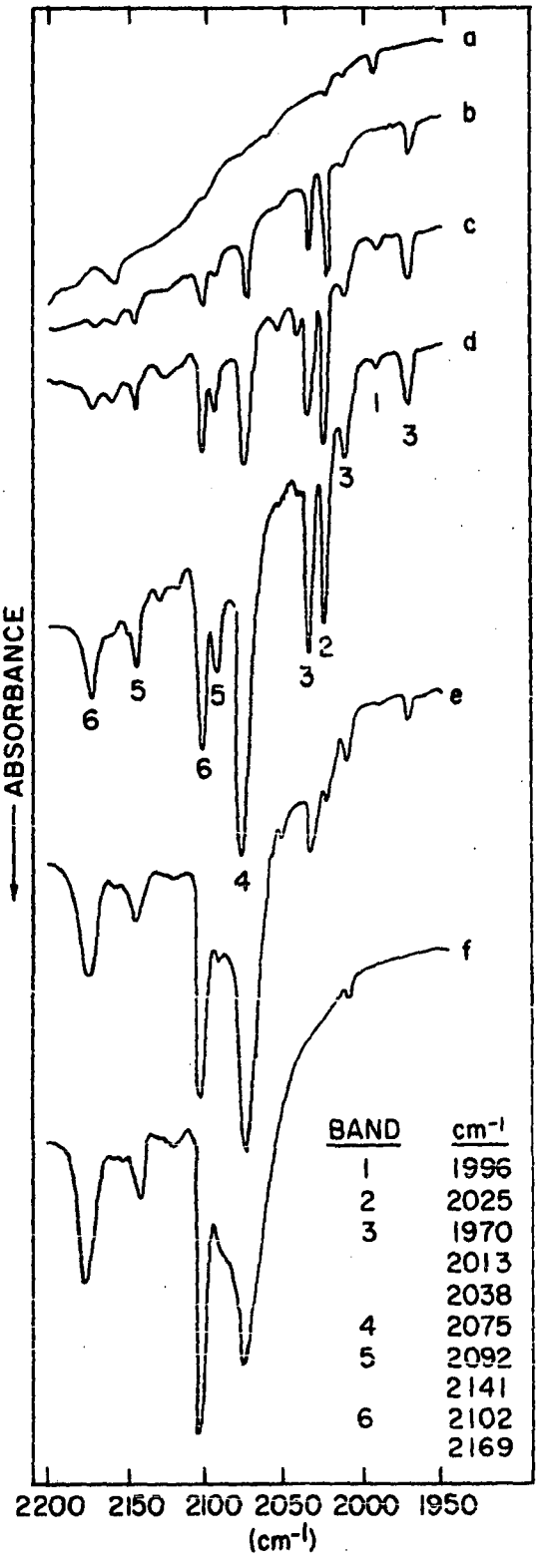
a
b
c
d
e
f
ABSORBANCE
1
3
3
2
3
5
5
6
6
4
BAND
cm⁻¹
1 1996
2 2025
3 1970
2013
2038
4 2075
5 2092
2141
6 2102
2169
2200 2150 2100 2050 2000 1950
(cm⁻¹)

behavior of the dinitrogen complexes in the matrix, six binary vanadium dinitrogen complexes have tentatively been identified. These complexes and the infrared bands which have been assigned to each are tabulated in Table 33. Unlike the vanadium carbonyl system, no bands which could be assigned to a dimeric species were observed.

Unlike the dinitrogen complexes of chromium, the dinitrogen complexes of vanadium do follow the trend of increasing frequency with increased number of coordinated ligands exhibited by the hexacarbonyl systems. Hence, the bonding in the vanadium dinitrogen complexes appears to be similar to the bonding found in the carbonyl complexes, while the bonding in the lower coordinated chromium dinitrogen complexes appears to be somewhat different than the bonding found in the carbonyl complexes. Since $Ni(N_2)_{1-4}$ and $Pd(N_2)_{1-3}$,[85] which have experimentally been shown to contain only end-bonded dinitrogen, obey the monotonically increasing frequency-coordination number relationship, it is reasonable to suggest that all the dinitrogen complexes of vanadium are end-bonded while the lower coordinated complexes of chromium are side-bonded. The unassigned band at 2156 cm^{-1} which was first observed for V in 0.25% N_2, could offer further support for this assumption. Since this band occurs in matrices with low N_2 concentrations, one reasonable assignment for this band would be side-bonded $V(N_2)$. If this assignment is correct, then the infrared frequency of the side-bonded dinitrogen complex would be $\sim$ 160 cm^{-1} to the blue of the frequency of the end-bonded dinitrogen complex.

Tentative structures for the remaining end-bonded dinitrogen complexes were determined by comparing the number of observed infrared bands with the

Table 33. Tentative assignments and the observed vibrational frequencies for $V(N_2)_n$, n = 1 - 6 in argon matrices

Species	$\nu(cm^{-1})$
$V(N_2)$	1996
$V(N_2)_2$	2025
$V(N_2)_3$	1970
	2013
	2038
$V(N_2)_4$	2075
$V(N_2)_5$	2092
	2141
$V(N_2)_6$	2102
	2169

number of infrared bands calculated for structures which have the appropriate stoichiometry. Using the structures calculated by Burdett[80] for low, intermediate and high spin d^5 ions which had been tabulated previously, the structures listed in Table 34 were determined for the vanadium dinitrogen complexes.

However, the matrix structure may not be the most stable structure of the free species. There is growing evidence that quasi-stable complexes may be formed from the interactions between the trapped species and the matrix. For example, the electronic spectrum of vanadium atoms trapped in argon and krypton matrices discussed in Section III was found to be similar to the electronic spectrum expected for the hypothetical complex $V(Ar)_6$. The solvation effects could influence the structures of the intermediate complexes. In fact, Kündig and Ozin[16] have suggested the structure of free $Cr(CO)_5$ is trigonal bipyramidal (D_{3h}) rather than the square pyramid (C_{4v}) structure reported by Graham et al.[93] They suggest the C_{4v} complex is actually $Cr(CO)_5$ S; where S = solvent. From the variation of the visible absorption band of $Cr(CO)_5$ in matrices composed of different gases, Perutz and Turner[94] have also concluded that $Cr(CO)_5$ S may be a better representation of the complex. However, they expressed doubt that the solvation effect was strong enough to influence the structure of the complex. Perhaps the structure of the partially coordinated complexes would be more accurately represented if they were expressed as the structure of solvated complexes of the form ML_nS_x.

Occasionally infrared bands were observed in matrices containing high N_2 concentrations which could have been due to solvated side-bonded dinitrogen.

Table 34. Observed structures and point group symmetry for $V(N_2)_n$, n = 1 - 6

Species	Structure	Point Group Symmetry
$V(N_2)$	linear	$C_{\infty v}$
$V(N_2)_2$	linear	$D_{\infty h}$
$V(N_2)_3$	Y-shaped	C_{2v}
$V(N_2)_4$	square planar or tetrahedral	D_{4h} T_d
$V(N_2)_5$	trigonal bipyramid	D_{3h}
$V(N_2)_6$	tetragonal bipyramid	D_{4h}

The unassigned bands at 2273 cm^{-1} in the chromium dinitrogen system and at 2218 cm^{-1} in the vanadium dinitrogen system are examples of these possible solvated bands. However, these assignements have not been confirmed.

Loosely bonded solvated complexes provide one explanation for the occurrence of partially coordinated dinitrogen complexes in N_2 matrices. Quasi-bonds between lattice bonded N_2 and the metal atom could sterically hinder the formation of the more stable higher coordinated complexes.

Cotton-Kraihanzel force constants have been calculated for the dinitrogen complexes of vanadium and are given in Table 35.

While the end-bonded vanadium dinitrogen and carbonyl complexes are isostructural, the two bands assigned to $V(N_2)_6$ are more widely separated than are the two bands assigned to $V(CO)_6$, suggesting that $V(N_2)_6$ may be more distorted from the ideal octahedral structure than $V(CO)_6$. Since the relative distortion in the complexes can be estimated by comparing their crystal field distortion parameters, the electronic spectrum of $V(N_2)_6$ was examined.

The electronic spectrum of $V(N_2)_6$ in a nitrogen matrix is shown in Figure 30. As expected, this spectrum was qualitatively similar to the electronic spectrum observed for $V(CO)_6$ in CO matrices. Since the massive overlap of the spectral features prevented a clear-cut resolution of the spectrum, the spectrum was resolved by using the procedure described previously. The spectral resolution which appears to best reproduce the major features of the observed spectrum is shown in Figure 30. Crystal field and Racah parameters were calculated from the four bands of lowest energy. The parameters which best reproduced the observed spectrum were used to assign

Table 35. Cotton-Kraihanzel force constants for $V(N_2)_{1-6}$

Species	$\nu(cm^{-1})$	Normal Mode	Force Constant (m dyn/A^o)
$V(N_2)$	1996	Σ^+	16.42[a]
$V(N_2)_2$	2025	Σ_u^+	16.90[a]
$V(N_2)_3$	1970	A_1	16.00[b]
	2013	A_1	16.70[c]
	2038	B_1	17.12[a]
$V(N_2)_4$	2075	E_u or T_2	17.75[a]
$V(N_2)_5$	2092	E'	18.04[a]
	2141	A_2''	18.90[b]
$V(N_2)_6$	2102	E_u	18.21[a]
	2169	A_{2u}	19.39[b]

[a] $K - K_r$.

[b] $K' - K_s$.

[c] $\bar{K} + \bar{K}_T$.

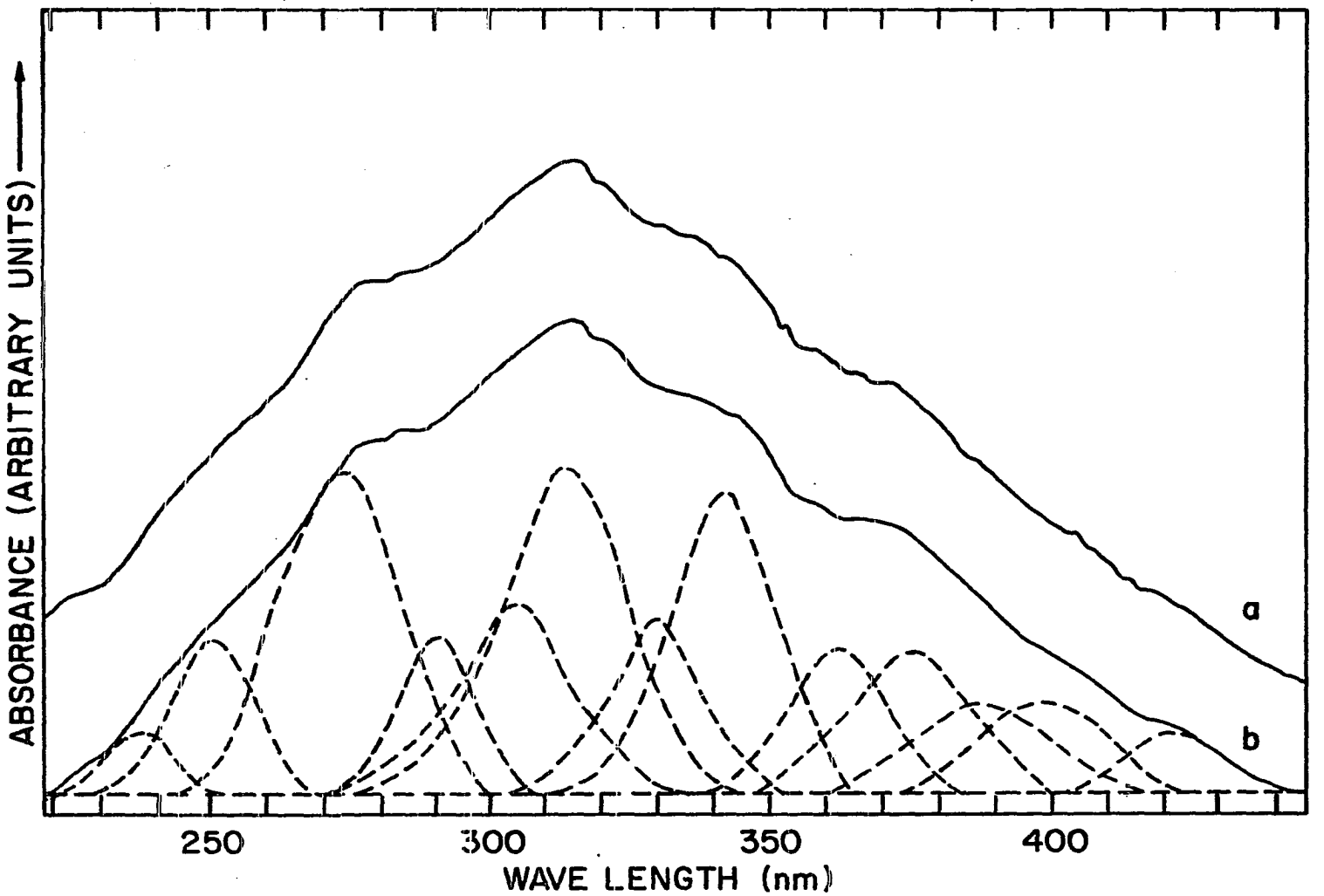

Figure 30. The electronic spectrum of $V(N_2)_6$ in a N_2 matrix. Trace a is the observed spectrum. Trace b is a gaussian resolution of the observed spectrum

the d-d bands in the spectrum. The charge transfer bands were assigned by analogy to the $V(CO)_6$ spectrum. Tentative assignments for the $V(N_2)_6$ electronic transitions are given in Table 36.

The crystal field and Racah parameters determined for $V(N_2)_6$ are compared to the parameters determined previously for $V(CO)_6$, $Cr(CO)_6$ and $Cr(N_2)_6$ in Table 37 and the calculated d orbital energies for these complexes are compared in Table 38. Although all the parameters have the same order of magnitude, the values for the d-d splitting parameters (Δ) of the dinitrogen complexes are slightly smaller numerically than are the Δ values for the corresponding carbonyl complexes, and the Δ values of the vanadium complexes are slightly smaller numerically than are the Δ values for the corresponding chromium complexes. In the crystal field model, smaller Δ values indicate weaker fields, which in turn imply less bonding for the dinitrogen complexes and for the vanadium complexes. Considering the apparent instability of the dinitrogen complexes and the presence of one less electron available for backbonding in the vanadium case, this picture is reasonable. However, this result contradicts the results of the infrared spectra which using the usual model,[27] predict that the dinitrogen complexes and the complexes of vanadium are more extensively π-bonded. The more exact MO formalism provides a resolution of this apparent contradiction. In this picture Δ measures the energy difference between the occupied π^* orbitals and the empty σ^* orbitals. A smaller value of Δ could indicate increased π bonding, decreased σ bonding, or both, as well as the decreased overall bond strength predicted by the crystal field model. Consequently, the dinitrogen complexes and/or the vanadium complexes could have weaker

Table 36. Tentative assignments for the electronic spectrum of $V(N_2)_6$

Transition	λ(nm)	$\bar{\nu}(cm^{-1})$
$^2E_g(2) \leftarrow {}^2B_{2g}$	422.0	23696
$^2E_g(3) \leftarrow {}^2B_{2g}$	398.8	25075
$^2B_{1g} \leftarrow {}^2B_{2g}$	387.0	25840
$^2A_{1g} \leftarrow {}^2B_{2g}$	375.5	26631
$^2Eg(4) \leftarrow {}^2B_{2g}$	362.2	27609
$^2Eg(5) \leftarrow {}^2B_{2g}$	(338.3)[a]	(29560)[a]
$^2E_u(1) \leftarrow {}^2B_{2g}$	341.8	29257
$^2A_{2u} \leftarrow {}^2B_{2g}$	329.0	30395
$^2E_u(2) \leftarrow {}^2B_{2g}$	313.5	31898
$^2B_{2u} \leftarrow {}^2B_{2g}$	291.0	34364
$^2B_{1u} \leftarrow {}^2B_{2g}$	273.0	36630
$^2A_{2u} \leftarrow {}^2B_{2g}$	250.5	39920
$^2A_{1u} \leftarrow {}^2B_{2g}$	227.5	43956

[a]Calculated value.

Table 37. Crystal field and Racah parameters for $V(N_2)_6$, $V(CO)_6$, $Cr(N_2)_6$ and $Cr(CO)_6$

	$V(N_2)_6$	$V(CO)_6$	$Cr(N_2)_6$	$Cr(CO)_6$[a]
$\Delta(cm^{-1})$	25850	29300	28800	32200
$Ds(cm^{-1})$	1315	1215	—	—
$Dt(cm^{-1})$	185	365	—	—
B (cm^{-1})	350	450	400	520
C (cm^{-1})	1400[b]	1800[b]	1600[b]	1700[b]

[a]Reference 91.

[b]Estimated value.

Table 38. Relative crystal field d orbital energies (in cm^{-1}) for $V(CO)_6$, $V(N_2)_6$, $Cr(CO)_6$ and $Cr(N_2)_6$

Orbital	$V(CO)_6$	$V(N_2)_6$	$Cr(CO)_6$	$Cr(CO)_6$
$E(b_{1g})^a$	19,630	17,950		
$E(e_g)^b$			19,320	17,280
$E(a_{1g})^a$	12,945	11,765		
$E(b_{2g})^a$	-9,645	-7,890		
$E(t_{2g})^b$			-12,880	-11,520
$E(e_g)^a$	-11,465	-10,910		

[a] D_{4h} symmetry.

[b] O_h symmetry.

metal-ligand bonds and still have lower ligand stretching frequencies because of more relative backbonding than is found in the corresponding carbonyl and/or chromium complex. In addition, nonempirical calculations[8] have shown that the ligand orbitals involved in sigma donation are antibonding with respect to the ligand molecular orbital framework, with the sigma orbitals in CO being more antibonding than are the corresponding orbitals in N_2. Thus increased σ donation is expected to increase the strength of the A-B bond. Since Mössbauer studies[95] have indicated that "CO is an appreciably better σ donor and/or π acceptor than N_2," it has been concluded that the weakening of the N-N bond is apparently caused by decreased σ donation.[8,85] Thus, the electronic and infrared results are consistent with a model of weaker metal-ligand bonds in the dinitrogen complexes.

Since the distortion parameters, Ds and Dt are of comparable magnitude for $V(CO)_6$ and $V(N_2)_6$, the larger separation of the infrared frequencies of $V(N_2)_6$ cannot be totally explained simply by assuming a larger distortion for the dinitrogen complex. Part of the increased separation must originate from quantitative differences in the bonding. As the bond length is increased both the sigma bonding and the π backbonding are expected to decrease, which results in a simultaneous weakening and strengthening of the ligand A-B bond, respectively. Since the CO complexes are more strongly sigma bonded, the CO bond in distorted $V(CO)_6$ is better buffered against the increased π bonding caused by the distortion than is the NN bond in $V(N_2)_6$. In addition, the π^* orbital involved in the backbonding is more localized on the carbon atom in CO, but is evenly distributed between both

nitrogen atoms in N_2.[8] Since this π^* orbital is necessarily smaller in the dinitrogen complex, increasing the bond length is expected to decrease the overlap between the d and π^* orbitals more in the dinitrogen complex than in the carbonyl complex, which would in turn lead to a greater increase in the N-N stretching frequency than in the CO stretching frequency.

C. Conclusions

From the observed trends in the dinitrogen complexes of chromium and vanadium, it is concluded that the dinitrogen complexes of chromium were side-bonded while those of vanadium are end-bonded. Tentative structures and force constants have been determined for each set of complexes.

From the values calculated for the d-d splitting parameter (Δ) and the observed infrared frequencies, some generalizations have been made about the bonding in the dinitrogen complexes. While N_2 produces a strong crystal field, it is a weaker ligand than is CO. N_2 is a poorer σ-donor and possibly also a poorer π-donor than is CO. However, because σ-donation strengthens the A-B bond, N_2 produces a larger shift in the vibrational frequency upon complexation than does CO.

Because of the better overlap which is created by the larger, less energetic d orbitals of vanadium, vanadium is a more efficient π donor than is chromium. However, chromium is known to form overall stronger metal ligand bonds than does vanadium.[96]

VII. THE HOMONUCLEAR DIATOMIC MOLECULES

A. Introduction

The homonuclear diatomic molecules of the first transition period have potential theoretical, astronomical, and high temperature importance. Although each of these molecules has been identified mass spectrometrically in the vapor in equilibrium with the liquid metal, in general, spectroscopic data for the molecules are lacking and only their dissociation energies have been established. The low concentration of the dimer in the equilibrium vapor has prevented the observation of their spectra by conventional techniques. However, Green and Gruen[39] observed the visible absorption spectrum of Nb_2 for the first time by using the technique of matrix isolation. In addition, other metal dimers, such as Mg_2,[97] Ca_2,[98] and Pb_2,[99] were observed to form in argon matrices as the result of surface diffusion during the deposition process. Thus, it was concluded the technique of matrix isolation could be used to study the previously unobserved absorption spectra of the homonuclear diatomic molecules of Mn, Fe and Ni.

Since the partial pressure of the dimer in the equilibrium vapor is quite small, the concentration of metal dimer in the matrix probably was supplemented by surface diffusion during the deposition process. Attempts to observe Ti_2, V_2 and Cr_2 failed, suggesting these metals do not diffuse through the matrix as readily as do Mn, Fe, and Ni, which were observed.

B. Results and Discussion

1. Mn_2

Mn_2 was observed in the vapor in equilibrium with Mn metal at 1500°K by Kant, Lin, and Strauss[100] and was possibly observed in the vapor in equilibrium with MnS at 1600°K by Wiedemeier and Gilles.[101] A series of sharp highly overlapping absorptions which was observed in the spectrum of Mn in Ar matrices, is shown in Figure 31. Since only Mn and Ar were intentionally deposited in the matrix, and since the average band spacing of 111 cm^{-1} is a reasonable vibrational spacing for a weakly bound molecule like Mn_2, this vibrational progression is assigned as the $A \leftarrow X$ transition of Mn_2. The assignments made assuming the longest wave length band is the 0 - 0 band are given in Table 39.

The results of an ab-initio calculation for the Mn_2 molecules by Nesbets[3] further supports this assignment. This calculation indicates that a weakly bound $^1\Sigma_u^+$ state occurs $\sim$ 7000 Å above the $^1\Sigma_g^+$ ground state, in good agreement with the proposed Mn_2 electronic transition. Consequently, this transition has been assigned as the $A(^1\Sigma_u^+) \leftarrow X(^1\Sigma_g^+)$ transition of Mn_2.

2. Fe_2

Lin and Kant[102] have observed Fe_2 in the vapor in equilibrium with liquid iron at temperatures greater than $\sim$ 1900°K. The visible absorption spectrum of Fe in an argon matrix (Figure 32) contained two vibrational progressions and a broad featureless absorption band. Since only Fe and Ar were present in the matrix and since the average vibrational spacings of 194 cm^{-1} and 218 cm^{-1} are reasonable metal dimer frequencies, these bands have

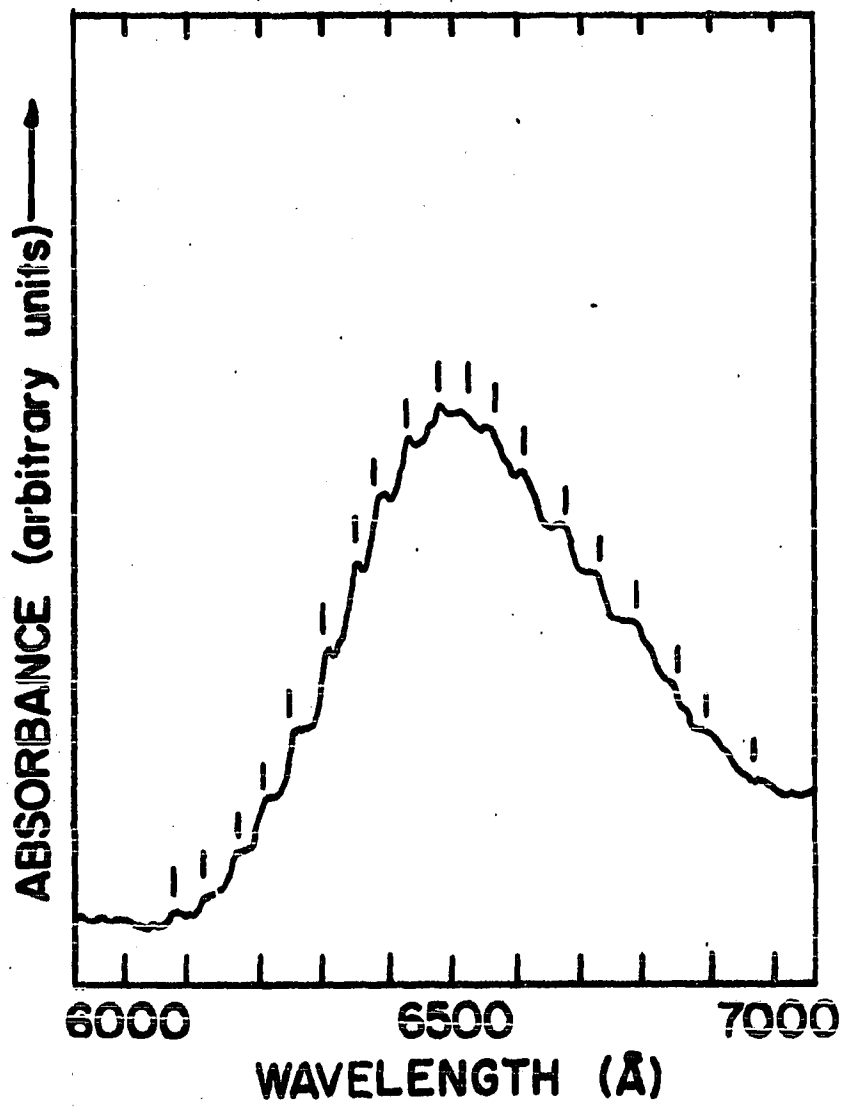

Figure 31. The A ← X absorption band of Mn_2 in an Ar matrix

Table 39. Assignments for the $A(^1\Sigma_u^+) \leftarrow X(^1\Sigma_g^+)$ transition of Mn_2 assuming the longest wavelength band is the 0 - 0 band

v'	λ(Å)	$\bar{\nu}(cm^{-1})$	$\Delta G'_{1/2}$ (cm^{-1})
0	6930	14430	94
1	6885	14524	96
2	6840	14620	116
3	6786	14736	145
4	6720	14881	98
5	6676	14979	120
6	6623	15099	94
7	6582	15193	106
8	6532	15309	106
9	6487	15415	108
10	6442	15523	114
11	6395	15637	104
12	6353	15741	104
13	6311	15845	122
14	6263	15967	121
15	6216	16088	122
16	6169	16210	117
17	6125	16327	118
18	6081	16445	.....
			Ave; 111

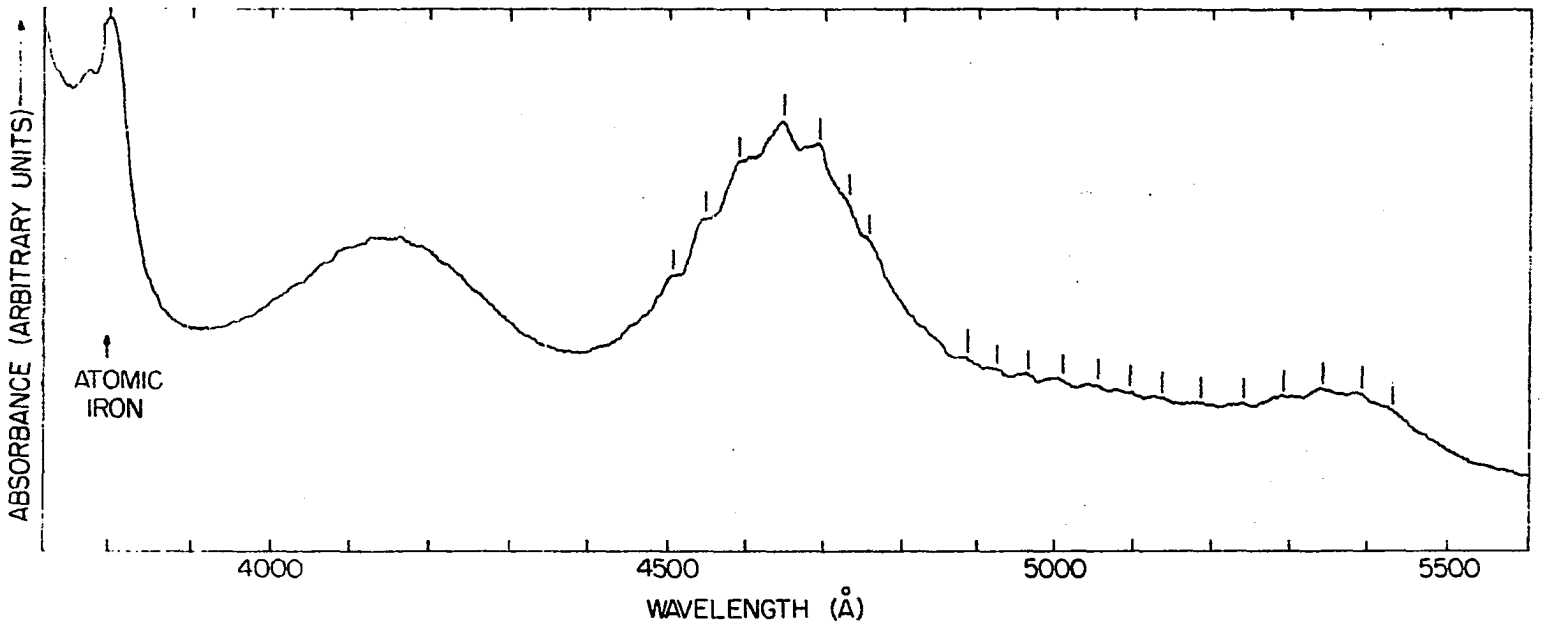

Figure 32. The A ← X, B ← X, and C ← X absorption bands of Fe_2 in an argon matrix

been assigned as the A ← X, B ← X, and C ← X absorption bands of Fe_2. The assignments made by assuming the longest wave length band is the 0 - 0 band are given in Table 40.

Nonempirical calculations have not been done for Fe_2. Consequently, because the calculation for Mn_2 indicated that rather complicated electron correlation effects occur in the transition-metal dimers, the states involved in the observed Fe_2 transitions could not be determined. However, the absorption spectrum of Fe_2 was estimated by using extended Hückel theory. The input parameters needed to reproduce this calculation are given in Table 41. Calculations were made for experimental bond lengths of 1.75 Å, 2.0 Å, and 2.25 Å, and the wave lengths expected for the first three visible absorption bands were calculated. Since the SCF calculation for Mn_2 indicated that there are rather extensive electron correlation effects operating in the metal dimers, an attempt was made to account for electron correlation by assuming that each M.O. which contained a significant amount of d character contained at least one d electron. The computed energy minimum is at ≈ 2.0 Å. The calculated orbital energy levels and wave functions for r = 2.0 Å are given in Table 42. As shown in Table 43, the first three calculated visible absorption bands are in good agreement with the observed 0 - 0 bands for Fe_2. While this cannot be regarded as conclusive evidence, it does support the assignment of these bands to Fe_2.

3. Ni_2

Ni_2 was observed by Kant[103] in the vapor in equilibrium with liquid Ni at temperature greater than 2000°K. A series of sharp absorptions with an

Table 40. Assignments for the three observed transitions of Fe_2 assuming the longest wavelength band is the 0 - 0 band

v'	λ(Å)	$\bar{\nu}$(cm^{-1})	$\Delta G'_{1/2}$ (cm^{-1})
		A ← X	
0	5448	18355	194
1	5391	18549	195
2	5335	18744	195
3	5280	18939	196
4	5226	19135	192
5	5174	19327	197
6	5122	19524	196
7	5071	19720	176
8	5026	19896	200
9	4976	20096	196
10	4928	20292	191
11	4880	20483	
		Ave.	194
		B ← X	
0	4740	21095	217
1	4692	21312	216
2	4645	21528	220
3	4598	21748	220
4	4552	21968	215
5	4508	22183	
		Ave.	218
		C ← X	

Continuous absorption with maxima at 4145Å.

Table 41. Input parameters for the EHMOT calculation of Fe_2 using Slater type orbitals

Orbital	H_{ii}(eu) [a]	Exponent [b]
3p	-60.00	4.259
3d	-8.70	3.083
4s	-7.10	1.550
4p	-3.80	1.000

$$H_{ij} = [0.875\ (H_{ii} + H_{jj})\ S_{ij}]^{c}$$

[a] Values for Fe with a d^7s^1 configuration taken from reference 42.

[b] Value calculated from the rules of G. Burns (reference 104).

[c] Reference 43.

Table 42. Eigenvalues and eigenvectors for Fe_2 at r_e = 2.0 Å

Symmetry Designation	E_i (e.V)	$3p_\sigma$	$3p_\pi$	$3d_\sigma$	$3d_\pi$	$3d_\delta$	4s	$4p_\sigma$	$4p_\pi$
σ_g^+	- 60.20	0.705		___			___	-0.001	
π_u	- 60.02		0.707		___				0.001
π_g	- 59.98		0.708		___				0.007
σ_u^+	- 59.80	0.709		___			0.008	0.005	
σ_g^+	- 9.03	-0.027		0.643			0.192	0.002	
π_u	- 8.86		0.004		0.698				0.006
σ_g^+	- 8.82	-0.027		-0.248			0.519	0.043	
δ_g	- 8.72					0.706			
δ_u	- 8.68					0.708			
π_g	- 8.53		0.003		0.716				-0.019
σ_u^+	- 8.32	0.014		0.723			-0.054	0.009	
σ_u^+	- 5.97	0.014		0.065			0.390	0.432	
π_u	- 4.88		-0.023		-0.026				0.547
σ_g^+	- 0.29	___		0.032			-0.404	0.917	
π_g	2.43		0.053		0.054				1.240
σ_u^+	50.47	0.172		0.074			2.130	1.301	

Table 43. Comparison of the observed and calculated 0 - 0 bands for the visible absorption spectrum of Fe_2[a]

Observed Spectrum (Å)	Calculated Spectrum (Å)
5448	5275
4740	4850
4145[b]	3600

[a] $r = 2.0$ Å.

[b] Intensity maximum of the continuous absorption.

average vibrational spacing of 192 cm^{-1} was observed in the spectrum of Ni isolated in argon. Since the vibrational spacing of this progression is comparable to the spacings observed for Fe_2, this progression is assigned as the A ← X transition of Ni_2. The assignments are given in Table 44.

Cooper, Clarke and Hare[105] have estimated the energy of the first electronic transition of Ni_2 to be ∿ 5500Å using extended Hückel theory. This prediction is in sufficiently good agreement to support the assignment of the observed transition as Ni_2.

C. Comparision with Interstellar Absorptions

The visible absorption spectrum of interstellar space contains several unassigned molecular bands.[106-108] Since several vapor phase molecules of refractory solids have been observed in interstellar atmospheres,[18] other, as yet unknown small molecules such as the transition metal dimers could be responsible for part of these unassigned interstellar absorptions.

The wave lengths of several of the better characterized interstellar absorption band maxima and the observed absorption maxima of Mn_2, Fe_2, and Ni_2 in argon matrices are compared in Table 45. None of the observed maxima match exactly. However, considering the time dependent nature of the wave length of the interstellar absorptions and the possible shifts in wave length and intensity caused by matrix interactions, the wave lengths are in sufficiently good agreement to suggest that these species could at least be partially responsible for the interstellar absorptions.

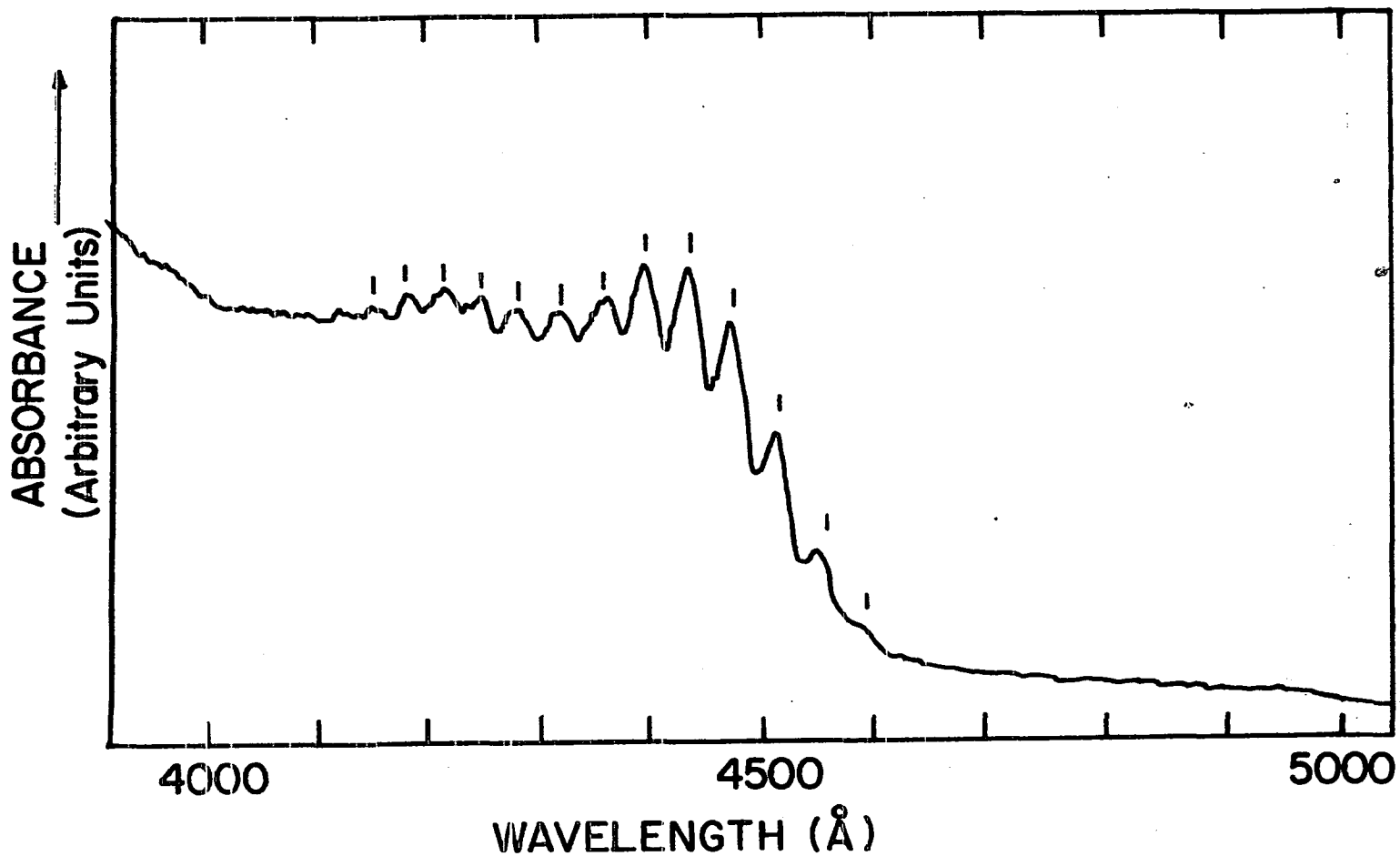

Figure 33. The A ← X absorption band of Ni_2 in an argon matrix

Table 44. Assignments for the A ← X transition of Ni_2 assuming the longest wavelength band is the 0 - 0 band

v'	λ(Å)	$\bar{\nu}(cm^{-1})$	$\Delta G'_{1/2}(cm^{-1})$
0	4590	21786	182
1	4552	21968	180
2	4515	22148	198
3	4475	22346	187
4	4438	22533	184
5	4402	22717	198
6	4364	22915	228
7	4321	23143	200
8	4284	23343	164
9	4254	23507	195
10	4219	23702	197
11	4184	23901	
			Ave, 192

Table 45. A comparison of the wavelength observed for the interstellar absorption band maxima with the wavelength observed for the absorption band maxima of Mn_2, Fe_2, and Ni_2 in argon matrices

Interstellar absorption maxima (Å)[a]	M_2 Absorption maxima (Å)
6200	6500[b]
5700	—
5100	5350[c]
4430	4650[c]
4100	4400[d]
3800	4145[c]

[a] From references 106-108.

[b] Mn_2.

[c] Fe_2.

[d] Ni_2.

D. Conclusions

The visible absorption spectra of Mn_2, Fe_2, and Ni_2 were examined in Ar matrices at 10°K. A comparison of the absorption maxima obtained for these compounds with the absorption maxima from interstellar space suggests these molecules may be important interstellar species.

VIII. SUGGESTIONS FOR FUTURE RESEARCH

There are many known molecules in the equilibrium vapor of refractory transition metal compounds which have not been investigated spectroscopically. For example, ground state vibrational frequencies have not been established for most of the transition metal borides, carbides, nitrides, silicides, phosphides, sulfides, selenides and tellurides. It would be interesting to compare the molecular properties and bonding in an isoelectronic series of molecules such as FeB, MnC, CrN, VO, and TiF to determine whether concepts explored in this thesis such as the Yanishevskii equation will reasonably explain the observed data.

The reaction between metal atoms and OCS certainly merits further study. Using techniques similar to those described by West and Broida,[66] it may be possible to use this reaction to generate "low temperature" transition metal vapor sulfides which could be studied without matrix effects and without several of the disadvantages inherent using conventional high temperature methods. Also it is possible that like many of the reactions between metal atoms and CO_2, this reaction may luminesce and have potential applicability in the laser industry.

It would be interesting to compare the Racah parameters for matrix isolated metal atoms with the parameters of free metal atoms to attempt to determine a possible origin of "secondary" matrix effects. Also it might be fun to look for metal-argon stretching frequencies in the near-microwave or far IR region using infrared (or microwave) absorption spectroscopy or Raman experiments. Observation of these frequencies would suggest that the metal atoms "bond" to the matrix to form pseudo-complexes.

Since few studies have been performed investigating the molecular properties of the dinitrogen complexes of the second and third period transition metals, it would be interesting to compare the structures and bonding found for the dinitrogen complexes of these metals to determine what if any differences are observed. Also it would be interesting to compare the structures and bonding found for other isoelectronic ligands such as CS, SiO, or BF with the structures and bonding in the dinitrogen and carbonyl complexes.

Finally, extended Hückel calculations could be used to further investigate the possibility of side-bonded dinitrogen groups in the lower coordinated dinitrogen complexes.

IX. APPENDIX A: EXTENDED HÜCKEL CALCULATIONS

The Hoffman EHMOT formalism has been extensively reviewed by McGlynn et al.,[109] so only a brief outline of the method will be given here.

Using the usual LCAO-MO format, the molecular orbital ϕ_j is expanded as a linear combination of Slater type orbitals (STO's).[40]

$$\phi_j = \sum_t C_{jt} \chi_t \tag{1}$$

where

$$\chi(\text{STO}) = (2\xi)^{n + \frac{1}{2}} (\tfrac{1}{2} n!)^{\frac{1}{2}} r^{n-1} e^{-\xi r} Y_l^m(\theta,\phi). \tag{2}$$

The Slater exponent (ξ) is

$$\xi = (z - \sigma)/n \tag{3}$$

where

z is the atomic number

σ is the atomic screening constant

n is a function of the quantum number.

The expansion coefficients (C_{jq}) are obtained by solving the secular equation

$$\sum_t (H_{st} - \epsilon_j S_{st}) C_{jt} = 0 \tag{4}$$

where

$$H_{st} = \langle \chi_s | \ddot{H} | \chi_t \rangle$$

$$S_{st} = \langle \chi_s | \chi_t \rangle \quad .$$

The orbital energies (ϵ_j) and the expansion coefficients (C_{jt}) are to be determined.

From the theorems of algebra, it is known that Equation 4 will have nontrivial solutions if, and only if, the determinate of the coefficients vanishes. That is

$$| H_{st} - \epsilon_j S_{st} | = 0 . \tag{5}$$

Equation 5 can be used to solve for the orbital energies, which in turn can be used in Equation 4 to determine the expansion coefficients.

In the extended Hückel formalism, the coulomb integrals (H_{tt}) are evaluated empirically from spectroscopic data. In this study, the charge dependent Valence Orbital Ionization Potentials (VOIP) of Basch *et al.*[42] were used to evaluate the coulomb integrals. In this method, the VOIPs are assumed to be a function of the total ionic charge (q)

$$\text{VOIP}(q) = A\, q^2 + Bq + C. \tag{6}$$

where A, B, and C are tabulated numerical constants which have been evaluated from known spectroscopic data. The total ionic charge (q) is determined from a Mulliken population analysis.[110] The input charge is cycled until

$$q_{in} = q_{out}.$$

For this reason, this method is also called the self-consistent charge-extended Hückel Method.

The exchange integrals are assumed to be a function of the coulomb integrals and are evaluated using either the Wolfsberg-Helmholz approximation[43]

$$H_{st} = \tfrac{1}{2}\, k\, S_{st}\, [H_{ss} + H_{tt}] \tag{7}$$

the Ballhausen-Gray approximation[111]

$$H_{st} = -k\, S_{st}\, [H_{ss} H_{tt}]^{\frac{1}{2}} \tag{8}$$

or the Cusachs approximation[112]

$$H_{st} = \tfrac{1}{2}\, S_{st}\, (2 - |S_{st}|\,)\, (H_{ss} + H_{tt})\,. \tag{9}$$

In all cases k is an arbitrary parameter ($1.0 \leq k \leq 2.0$) which can be adjusted to obtain agreement between the calculated and experimental data.

Although the atomic screening parameters could also be arbitrarily adjusted to produce agreement between the calculations and experiments, these parameters are generally evaluated empirically by using one of three sets of rules which have been developed by Slater,[40] Burns,[104] and Clementi and Raimondi,[41] respectively.

The computer program used to evaluate ε_i, C_{jt} and the Mulliken population analysis has been described previously by Owzarski[50] and will not be discussed here.

X. APPENDIX B: THIRD LAW CALCULATIONS OF THERMODYNAMIC PROPERTIES OF THE TRANSITION METAL SULFIDES

By using simple formulas such as those given in Lewis, Randall, Pitzer, and Brewer,[113] thermodynamic properties of ideal gases can be evaluated from spectroscopic and other molecular data. In this appendix, the values of three of the more useful thermodynamic properties, the enthalpy, the entropy, and the free energy function have been tabulated in 100 degree increments from 300°K to 3000°K for the first period transition metal sulfides.

To a first approximation, any extensive thermodynamic property (χ) can be written as a sum of terms

$$\chi = \chi_{tr} + \chi_{el} + \chi_{R} + \chi_{vib}$$

where

χ_{tr} = translational component

χ_{el} = electronic component

χ_{R} = rotational component

χ_{vib} = vibrational component.

The equations needed to compute each component of the enthalpy (H), the entropy (s), and the free energy function (fef) are listed in Table 46. The molecular properties used in this calculation are listed in Table 47.

In addition, an attempt was made to estimate the low lying electronic states of these sulfides. The states and estimated energies used to compute the internal electronic energies are given in Table 48.

Table 46. The equations needed to calculate H, S, and fef ($-\frac{F - H_o}{T}$) from molecular data

Translational Component

$$(H - H_o) = 5/2\ RT$$

$$S = R(3/2\ \ln M + 5/2\ \ln T) - 2.315\ \text{cal/dg}$$

$$-\left(\frac{F - H_o}{T}\right) = R(3/2\ \ln M + 5/2\ \ln T) - 7.283\ \text{cal/dg}$$

Electronic Component

$$H - H_o = RT(Q'/Q)$$

$$S = R(\ln Q + Q'/Q) - \left(\frac{F - H_o}{T}\right) = R\ \ln Q$$

$$Q = \sum_i g_i\, e^{-\varepsilon_i/kT}$$

$$Q' = \sum_i g_i(\varepsilon_i/kT)\, e^{-\varepsilon_i/kT}$$

Rotational Component

$$H - H_o = RT(1 - y/3 - y^2/45 - \ldots)$$

$$S = R(1 - \ln y - \ln\sigma - y^2/90 - \ldots)$$

$$-\frac{F - H_o}{T} = R(-\ln y - \ln\sigma + y/3 + y^2/90 + \ldots)$$

$$y = \frac{hcB}{kT} = \frac{h^2}{8\pi^2\ IkT}$$

σ = 1 for unsymmetrical molecule

= 2 for a symmetrical molecule

Table 46. (Continued)

Vibrational Component

$$H - H_o = RT(u/e^u - 1)$$

$$S = R\left(\frac{u}{e^u - 1} - \ln\left(1 - e^{-u}\right)\right)$$

$$-\frac{F - H_o}{T} = R \ln\left(1 - e^{-u}\right)$$

$$u = \frac{h\nu}{kT} = \frac{hc\omega}{kT} = 1.4387\ \frac{\omega}{T}$$

Table 47. Molecular properties for the first period transition metal sulfides

Molecule	M(Amu)	w(cm^{-1})	r(Å)	ground state
ScS	77	562.07	2.1354	$^2\Sigma^+$
TiS	80	562.18	2.0825	$^3\Delta$
VS	83	591	2.0	$^4\Sigma^-$
CrS	84	566	2.05	$^4\pi$
MnS	87	516	2.05	$^6\Sigma^+$
FeS	88	550	2.05	$^5\Sigma^+$
CoS	91	545	2.05	$^4\Delta$
NiS	91	544	2.00	$^3\Sigma^-$
CuS	96	414	2.00	$^2\pi$

Table 48. Estimated low lying electronic states for the transition metal sulfides

Molecule	State	Degeneracy (g_1)	Energy (1000 cm^{-1})
ScS	$^2\Sigma^+$	2	0.0
	$^2\Delta^+$	4	0.6
	$^2\pi$	4	10.0
TiS	$^3\Delta$	6	0.0
	$^1\Delta$	2	0.6
	$^1\Sigma$	1	3.0
	$^3\pi$	6	10.0
VS	$^4\Sigma^-$	4	0.0
	$^2\Sigma^-$	2	1.0
	$^2\Gamma$	4	3.0
	$^2\Sigma^+$	2	6.0
	$^2\Delta$	4	6.0
	$^4\pi$	8	11.0
CrS	$^5\pi$	10	0.0
	$^3\pi$	6	1.0
	$^3\mathcal{H}$	6	5.0
	$^3\pi$	6	6.0
	$^1\mathcal{H}$	2	7.0
	$^1\pi$	2	9.0

Table 48. (Continued)

Molecule	State	Degeneracy (g_1)	Energy (1000 cm^{-1})
	$^3\Phi$	6	9.0
MnS	$^6\Sigma^+$	6	0.0
	$^4\Sigma^+$	4	1.0
	$^4\Gamma$	8	3.0
	$^4\Delta$	8	4.0
	$^4\Sigma^-$	4	5.0
	$^2\Gamma$	4	5.0
	$^2\Delta$	4	5.0
	$^4\Sigma^-$	4	6.0
	$^2\Sigma^-$	2	7.0
	$^2\Sigma^-$	2	8.0
	$^2\Pi$	4	9.0
	$^2\Gamma$	4	9.0
	$^2\Delta$	4	10.0
	$^2\Delta$	4	12.0
FeS	$^5\Sigma^+$	5	0.0
	$^3\Gamma$	6	3.0
	$^3\Delta$	6	4.0
	$^3\Sigma^-$	3	5.0
	$^3\Sigma^-$	3	6.0

Table 48. (Continued)

Molecule	State	Denencracy (g_1)	Energy (1000 cm^{-1})
	$^1\Sigma^+$	2	9.0
	$^1\Gamma$	2	9.0
	$^2\mathfrak{X}$	4	9.0
	$^1\Delta$	2	10.0
	$^2\Delta$	4	12.0
CoS	$^4\Delta$	8	0.0
	$^2\Delta$	4	2.0
	$^2\Sigma^-$	2	3.0
	$^2\Delta$	4	5.0
	$^2\Gamma$	4	6.0
	$^2\Sigma^+$	2	9.0
NiS	$^2\Sigma^-$	2	0.0
	$^1\Delta$	2	4.0
	$^1\Sigma^+$	2	7.0
CuS	$^2\pi$	4	0.0

The computed values for the entropy, the enthalpy and the free energy function are listed in Tables 49 - 57.

Table 49. Enthalpy (in Kcal), entropy (in e.u.'s) and the free energy function (in e.u.'s) for ScS

Temp	(H-Ho)	S	$-(\frac{F-Ho}{T})$
298	2.19	56.64	49.31
400	3.03	59.06	51.50
500	3.88	60.95	53.20
600	4.74	62.53	54.63
700	5.61	63.87	55.86
800	6.48	65.04	56.93
900	7.37	66.08	57.89
1000	8.25	67.01	58.76
1100	9.14	67.86	59.55
1200	10.04	68.64	60.27
1300	10.95	69.37	60.94
1400	11.86	70.05	61.57
1500	12.79	70.68	62.16
1600	13.73	71.29	62.71
1700	14.67	71.86	63.23
1800	15.63	72.41	63.73
1900	16.60	72.93	64.20
2000	17.58	73.44	64.65
2100	18.57	73.92	65.08
2200	19.58	74.38	65.48

Table 49. (Continued)

Temp	(H-Ho)	S	$-(\frac{F-Ho}{T})$
2300	20.58	74.83	65.89
2400	21.60	75.27	66.27
2500	22.62	75.68	66.64
2600	23.65	76.09	66.99
2700	24.69	76.48	67.34
2800	25.73	76.86	67.67
2900	26.77	77.22	67.99
3000	27.82	77.58	68.31

Table 50. Enthalpy (in Kcal), entropy (in e.u.'s) and the free energy function (in e.u.'s) for TiS

Temp	(H-Ho)	S	$-(\frac{F-Ho}{T})$
298	2.23	59.08	51.61
400	3.10	61.61	53.85
500	3.98	63.56	55.60
600	4.87	65.18	57.07
700	5.76	66.56	58.33
800	6.66	67.76	59.44
900	7.56	68.82	60.42
1000	8.46	69.77	61.31
1100	9.37	70.63	62.12
1200	10.27	71.42	62.86
1300	11.18	72.14	63.55
1400	12.08	72.82	64.19
1500	12.99	73.44	64.78
1600	13.90	74.03	65.34
1700	14.81	74.58	65.87
1800	15.72	75.10	66.37
1900	16.64	75.60	66.84
2000	17.55	76.07	67.29
2100	18.47	76.52	67.72
2200	19.40	76.94	68.12
2300	20.32	77.35	68.52

Table 50. (Continued)

Temp	(H-Ho)	S	$-(\frac{F-Ho}{T})$
2400	21.24	77.75	68.90
2500	22.17	78.13	69.26
2600	23.11	78.50	69.61
2700	24.05	78.85	69.94
2800	24.99	79.19	70.27
2900	25.94	79.53	70.58
3000	26.90	79.85	70.89

Table 51. Enthalpy (in Kcal), entropy (in e,u,'s) and the free energy function (in e.u.'s) for VS

Temp	(H-Ho)	S	$-(\frac{F-Ho}{T})$
300	2.19	58,07	50.74
400	3.05	60,56	52,93
500	3,94	62.53	54.66
600	4,84	64,19	56,11
700	5,77	65,62	57,37
800	6,71	66,87	58,48
900	7.66	67,99	59,48
1000	8,62	69.00	60,38
1100	9.59	69,92	61,21
1200	10.57	70,77	61,97
1300	11.55	71,56	62,68
1400	12,54	72,30	63,34
1500	13.54	72,98	63,96
1600	14.54	73.63	64,54
1700	15.54	74.24	65.10
1800	16.56	74.82	65.62
1900	17.57	75.37	66,12
2000	18.59	75.89	66.59
2100	19,61	76,39	67,05
2200	20,63	77,88	67,50
2300	21.66	77.32	67,90

Table 51. (Continued)

Temp	(H-Ho)	S	$-(\frac{F-Ho}{T})$
2400	22.69	77.76	68.30
2500	23.72	78.18	68.69
2600	24.75	78.58	69.06
2700	25.78	78.97	69.42
2800	26.81	79.34	69.77
2900	27.84	79.71	70.11
3000	28.88	80.06	70.43

Table 52. Enthalpy (in Kcal), entropy (in e.u.'s) and the free energy function (in e.u.'s) for CrS

Temp	(H-Ho)	S	$-(\frac{F-Ho}{T})$
298	2.20	60.08	52.71
400	3.07	62.60	54.92
500	3.97	64.59	56.66
600	4.88	66.26	58.12
700	5.81	67.69	59.39
800	6.74	68.93	60.51
900	7.67	70.03	61.51
1000	8.61	71.01	62.41
1100	9.54	71.90	63.23
1200	10.48	72.72	63.99
1300	11.41	73.47	64.69
1400	12.35	74.17	65.34
1500	13.30	74.82	65.95
1600	14.25	75.43	66.53
1700	15.20	76.01	67.07
1800	16.16	76.56	67.58
1900	17.13	77.08	68.07
2000	18.10	77.58	68.53
2100	19.08	78.05	68.97
2200	20.07	78.55	69.46
2300	21.05	78.95	69.80

Table 52. (Continued)

Temp	(H-Ho)	S	$-(\frac{F-Ho}{T})$
2400	22.04	79.37	70.19
2500	23.04	79.78	70.57
2600	24.04	80.17	70.93
2700	25.04	80.55	71.28
2800	26.06	80.92	71.62
2900	27.07	81.28	71.94
3000	28.09	81.62	72.26

Table 53. Enthalpy (in Kcal), entropy (in e.u.'s) and the free energy function (in e.u.'s) for MnS

Temp	(H-Ho)	S	$-(\frac{F-Ho}{T})$
298	2.22	59.34	51.89
400	3.07	61.89	54.13
500	4.02	63.92	55.89
600	4.95	65.62	57.37
700	5.90	67.09	58.66
800	6.87	68.38	59.80
900	7.86	69.55	60.82
1000	8.87	70.61	61.74
1100	9.90	71.59	62.59
1200	10.94	72.50	63.38
1300	12.01	73.35	64.12
1400	13.09	74.15	64.81
1500	14.18	74.91	65.45
1600	15.29	75.62	66.07
1700	16.40	76.30	66.65
1800	17.52	76.94	67.20
1900	18.65	77.55	67.73
2000	19.78	78.13	68.24
2100	20.90	78.68	68.72
2200	22.03	79.17	69.18
2300	23.16	79.70	69.63

Table 53. (Continued)

Temp	(H-Ho)	S	$-(\frac{F-Ho}{T})$
2400	24.28	80.18	70.06
2500	25.40	80.64	70.48
2600	26.52	81.07	70.88
2700	27.63	81.49	71.26
2800	28.74	81.90	71.63
2900	29.84	82.29	71.99
3000	30.94	82.66	72.34

Table 54. Enthalpy (in Kcal), entropy (in e.u.'s) and the free energy function (in e.u.'s) for FeS

Temp	(H-Ho)	S	$-(\frac{F-Ho}{T})$
298	2.19	58.89	51.54
400	3.04	61.32	53.73
500	3.89	63.22	55.45
600	4.76	64.81	56.88
700	5.64	66.17	58.11
800	6.55	67.39	59.20
900	7.49	68.49	60.17
1000	8.44	69.50	61.05
1100	9.43	70.43	61.86
1200	10.44	71.31	62.61
1300	11.47	72.14	63.31
1400	12.52	72.92	63.97
1500	13.59	73.66	64.59
1600	14.68	74.35	65.18
1700	15.77	75.02	65.74
1800	16.87	75.65	66.27
1900	17.98	76.25	66.78
2000	19.10	76.82	67.27
2100	20.21	77.37	67.74
2200	21.34	77.88	68.18
2300	22.45	78.38	68.62

Table 54. (Continued)

Temp	(H-Ho)	S	$-(\frac{F-Ho}{T})$
2400	23.56	78.86	69.04
2500	24.68	79.31	69.44
2600	25.79	79.75	69.83
2700	26.89	80.16	70.20
2800	28.00	80.56	70.57
2900	29.10	80.95	70.92
3000	30.19	81.32	71.26

Table 55. Enthalpy (in Kcal), entropy (in e.u.'s) and the free energy function (in e.u.'s) for CoS

Temp	(H-Ho)	S	$-(\frac{F-Ho}{T})$
298	2.20	59.88	52.52
400	3.04	62.31	54.71
500	3.90	64.22	56.43
600	4.78	65.83	57.87
700	5.67	67.21	59.10
800	6.58	68.42	60.20
900	7.51	69.51	61.17
1000	8.44	70.50	62.06
1100	9.38	71.39	62.86
1200	10.33	72.22	63.61
1300	11.29	72.99	64.30
1400	12.26	73.70	64.95
1500	13.22	74.37	65.55
1600	14.20	75.00	66.13
1700	15.18	75.59	66.66
1800	16.16	76.15	67.18
1900	17.14	76.69	67.66
2000	18.13	77.19	68.13
2100	19.12	77.67	68.57
2200	20.11	78.05	69.00
2300	21.10	78.58	69.40

Table 55. (Continued)

Temp	(H-Ho)	S	$-(\frac{F-Ho}{T})$
2400	22.10	79.00	69.79
2500	23.09	79.41	70.17
2600	24.08	79.80	70.53
2700	25.08	80.17	70.88
2800	26.07	80.53	71.22
2900	27.07	80.88	71.55
3000	28.06	81.22	71.86

Table 56. Enthalpy (in Kcal), entropy (in e.u.'s) and the free energy function (in e.u.'s) for NiS

Temp	(H-Ho)	S	$-(\frac{F-Ho}{T})$
298	2.20	57.93	50.57
400	3.04	60.36	52.77
500	3.89	62.26	54.48
600	4.75	63.83	55.91
700	5.63	65.18	57.14
800	6.51	66.35	58.22
900	7.40	67.40	59.18
1000	8.29	68.34	60.05
1100	9.19	69.20	60.85
1200	10.10	69.99	61.58
1300	11.02	70.73	62.25
1400	11.94	71.41	62.88
1500	12.87	72.05	63.47
1600	13.81	72.66	64.03
1700	14.75	73.23	64.55
1800	15.70	73.77	65.05
1900	16.65	74.29	65.52
2000	17.61	74.78	65.97
2100	18.57	75.25	66.40
2200	19.53	75.70	67.81
2300	20.50	76.13	67.21

Table 56. (Continued)

Temp	(H-Ho)	S	$-(\frac{F-Ho}{T})$
2400	21.47	76.54	67.59
2500	22.44	76.93	67.96
2600	23.41	77.32	68.31
2700	24.38	77.68	68.65
2800	25.36	78.04	68.98
2900	26.33	78.38	69.30
3000	27.30	78.71	69.61

Table 57. Enthalpy (in Kcal), entropy (in e.u.'s) and the free energy function (in e.u.'s) for CuS

Temp	(H-Ho)	S	$-(\frac{F-Ho}{T})$
298	2.26	59.07	51.50
400	3.13	61.57	53.76
500	3.99	63.51	55.52
600	4.87	65.10	56.99
700	5.75	66.46	58.25
800	6.64	67.64	59.35
900	7.52	68.69	60.33
1000	8.41	69.62	61.21
1100	9.30	70.47	62.02
1200	10.19	71.24	62.75
1300	11.08	71.96	63.44
1400	11.97	72.62	64.07
1500	12.86	73.23	64.66
1600	13.75	73.81	65.21
1700	14.64	74.35	65.73
1800	15.54	74.86	66.23
1900	16.43	75.34	66.69
2000	17.32	75.80	67.14
2100	18.21	76.23	67.56
2200	19.11	76.67	67.93
2300	20.00	77.05	68.35

Table 57. (Continued)

Temp	(H-Ho)	S	$-(\frac{F-Ho}{T})$
2400	20.89	77.43	68.72
2500	21.79	77.79	69.08
2600	22.68	78.14	69.42
2700	23.57	78.48	69.75
2800	24.47	78.80	70.07
2900	25.36	79.12	70.37
3000	26.26	79.42	70.67

XI. BIBLIOGRAPHY

1. R. J. Ackermann and E. G. Rauh, J. Phys. Chem. 67, 2596 (1963).

2. K. D. Carlson and C. R. Claydon, in Advances in High Temperature Chemistry, edited by L. Eyring (Academic Press, New York, 1967) Vol. 1, p. 43.

3. R. K. Nesbet, Phys. Rev. 135, A460 (1964).

4. K. D. Carlson, E. Ludewa, and C. Moser, J. Chem. Phys. 43, 2408 (1965).

5. K. D. Carlson and R. K. Nesbet, J. Chem. Phys. 41, 1051 (1964).

6. K. D. Carlson and C. Moser, J. Chem. Phys. 44, 3259 (1966).

7. P. S. Bagus and H. J. T. Preston, J. Chem. Phys. 59, 2986 (1973).

8. K. G. Caulton, R. L. DeKock and R. F. Fenske, J. Am. Chem. Soc. 92, 515 (1970).

9. E. Whittle, D. A. Dows and G. C. Pimentel, J. Chem. Phys. 22, 1943 (1954).

10. L. Andrews, in Vibrational Spectroscopy of Trapped Species, edited by H. E. Hallam (John Wiley & Sons, New York, 1973) p. 179.

11. M. J. Linevsky, J. Chem. Phys. 34, 587 (1961).

12. A. Snelson, in Vibrational Spectroscopy of Trapped Species, edited by H. E. Hallam (John Wiley & Sons, New York, 1973) p. 203.

13. A. J. Rest and J. J. Turner, Chem. Commun., 1026 (1969).

14. R. K. DeKock, Inorg. Chem. 10, 1205 (1971).

15. G. A. Ozin and A. Van der Voet, Accounts of Chemical Research 6, 313 (1973).

16. E. P. Kündig and G. A. Ozin, J. Am. Chem. Soc. 96, 3820 (1974).

17. H. E. Hallam, in Vibrational Spectroscopy of Trapped Species, edited by H. E. Hallam (John Wiley & Sons, New York, 1973) p. 67.

18. W. Weltner, Jr., Science 155, 155 (1967).

19. C. J. Cheetham and R. F. Barrow, in Advances in High Temperature Chemistry, edited by L. Eyring (Academic Press, New York, 1967) Vol. 1, p. 43.

20. M. Marcano and R. F. Barrow (unpublished), reported by R. F. Barrow and C. Cousins, in Advances in High Temperature Chemistry, edited by L. Eyring (Academic Press, New York, 1971) Vol. 4, p. 161.

21. N. S. McIntyre, K. C. Lin and W. Weltner, Jr., J. Chem. Phys. 56, 5576 (1972).

22. M. Marcano and R. F. Barrow, J. Phys, B3, L. 121 (1970).

23. R. M. Clements and R. F. Barrow, Trans. Faraday Soc. 65, 1163 (1969).

24. M. Biron, C. R. Acad. Sci. 258, 4228 (1964).

25. F. A. Cotton and G. Wilkinson, Advanced Inorganic Chemistry (Interscience Publishers, New York, 1972) 3rd edition, p. 829.

26. H. A. Jahn and E. Teller, Proc. Roy. Soc. (London) A161, 220 (1937).

27. P. S. Braterman, Structure and Bonding 10, 57 (1972).

28. B. J. Ransil, Rev. Mod. Phys. 32, 245 (1960).

29. J. K. Burdett, M. A. Graham and J. J. Turner, J. Chem. Soc., Dalton, 1972, 1620.

30. J. M. Brom, Jr., Ph.D. Thesis, Iowa State University (1970) (unpublished).

31. D. M. Mann and H. P. Broida, J. Chem. Phys. 55, 34 (1971).

32. A. J. Barnes, in Vibrational Spectroscopy of Trapped Species, edited by H. E. Hallam (John Wiley & Sons, New York, 1973) p. 203.

33. F. Schoch and E. Kay, J. Chem. Phys. 59, 718 (1973).

34. W. R. M. Graham and W. Weltner, Jr., J. Chem. Phys. 56, 4400 (1972).

35. D. H. Corliss and W. R. Bozman, National Bureau of Standards Monograph 53, 1962.

36. D. M. Gruen and D. H. W. Carstens, J. Chem. Phys. 54, 5206 (1971).

37. C. E. Moore, National Bureau of Standards Monograph 467, 1 (1947).

38. C. E. Moore, National Bureau of Standards Monograph 467, 2 (1952).

39. D. W. Green and D. M. Gruen, J. Chem. Phys. 57, 4462 (1972).

40. J. C. Slater, Phys. Rev. 36, 57 (1930).

41. E. Clementi and D. L. Raimondi, J. Chem. Phys. 38, 2686 (1963).

42. H. Basch, A. Viste, and H. B. Gray, Theoret. Chim. Acta. (Berl.) 3, 458 (1965).

43. M. Wolfsberg and L. Helmholz, J. Chem. Phys. 20, 837 (1952).

44. R. F. Barrow and C. Cousins, in Advances in High Temperature Chemistry, edited by L. Eyring (Academic Press, New York, 1971) Vol. 4, p. 161.

45. R. H. Hauge and J. L. Margrave, High Temp. Sci. 4, 170 (1972).

46. V. M. Yanishevskii, Opt. Spectrosk. 33, 636 (1972).

47. C. Chang, High Temp. Sci. 6, 276 (1974).

48. E. D. Cater, A. Facsimile Report No. COO-1182-36, 1973 (unpublished).

49. T. P. Owzarski and H. F. Franzen, J. Chem. Phys. 60, 1113 (1974).

50. T. P. Owzarski, M. S. Thesis, Iowa State University (1973) (unpublished).

51. N. S. McIntyre, K. R. Thompson, and W. Weltner, Jr., J. Phys. Chem. 75, 3243 (1971).

52. W. Weltner, Jr. and D. McLeod, Jr., J. Chem. Phys. 42, 882 (1965).

53. R. L. DeKock and W. Weltner, Jr., J. Phys. Chem. 75, 514 (1971).

54. S. D. Gabelnick, G. T. Reedy, and M. G. Chanasov, J. Chem. Phys. 60, 1167 (1974).

55. W. Weltner, Jr. and D. McLeod, Jr., J. Mol. Spectrosc. 17, 276 (1965).

56. W. Weltner, Jr. and D. McLeod, Jr., J. Phys. Chem. 69, 3488 (1965).

57. M. Allavena, R. Rysnik, D. White, V. Calder, and D. E. Mann, J. Chem. Phys. 50, 3399 (1969).

58. B. Meyer, T. Stroyer-Hansen, and T. V. Oomen, J. Mol. Spectrosc. 42, 335 (1972).

59. B. Meyer and T. Stroyer-Hansen, J. Phys. Chem. 76, 3968 (1972).

60. R. T. Birge and H. Sponer, Phys. Rev. 28, 259 (1926).

61. J. Pacansky and V. Calder, J. Chem. Phys. 53, 4519 (1970).

62. G. Herzberg, Infrared and Raman Spectra of Polyatomic Molecules (Van Nostrand Co., Inc., New York, 1945) p. 160.

63. J. G. Edwards, H. F. Franzen and P. W. Gilles, J. Chem. Phys. 54, 545 (1971).

64. M. Ninomiya, J. Phys. Soc. Japan 10, 829 (1955).

65. R. F. Barrow and M. Senior, Nature 223, 1359 (1969).

66. J. B. West and H. P. Broida, J. Chem. Phys, 62, 2566 (1975).

67. W. Weltner, Jr. in Advances in High Temperature Chemistry, edited by L. Eyring (Academic Press, New York, 1967) Vol. 2, p. 85.

68. E. P. Kündig, M. Moskovits, and G. A. Ozin, Can. J. Chem., 50, 3587 (1972).

69. E. P. Kündig, D. McIntosh, M. Moskovits, and G. A. Ozin, J. Am. Chem. Soc. 95, 7234 (1973).

70. J. S. Ogden, Chem. Commun., 978 (1971).

71. J. L. Slater, R. K. Sheline, K. C. Lin and W. Weltner, Jr., J. Chem. Phys. 55, 5129 (1971).

72. J. L. Slater, T. C. DeVore and V. Calder, Inorg. Chem. 12, 1918 (1973).

73. J. L. Slater, T. C. DeVore and V. Calder, Inorg. Chem. 13, 1808 (1974).

74. H. Haas and R. K. Sheline, J. Am. Chem. Soc. 88, 3219 (1966).

75. S. Evans, J. C. Green, A. F. Orchard, T. Saito, and D. W. Turner, Chem. Phys. Letters 4, 361 (1969).

76. D. W. Pratt and R. J. Myers, J. Am. Chem. Soc. 89, 6470 (1967).

77. H. J. Keller, P. Laubereau and D. Nothe, Z. Naturforsch. 24b, 257 (1969).

78. J. C. Bernier and O. Kahn, Chem. Phys. Letters 19, 414 (1973).

79. H. Huber, E. P. Kündig, G. A. Ozin and A. J. Poe, J. Am. Chem. Soc. 97, 308 (1975).

80. J. K. Burdett, J. Chem. Soc., Faraday Trans. 2, 70, 1599 (1974).

81. F. A. Cotton and G. Wilkinson, Advanced Inorganic Chemistry (Interscience Publishers, New York, 1972) 3rd edition, p. 693.

82. F. A. Cotton and C. S. Kraihanzel, J. Am. Chem. Soc., 84, 4432 (1962); Inorg. Chem. 2, 533 (1963).

83. G. Racah, Phys. Rev. 62, 438 (1942).

84. Y. Tanabe and S. Sugano, J. Phys. Soc. Japan 2, 753 (1974).

85. H. Huber, E. P. Kündig, M. Moskovits, and G. A. Ozin, J. Am. Chem. Soc. 95, 332 (1973).

86. D. W. Green, J. Thomas and D. M. Gruen, J. Chem. Phys. 58, 5433 (1973).

87. E. P. Kundig, M. Moskouits and G. A. Ozin, Can. J. Chem. 51, 2710 (1973).

88. G. A. Ozin and A. Vander Voet, Can. J. Chem. 51, 3332 (1973).

89. K. B. Yatsimirskii and Yu. A. Kraglyak, Dok. Akad. Nauk SSSR 186, 885 (1969).

90. F. A. Cotton and G. Wilkinson, Advanced Inorganic Chemistry (Interscience Publishers, New York, 1972) 3rd edition, chapter 22.

91. N. A. Beach and H. B. Gray, J. Am. Chem. Soc. 90, 5713 (1968).

92. H. B. Gray and N. A. Beach, J. Am. Chem. Soc. 85, 2922 (1963).

93. M. A. Graham, M. Poliakoff, and J. J. Turner, J. Chem. Soc. A, 2939 (1971).

94. R. N. Perutz and J. J. Turner, Inorg. Chem. 14, 262 (1975).

95. G. M. Bancroft, M. J. Mays, and B. E. Prater, Chem. Commun., 585 (1969).

96. D. R. Bidinosti and N. S. McIntyre, Can. J. Chem. 45, 641 (1967).

97. L. Brewer and J. L. F. Wang, J. Mol. Spectrosc. 40, 95 (1971).

98. J. E. Francis, Jr. and S. E. Webber, J. Chem. Phys. 56, 5879 (1972).

99. L. Brewer and C. Chang, J. Chem. Phys. 56, 1728 (1972).

100. A. Kant, S. Lin, and B. Strauss, J. Chem. Phys. 49, 2765 (1965).

101. H. Wiedemeier and P. W. Gilles, J. Chem. Phys. 42, 2765 (1965).

102. S. Lin and A. Kant, J. Phys. Chem. 73, 2450 (1969).

103. A. Kant, J. Chem. Phys. 41, 1872 (1964).

104. G. Burns, J. Chem. Phys. 41, 1521 (1964).

105. W. F. Cooper, G. A. Clarke, and C. R. Hare, J. Phys. Chem. 76, 2268 (1972).

106. H. Sheldon, Nature 222, 757 (1969).

107. P. G. Manning, Nature 228, 844 (1970).

108. P. G. Manning, Nature 239, 87 (1972).

109. S. P. McGlynn, L. G. Vanquickenborne, M. Kinoshita, and D. G. Carroll, Introduction to Applied Quantum Theory, (Holt, Rhinehart, and Winston, New York, 1972).

110. R. S. Mulliken, Journal of Chemical Physics 23, 1833 (1955).

111. C. J. Ballhausen and H. B. Gray, Inorg. Chem. 1, 111 (1962).

112. L. C. Cusachs, J. Chem. Phys. 43, 5157 (1965).

113. G. N. Lewis, M. Randall, K. S. Pitzer, and L. Brewer, Thermodynamics (McGraw Hill Book Company, New York, 1961), 2nd ed.

XII. ACKNOWLEDGMENTS

The author is deeply indebted to Professor H. F. Franzen for his invaluable contributions to this work. Also the patience, encouragement, and extreme confidence which he conveyed to the author are deeply appreciated.

The author wishes to thank Dr. V. Calder, Dr. J. L. Slater and Dr. J. M. Brom, Jr., for sharing some of their expertise about the techniques of matrix isolation. Without their assistance, none of this work could have been accomplished.

Also the author is grateful to the residents of the third floor of Spedding Hall, especially Dave Leebrick, Dick Tuenge, Tom Owzarski, and Jim Owens for the chemical insight they have provided. In addition, Dave and Dick deserve special commendation for turning the cryostat; a small but important part of each experiment.

Finally, the author wishes to convey special praise to his wife, Doreen. Without her love and understanding, none of this work would have been accomplished.